4-20-2011

Self-Ordered Search: A Novel fMRI Task to Study Working Memory in Children with Catastrophic Disease

Matthew Alan Scoggins

To the University Council:

The Dissertation Committee for Matthew Alan Scoggins certifies that this is the final approved version of the following electronic dissertation: “Self-ordered search: A novel fMRI task to study working memory in children with catastrophic disease”.

Eugene Eckstein, Ph.D.
Major Professor

We have read this dissertation and recommend its acceptance:

Heather M. Conklin, Ph.D.

Amy DeJongh-Curry, Ph.D.

Erno Lindner, Ph.D.

Robert J. Ogg, Ph.D.
Research Advisor

Accepted for the Graduate Council:

Karen D. Weddle-West, Ph.D.
Vice Provost for Graduate Programs

SELF-ORDERED SEARCH: A NOVEL FMRI TASK TO STUDY WORKING MEMORY IN CHILDREN WITH CATASTROPHIC DISEASE

by

Matthew Alan Scoggins

A Dissertation

Submitted in Partial Fulfillment of the

Requirements for the Degree of

Doctor of Philosophy

Major: Biomedical Engineering

The University of Memphis

and

The University of Tennessee

May 2011

Acknowledgements

I would like to thank Dr. Robert Ogg for his guidance and invaluable help and insights in the research presented here. I would also like to thank Dr Eugene Eckstein, Dr. Heather Conklin, Dr. Amy DeJongh-Curry and Dr. Erno Lindner for their insightful comments, in-depth suggestions and support over my graduate education. Additionally, I would like to thank Martha McCool and Jason Ashford for their help in recruiting and data acquisition in the EXFXN2 protocol; Dr. Thomas Merchant and Anne Madey for their help in recruiting and data acquisition in the RT1 protocol; Samina Taherbhoy and Carlos Parra for their assistance in running the eye-tracking system and fMRI experiments; Dr. Ping Zou for her assistance with analysis of the data; Kim Johnson for data management and processing; and particularly Mrs. Melissa Jones for being the frontal lobes of the functional neuroimaging lab.

Abstract

Scoggins, Matthew Alan. Ph. D. The University of Memphis. May/2011. Self-ordered Search: A novel fMRI task to study working memory in children with catastrophic disease. Major Professor: Eugene Eckstein, PhD.

Children treated for brain tumors are at increased risk for developing cognitive deficits. The self-ordered search (SOS) is a computerized neuropsychological test used to investigate working memory, a cognitive system whose function is integral to many high level cognitive processes. Functional MRI (fMRI) provides important opportunities to characterize neural correlates of SOS performance non-invasively**.** Implementation of the SOS task presents challenges in the unique environment of the MRI scanner. First, SOS requires participants to select a single stimulus from a set. Second, SOS is a behaviorally driven task that entails variable event timing among participants which complicates group analysis of fMRI data. The work presented here consists of the implementation, validation and application of the SOS for fMRI and associated analysis techniques. Eye-tracking with a MRI-safe response device was used as an interface for the fMRI task, allowing the participant to select an individual stimulus from a two-dimensional array. Performance information was used to generate individual subject design matrices for fMRI analysis, preserving important behavioral measures (time to completion). Healthy volunteers and patients treated for childhood brain tumors performed the SOS task and N-back task, a commonly used working memory task for fMRI. The eye-tracking interface performed well after initial problems with equipment and calibration routine were solved. Activation patterns identified by general linear model (GLM) analysis were similar between the SOS and N-back tasks and included dorsolateral prefrontal cortex, ventral prefrontal cortex, dorsal cingulate, bilateral premotor, and parietal areas.

Independent component analysis identified task-correlated components that were consistent with the GLM. Increasing activation across the general network was associated with fewer errors during the N-back task. Differences in activation between the patient group and healthy group were identified in the parietal and retrosplenial cortex. Analysis of the performance data suggests differences between the healthy and patient groups. Our novel eye-tracking interface provides a natural interface that controls for movement and motor planning associated complex response devices. The SOS for fMRI provides a new tool that will allow us to investigate deficits of working memory in children treated for brain tumors.

Table of Contents

List of Tables

List of Figures

List of Abbreviations

AC	anterior commissure
BA	Brodmann's area
BOLD	blood oxygen level dependent
CBF	cerebral blood flow
CBV	cerebral blood volume
CNS	central nervous system
DLPFC	dorsolateral prefrontal cortex
DMN	default mode network
DTI	diffusion tensor imaging
DX	diagnosis
EPI	echo planar imaging
FA	fractional anisotropy
fMRI	functional magnetic resonance imaging
FOV	field of view
FWE	family-wise error
FWHM	full width half maximum
GIFT	Group ICA of fMRI Toolbox
GLM	general linear model
HRF	hemodynamic response function
ICA	independent component analysis
IQ	intelligence quotient
IRB	institutional review board

MDL	minimum description length
MNI	Montreal Neurological Institute
MRI	magnetic resonance imaging
PC	posterior commissure
PCA	principle component analysis
PCL	Presentation Control Language
PET	positron emission tomography
PFC	prefrontal cortex
RAN	rapid automatized naming
RFT	random field theory
RT	radiation therapy
SDL	Scenario Description Language
SNR	signal-to-noise
SOS	self-ordered search
TE	echo time
TR	repetition time
WASI	Wechsler abbreviated scale of intelligence
WM	working memory

Chapter 1: Introduction

Neurocognitive Sequelae in Survivors of Childhood Cancer

Long-term survival rates for children diagnosed with brain tumors have risen greatly over the past few decades [Linaberry & Ross, 2008]. This is due in large part to aggressive, comprehensive therapies that can include surgical resection, chemotherapy and radiation therapy (RT). Unfortunately, treatment often comes with a price. Disease and treatment induced damage leave this patient population particularly vulnerable to cognitive deficits that often result in academic failure, high jobless rates, and other challenges that affect long-term quality of life [Palmer et al., 2001; Waber et al., 2006]. Neurocognitive testing has shown survivors develop deficits in reading, spelling, math and general Intelligence Quotient (IQ) at a higher percentage than the normal population [Mulhern et al., 2004]. A progressive decline in IQ has been well documented in survivors of childhood cancers [Palmer et al., 2001; Spiegler et al., 2004; Palmer et al., 2007; Mulhern et al., 2005] and is likely due to a slower rate of acquiring new knowledge as opposed to the loss of prior knowledge [Palmer et al., 2001]. The severity of IQ decline has been linked to age of the patient at treatment, radiation dose and irradiated brain volume among other clinical factors [Duffner et al., 1988; Palmer et al., 2001; Palmer et al., 2007; Packer et al., 1989].

Radiation therapy is frequently critical to treatment; however, it is known to cause damage to healthy cerebral white matter and disrupt normal white matter development. The rate of white matter loss is directly correlated to the radiation dose and age at RT [Palmer et al., 2002; Reddick et al., 2000; Reddick et al. 2005]. White matter integrity can be characterized non-invasively using Fractional Anisotropy (FA), a measure of

directional coherence of the diffusion of water molecules derived from Diffusion Tensor Imaging (DTI) MRI. Palmer et al. (2007) documented significant parametric decreases in (FA) (i.e. degeneration of white matter) in 3 patient groups stratified by RT dose compared to a healthy control group. The percent decrease in FA was directly correlated with verbal-, performance- and full-scale IQ. Mulhern et al. (2004) documented less severe cognitive deficits in survivors of ependymoma when RT was restricted to the posterior fossa in comparison to full craniospinal radiation.

While early studies primarily examined global outcome measures such as IQ in survivors of childhood brain tumors, focus is shifting to investigate specific underlying processes such as attention, working memory, processing speed and reading. Survivors have shown deficits in processing speed, attention, and memory [Palmer et al., 2007; Reeves et al., 2006]. Working memory (WM) is a key cognitive process that supports higher level functions such as reading comprehension, math and goal oriented behaviors. WM may be a core deficit that underlies the observed global decline of IQ. Conklin et al. (2011) demonstrated that children treated for brain tumors with conformal radiation therapy show significant impairment on clinical measures of WM when compared to healthy controls and solid-tumor patients who received no radiation therapy.

Functional-MRI

Functional-MRI, or fMRI, is a non-invasive, non-ionizing method of neuroimaging that is used to detect brain activation. Functional-MRI is based on the blood oxygen level dependent (BOLD) signal [Ogawa et al., 1990]. Oxygenated hemoglobin and deoxygenated hemoglobin have different magnetic properties [Pauling and Coryell, 1936]. Functional-MRI exploits this phenomenon to detect changes in blood

oxygenation, a secondary marker related to neuronal activation. Active neurons use the locally available oxygen. An increased oxygen demand starts a neurovascular cascade that leads to a localized increase in cerebral blood volume and blood flow. This brings an increased supply of fresh oxygenated blood that changes the relative concentrations of oxygenated- and deoxygenated hemoglobin which result in a detectible MRI signal change.

Functional-MRI is performed using a standard clinical MR imager and typically involves an individual performing some motor, sensory, or cognitive task while lying in the MRI. Experiments can be designed to look at any number of neurological events, or investigate how underlying neural networks participate in complex behaviors. Each fMRI task generates time-series data (typically 120-400 image volumes), as full brain images are acquired at the rate of an image every 2 seconds. Functional data is analyzed to detect brain activation and organization via both model-driven and data-driven techniques. The General Linear Model (GLM) is an example of model-driven method of fMRI analysis and is well established in the field of fMRI. Recently, however, interest is growing in data-driven techniques, such as Independent Component Analysis (ICA). Data-driven methods implement higher order multivariate statistics to identify unique neural networks based on signal coherence. These analysis techniques are complementary, not exclusionary.

Project Overview

The Self-ordered Search (SOS) is a computerized neuropsychological task developed to study working memory performance in typically developing children. The SOS has been used successfully in a clinical laboratory and positron emission

tomography (PET) neuroimaging studies. Functional-MRI provides important opportunities to characterize neural correlates of SOS performance without the injection of a radioactive tracer required in PET imaging. However, implementation of the SOS task presents challenges in the unique environment of the MRI scanner. First, SOS requires participants to select a single stimulus from a set. Second, SOS is a behaviorally driven task that entails variable event timing among participants which complicates group analysis of fMRI data. The work presented here consists of the implementation, validation and application of an fMRI version of the SOS and associated analysis techniques.

Implementation

Eye-tracking has been used in fMRI to monitor task compliance. Here we used eye-tracking as an interface for an fMRI task, allowing the participant to select an individual stimulus from a multi-dimensional array. Functional-MRI task design has typically been limited to simple stimuli presented serially on a projection screen. During the task a participant is asked to respond to a specified condition using an MRI-compatible response device. Eye-tracking provided an "out-of-the-way" interface that allows fMRI tasks to become more natural and interactive. In the case of the self-ordered search task, an individual was able to select a single object or word from a set of stimuli by looking at (fixating on) the desired stimulus and squeezing a MRI-safe pneumatic button.

Current fMRI task designs frequently follow one of two forms (1) a simple box-car form with fixed timing (e.g., alternating blocks of 20 s of rest and 20 s of a visual stimulus) or (2) an event related design in which brief stimuli are presented at pseudo-

random times during the imaging session. In contrast, the self-ordered search is a behaviorally driven task, i.e., progression through the task is based on fulfilling some condition (selecting a proper stimulus) rather than reaching a fixed time limit of a certain condition. A behaviorally-driven task design preserves an important behavioral measure (time to completion) at the cost of complicating fMRI analysis. We modified current fMRI analysis software to extract the timing variables from recorded task log files and generated subject specific design models.

Validation

A group of healthy volunteers performed the fMRI-based SOS task and N-back task, another prototypical measure of WM that has been widely used in fMRI studies and serves as a "gold standard". We constructed group mean activation maps for each task and identified areas of activation that are related to task performance and other cognitive and demographic measures such as IQ and age. Independent Component Analysis (ICA) was used to investigate functional connectivity of neural networks during the SOS and N-back tasks. Differences between the SOS and N-back are examined. We investigated differences between performance in a clinical setting and fMRI setting to determine if activation patterns were representative of clinical measures of task performance.

Application

Having established the neural correlates of the SOS in a group of healthy individuals, we began to explore the hypothesis that deficits in working memory in children treated with radiation therapy for brain tumors are related to altered neural networks. A group of children enrolled on a clinical protocol for treatment of brain tumors with conformal radiation therapy at St. Jude Children's Research Hospital

performed the SOS and N-back tasks. We identified group differences in mean activation maps and functional connectivity components between patients and healthy controls during the two WM tasks and related those to clinical variables.

Chapter 2: Working Memory

Working Memory

WM is a limited capacity, temporary storage system for the "on-line" maintenance and manipulation of data [Baddeley & Hitch, 1974; Baddeley, 1986; Goldman-Rakic, 1987]. The original model of WM was proposed by Baddeley and Hitch in 1974 to describe how short-term memory actively participates in higher order cognitive processes. Baddeley and Hitch's original model is a multi-modular system consisting of 3 components: the central executive, the visuospatial sketchpad, and the phonological loop. The central executive is a limited-capacity attentional system that directs the other two slave-systems and is responsible for selecting and performing cognitive processing strategies. The visuospatial sketchpad is responsible for maintaining visual and spatial information. The phonological loop acts as an articulatory rehearsal system. Although Baddeley's model of WM arose from experimental psychology, it has generated interest from multiple disciplines such as primate electrophysiology, human electrophysiology, neuropsychology, and neuroimaging.

WM function is integral to many higher level cognitive processes. As such, it is not surprising that performance measures of WM are highly correlated with general IQ [Wechsler D, 2003; Conklin et al., 2011]. More specifically, WM is directly associated with reading and language comprehension [Swanson HL, 1999; Hanten G et al., 1999; De Jonge P, 1996, Baddeley, 1992] and measures of mathematical abilities [Swanson HL, 1999; Ayr LK et al., 2005]. In fact, a significant portion of age related improvements in general IQ can be attributed to developmental improvements in WM [Wechsler D, 2003]

and the acquisition of more complex and cognitively demanding processes of WM [Fry A & Hale S, 1998].

Development of WM capabilities follows an extended course that continues into early adulthood. Basic foundations of WM are generally in place by early childhood and performance on simple tasks of WM stabilizes by preteens. The acquisition of executive processes of WM continues into adolescence, with performance on self-ordered tasks stabilizing around age 16 [Luciana et al., 2005; Conklin et al., 2007]. Additionally, the capacity to hold increased amounts of information in WM increases throughout adolescence [Klingberg et al., 2002; Luciana et al., 1998; Swanson HL, 1999].

Prefrontal Cortex

The prefrontal cortex (PFC) has been implicated as an important neural substrate that supports many higher level functions, including WM. This link is supported by single electrode recordings in the PFC of primates performing delayed match to sample tasks [Goldman-Rakic, 1995], lesion studies in primates [Goldman-Rakic, 1987] and humans [Petrides et al., 1982] and functional neuroimaging studies using PET and functional-MRI with various WM tasks.

The PFC is thought to contain modular circuits that are designed to handle specific types of information and/or specific processes [Smith & Jonides, 1998]. Sensory information often arrives to the frontal cortex via both ventral and dorsal pathways as demonstrated by Parker et al. (2005). As a result, it is not surprising that both dorsal- and ventral-PFC regions have been linked to WM tasks. Both areas have been shown to exhibit activation during WM tasks; however, there is evidence that each area participates in WM in different ways. The ventral-PFC is more active when tasks involve holding and

organizing information in memory [D'Esposito et al., 2000; Petrides et al., 1993]. The dorsolateral-PFC (DLPFC) is also active during such tasks, but exhibits enhanced activation when tasks involve monitoring and/or manipulation of the data [D'Esposito et al., 2000; Petrides et al., 1993]. Several studies provide additional support of DLPFC involvement in WM tasks that involve monitoring of data. Particularly, it has been shown that activation of the DLPFC is positively associated to increased demand on WM [Curtis et al., 2000; Klingberg et al., 2002; Nelson et al., 2000; D'Esposito et al., 2000; Owen et al., 2005].

Resembling the processing separation between dorsal-PFC and ventral-PFC areas, studies suggest a hemispheric lateralization of activation that is dependent upon type of information involved. Spatial WM appears to exhibit stronger activation in the right-DLPFC, while WM tasks involving verbal stimuli induced enhanced left-DLPFC activation [Nelson et al., 2000; Owen at al., 2005]. However, nameable objects have been shown to induce bilateral activation of the DLPFC [Nelson et al., 2005].

Conflicting evidence exists describing how activation of the DLPFC is associated with behavioral performance on WM tasks. For example, Curtis et al., (2000) demonstrated a positive correlation between percent-change in relative cerebral blood flow in the DLPFC with performance on the self-ordered search task. These results are contrary to those of D'Esposito (2000) who found less activation in the DLPFC suggested better performance.

The prefrontal cortex is one of the last regions to develop in the normal human brain [Casey et al., 2000; Gogtay et al., 2004]. Maturation is typically defined by two concurrent processes: synaptic pruning (the loss of gray matter) and myelination

(increase in cerebral white matter). Myelination of axons is associated with increased signal transduction speed that results in the faster processing and more efficient sharing of information between brain regions [Paus, 2005]. Synaptic pruning and myelination are evident in early childhood and continue into early adulthood as evidenced by several MRI studies. Barnea-Goraly et al. (2005) used DTI-MRI to show FA increases with age. More importantly, progression of both processes has been strongly correlated to age related changes in performance measures in neuropsychological testing [Casey et al., 2005; Barnea-Goraly et al., 2005].

As discussed previously, radiation therapy is known to damage existing white matter and to interrupt normal patterns of white matter development in children treated for brain tumors. Given that the prefrontal cortex is one of the last brain regions to mature, it is likely this area is highly susceptible to treatment induced insults that alter the normal trajectory of WM development.

Self-ordered Search

The Self-ordered Search (SOS) is a computerized neuropsychological task that has been used to study development of working memory in healthy children [Conklin et al., 2007; Luciana M et al., 2005]. The SOS was modeled after the paper-based tests described by Petrides and Milner (1982). The SOS engages WM by requiring the "on-line" updating and monitoring of information. A participant is presented with a set of words or object-stimuli, and asked to select each stimulus once and only once. The stimuli rearrange after a selection. The demand on WM can be modified by varying the number of stimuli. The specifics of the SOS task are explained in detail in Chapter 4.

The validity and usefulness of the SOS as a psychometric of WM has been established in several recent experiments. The SOS has been shown to be more sensitive to group differences between healthy controls, patients diagnosed with schizophrenia, and patients' relatives compared to digit-span tasks and delayed-response tasks, widely used clinical measures of WM [Conklin et al., 2005]. Recently, Conklin et al. (2011) demonstrated group differences in working memory between children being treated with CNS directed radiation therapy, children undergoing treatment for solid brain tumors without CNS directed radiation therapy, and healthy siblings.

Self-ordered tasks have been featured in two Positron Emission Tomography (PET) studies. Petrides et al. (1993) demonstrated activation of the frontal cortex in humans performing a verbal version of a self-ordered task. Similarly, Curtis et al., 2000 demonstrated that the object-SOS activated areas in the prefrontal cortex. Notably, percent increase in relative cerebral blood flow showed positive correlation with performance on the SOS object task. Together, these studies provide supporting evidence for the hypothesis that the PFC is a neural substrate of the SOS and WM.

To date, these PET studies appear to be the only existing functional neuroimaging studies using the SOS tasks in humans. PET, however, is an invasive imaging modality that requires injection of radioactive nucleotides (tracers). In addition, PET suffers from poor spatial resolution. Functional-MRI provides important opportunities for characterizing neural correlates of SOS performance without radiation and injection. However, as previously mentioned, implementation of the SOS task presents challenges in the unique environment of the MRI scanner. First, SOS requires participants to select a single stimulus from a set. Second, SOS is a behaviorally driven task that results in

variable event timing between participants which complicates group analysis of fMRI data. Implementation of the SOS for fMRI is discussed in Chapter 4.

Chapter 3: Functional-MRI

Functional-MRI

Functional-MRI (fMRI) is a non-invasive, non-ionizing method of neuroimaging that is used to detect brain activation. Functional-MRI can be performed using a standard clinical MR imager. Research with fMRI has grown exponentially, and fMRI is now a predominant form of neuroimaging used in both clinical and research settings.

BOLD Signal

Functional-MRI exploits the magnetic properties of hemoglobin to detect changes in blood oxygenation, a secondary marker related to neuronal activation. Similar to most biological tissue, oxygenated hemoglobin is diamagnetic. Deoxygenated hemoglobin, however, is paramagnetic and causes distortion in the local magnetic field resulting in shortened T2* relaxation times and MR signal loss. In 1990, Ogawa et al. demonstrated that changes in local susceptibility due to the changing oxygen level of blood can be used as contrast for MR imaging. Ogawa and colleagues termed this contrast the Blood Oxygen Level Dependent (BOLD) signal [Ogawa et al., 1990].

Although the underlying processes that cause the BOLD signal are not fully understood, there exists a neurovascular coupling between neuronal activation and hemodynamic responses. As neural activity increases, cerebral metabolism and oxygen consumption increase which leads to localized changes in the level of blood oxygenation. The increases in metabolism and oxygen demand lead to increases in cerebral blood volume (CBV) and cerebral blood flow (CBF) that result in an influx of fresh oxygenated blood to the active neurons. The changes in the relative concentration of deoxygenated hemoglobin and oxygenated hemoglobin lead to a detectible MRI signal change.

The canonical Hemodynamic Response Function (HRF) is the typical system response to a brief stimulus (Figure 3-1 top panel) [Friston et al, 2000; Zou et al., 2005]. Oxygen consumption by activated neurons leads to an initial negative dip in the MR signal as the relative concentration of deoxygenated hemoglobin increases. After approximately 2 seconds, the cascade of fresh oxygenated blood to the area has begun and the signal change becomes positive. The influx of fresh blood exceeds the oxygen demand of the neuronal population and causes a significant positive signal change (2-10%) that is proportional to the underlying neuronal activation [Logothetis, 2004] and strength of the magnetic field [Kruger et al. 2001]. The peak signal change occurs approximately 6 seconds after stimulus, followed by a return to baseline with an observed period of prolonged negative post-stimulus undershoot [Buxton et al., 1999]. Sustained activation (Figure 3-1 lower panel) generates a stronger peak signal that plateaus for the duration of the stimulus.

Task Design

Functional-MRI involves an individual performing a motor, sensory, or cognitive task while lying in the MRI.[1] Experiments can be designed to look at any number of neurological events. Task designs for fMRI can be complex but typically take one of two forms: a block design or an event related design (Figure 3-2).

Block designs, or box-car designs, comprise alternating epochs of specific conditions. For example, an individual might be shown a green light for 20 seconds during which they have been instructed to tap his or her fingers, followed by 20 seconds of a red light to signify a cessation of finger tapping. The green/red blocks are usually

[1] Recently interest has grown in task-free or "resting state" fMRI called functional connectivity MRI (fcMRI). FcMRI identifies inherent functional networks in the brain during rest via multivariate analysis of temporal coherence in signal changes among brain regions.

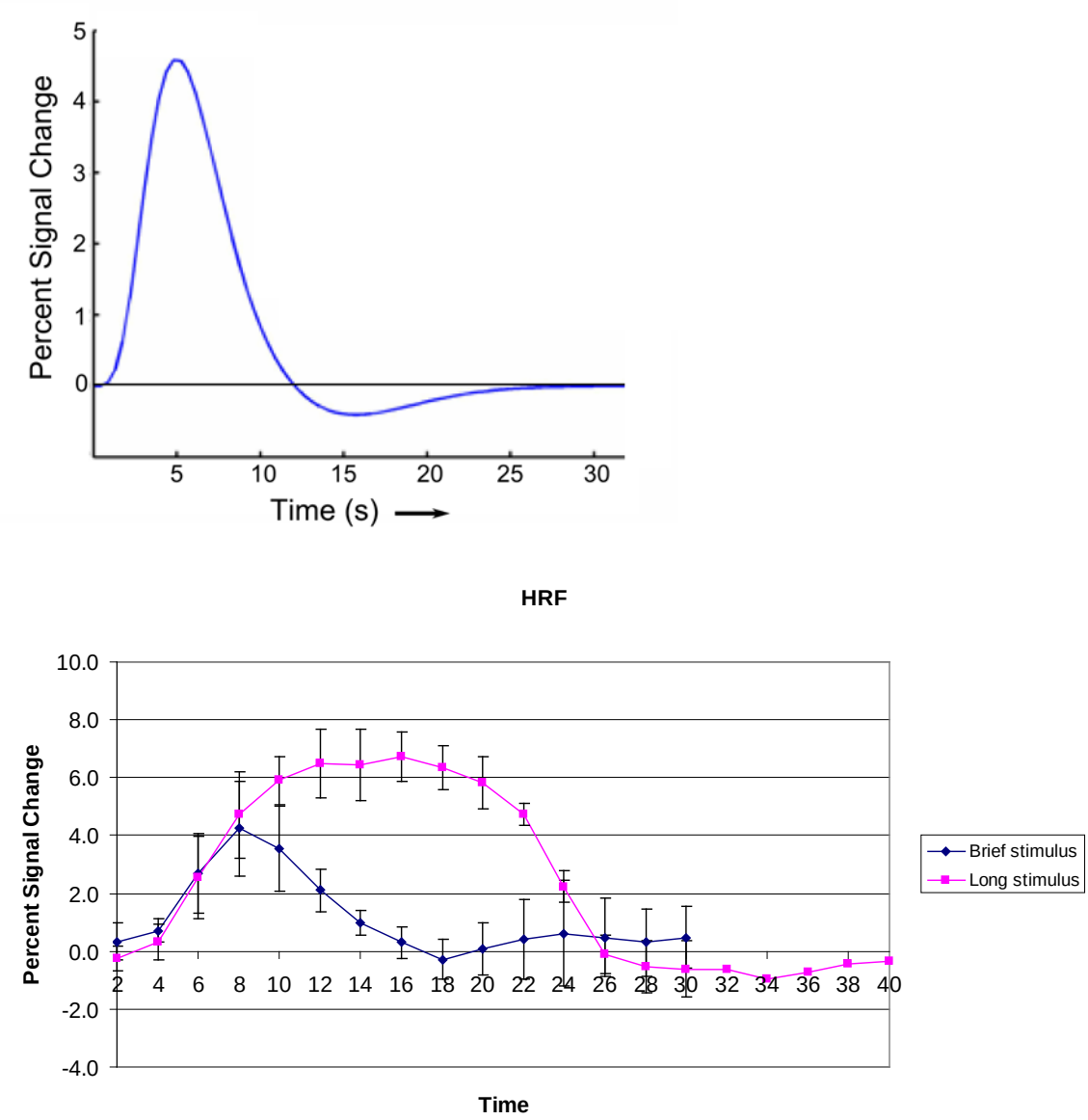

Figure 3-1. Hemodynamic response function (HRF). Top panel shows the canonical HRF response for an impulse stimulus. Bottom panel shows experimental data from the visual cortex during a flashing checkerboard experiment. The blue line shows response to a brief 2 s black and white checkerboard alternating at 8 Hz. The pink line shows response to the same alternating checkerboard for 20 s.

repeated several times to increase sensitivity to the BOLD effect. The statistical power for block designs is increased when compared to event-related design of the same length [Friston et al., 1999]. Block paradigms investigate sustained activation and are insensitive to transient activation; however parameter estimates during analysis are affected by all activity (sustained, transient, or artifactual) during the entire block.

Block designs can be constructed with more than 2 conditions. A common practice is the introduction of parametric modulation of task conditions. For example, the cognitive demand of a task can be varied across block conditions. Areas of the brain that respond with increased activation are more likely directly involved in the task under investigation. Parametric block designs also allow for investigation of recruitment of additional areas of the brain during difficult tasks.

Event related designs typically involve pseudo-random presentations of short stimuli. The type of stimuli can be mixed and separated in analysis. The statistical power of event related designs is less sensitive than block designs for detection of activation, but this design scheme offers several advantages. It is sensitive to transient activation which allows for investigation and characterization of the hemodynamic response and BOLD signal changes [Buxton et al., 2004] across different brain regions and different trials [Kruggel & Cramon, 1999].

There exist many variations of fMRI task designs. For example, block and event-related designs can be combined to create mixed designs. Mixed designs allow for the separation of transient and sustained activations [Visscher et al., 2003]. For the self-ordered search task used in this project we introduce a new variant, a behaviorally modified block design (Chapter 4).

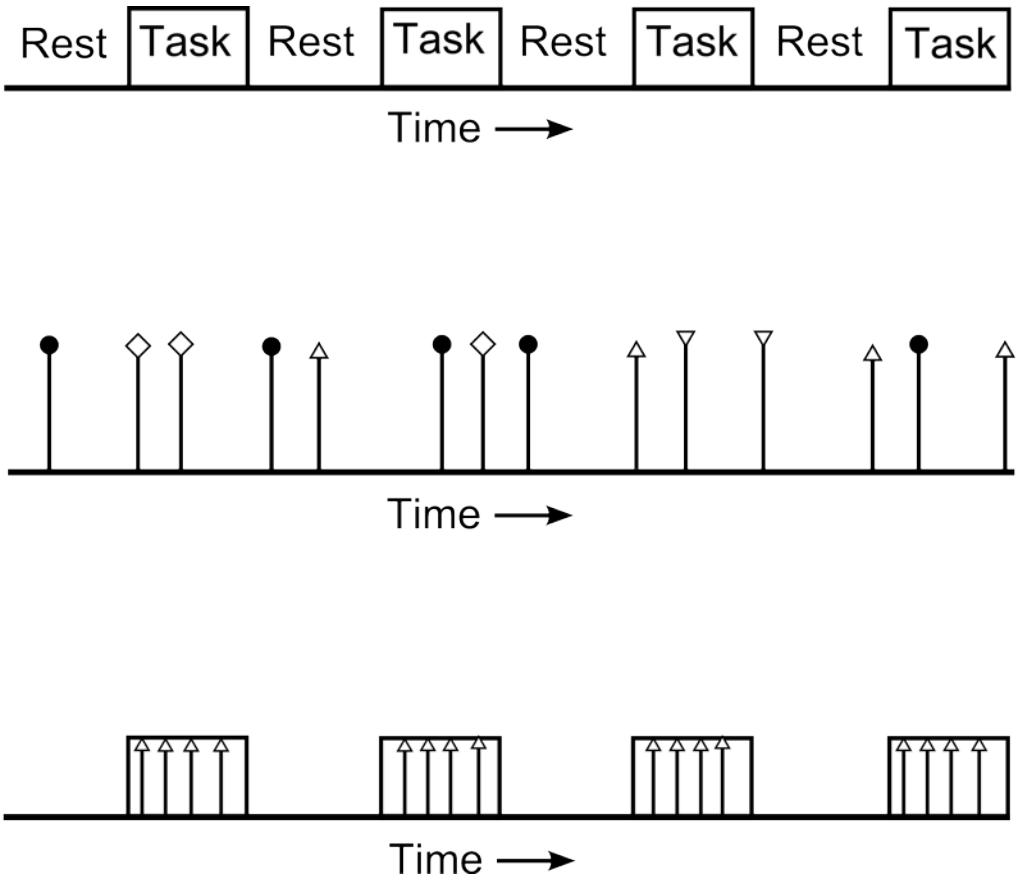

Figure 3-2. Common task designs in fMRI. A block-design (top) consists of epochs of fixed duration that are sensitive to sustained activation. Event-related designs (middle) contain randomized short stimuli and are sensitive to transient activation. Mixed designs (bottom) capture and separate both transient and sustained activation patterns.

Analysis of fMRI data

As previously discussed, an fMRI experiment involves an individual performing some cognitive, sensory, or motor task while lying in an MRI scanner. During this time, images are acquired approximately every 2 seconds. Typical fMRI tasks are between 2 and 10 minutes in duration, resulting in 60 to 300 image volumes. Each image typically consists of around 10^5 voxels. Debate still exists in the fMRI community about how to appropriately analyze these data sets to determine underlying neural activity. Analysis techniques can be characterized as model driven or data driven. However, before any statistical analysis is performed, fMRI time series images under go several preprocessing steps including: time series realignment, spatial normalization and spatial smoothing.

Preprocessing

Functional MRI analysis assumes that an image voxel represents the same neuroanatomy over the entire functional exam. As such, head motion during a functional sequence introduces confounding information, decreases signal to noise, and can produce "false" activation, particularly if head motion is correlated to task design. Participants in fMRI experiments show movement even when restrained by vacuum bags, padding and other restraining methods. In an effort to remove patient movement from image data, the time series data is realigned to a reference image, typically the first image of the series. A rigid-body affine transformation matrix is estimated for each image in the series using an appropriately selected objective function. A rigid-body affine transform consists of 6 parameters that define translation (x,y,z) and rotation (pitch, roll, yaw) and can be represented by the following matrix expression:

$$\boldsymbol{M} = \begin{bmatrix} 1 & 0 & 0 & \boldsymbol{T_x} \\ 0 & 1 & 0 & \boldsymbol{T_y} \\ 0 & 0 & 1 & \boldsymbol{T_z} \\ 0 & 0 & 0 & 1 \end{bmatrix} \begin{bmatrix} 1 & 0 & 0 & 0 \\ 0 & \cos(\theta) & \sin(\theta) & 0 \\ 0 & -\sin(\theta) & \cos(\theta) & 0 \\ 0 & 0 & 0 & 1 \end{bmatrix} \begin{bmatrix} \cos(\phi) & 0 & \sin(\phi) & 0 \\ 0 & 1 & 0 & 0 \\ -\sin(\phi) & 0 & \cos(\phi) & 0 \\ 0 & 0 & 0 & 1 \end{bmatrix} \begin{bmatrix} \cos(\gamma) & \sin(\gamma) & 0 & 0 \\ -\sin(\gamma) & \cos(\gamma) & 0 & 0 \\ 0 & 0 & 1 & 0 \\ 0 & 0 & 0 & 1 \end{bmatrix}$$

where T_x, T_y, and T_y are translation coefficients and θ, φ, and γ are the angles of rotation around the x, y, and z axes respectively.

In order to investigate group activation patterns, patients' brains must be taken to a common brain template, a process called spatial normalization. Spatial normalization is similar to the realignment process discussed previously, but the rigid body assumption is too strict to account for the variability in size and shape of cortical structures across subjects. Removing the rigid body constrictions from our affine transformation results in a 12 parameter transformation that now includes scaling and shearing. These processes are done in conjunction with the translation and rotation and are represented mathematically by the following matrices:

$$\boldsymbol{M}_{scale} = \begin{bmatrix} \boldsymbol{S_X} & 0 & 0 & 0 \\ 0 & \boldsymbol{S_Y} & 0 & 0 \\ 0 & 0 & \boldsymbol{S_Z} & 0 \\ 0 & 0 & 0 & 1 \end{bmatrix}$$

$$\boldsymbol{M}_{shear} = \begin{bmatrix} 1 & \boldsymbol{R_{XY}} & \boldsymbol{R_{XZ}} & 0 \\ 0 & 1 & \boldsymbol{R_{YZ}} & 0 \\ 0 & 0 & 1 & 0 \\ 0 & 0 & 0 & 1 \end{bmatrix}$$

The affine transformation is typically followed by a non-linear warping. For further details see Friston et al. (2007).

The last preprocessing step is spatial smoothing. Spatial smoothing is implemented using standard image filtering techniques. Each image voxel is convolved with a Gaussian kernel of a specified width. Following match-filter theory, the optimum size for our smoothing kernel should conform to the size of the activated area of interest, if known [Friston et al., 2007]. The resulting voxel value is a weighted sum of the original voxel and it nearest neighbors. Smoothing is essentially a low-pass filter that decreases high frequency noise, resulting in an increased Signal-to-noise (SNR) ratio. According the central limit theorem, smoothing also promotes a more normal distribution that leads well behaved errors during statistical analysis. Also, smoothing is necessary for multiple comparison corrections as discussed below.

General Linear Model and Statistical Parametric Maps

The General Linear Model (GLM) is a model-driven method of analysis that has been well established in fMRI. The GLM can be expressed mathematically by the following matrix equation:

$$\boldsymbol{Y} = \boldsymbol{X}\beta + \varepsilon$$

where $\boldsymbol{Y}$ is the observed signal; $\boldsymbol{X}$ is the design matrix; β is a vector of parameters to be estimated; and ε is a vector of normally distributed errors. Each column of the design matrix represents an exploratory variable or confound. In fMRI, an exploratory variable is a task-condition represented by a box-car function convolved with the hemodynamic response function [Friston et al. 1995]. The design matrix essentially models the expected BOLD signal for voxels exhibiting signal changes related to task-induced cortical

activity. Parameter estimation ($\hat{\beta}$) is performed using the method of ordinary least squares:

$$\hat{\beta} = \left(\boldsymbol{X}^{T}\boldsymbol{X}\right)^{-1}\boldsymbol{X}^{T}\boldsymbol{Y}$$

GLM analysis of fMRI data treats each voxel independently. After parameter estimation, activation effects between task conditions (e.g. finger taps > rest) are specified to create contrast images [Friston et al., 1995]. To determine activation patterns, one tests the null-hypothesis that a distribution of estimated β-weights for an image voxel is the same across experimental conditions.

The sheer volume of data in an fMRI experiment increases the likelihood of false-positives, or Type I errors. As previously stated, fMRI data sets typically have approximately 10^5 voxels. Selecting an alpha-value at 0.05 would on average return 5000 false "active" voxels. Multiple comparison correction becomes a necessity for determining activation patterns in a GLM analysis. The Bonferroni correction is a common method of controlling for type I errors. However, it is too conservative a measure because the number of voxels is large and voxels are spatially correlated. Therefore the Bonferroni correction increases the likelihood of false-negatives. Gaussian Random Field Theory (RFT) is used for multiple comparison corrections of fMRI data [Worsley and Friston, 1995]. RFT calculates the adjusted statistical threshold based on spatial correlation (smoothness) of the image data and an image property called the Euler Characteristic. This combination of the GLM and RFT has been labeled statistical parametric mapping. For an in-depth discussion see Friston et al (2007).

The procedures described above comprise the 1st-level of a two part mixed-effect analysis. The GLM and RFT are performed on each subject's fMRI data independently to examine fixed-effects within an individual. However, to make inferences about a population we need to consider the variability of the task effect on each person in a 2nd-level, or random-effects analysis [Holmes & Friston, 1998]. In the 2nd-level random effects analysis, contrast images from the fixed effects analysis of each participant are used as variables in the GLM to identify group patterns of activation and areas of the brain in which activity is related to behavioral performance.

Independent Component Analysis

GLM analysis of fMRI establishes a set of image voxels that exhibit significantly correlated signal change with experimental conditions. As mentioned previously, all activation during task block contributes to parameter estimates in the GLM. It is possible, however, for voxels to be significantly correlated to the task yet be uncorrelated to each other [McKeown & Sejnowski, 1998]. Independent component analysis (ICA) has recently been implemented as an exploratory method of analysis for detecting and separating activation patterns that may or may not be task related. ICA is a method of blind source separation that uses multivariate analysis techniques to extract statistically independent, non-Gaussian sources from signal mixtures. This is a heuristic process that emerged from information theory [Bell & Sejnowski, 1995; Comon, 1994].

A predominant example given to explain ICA is the cocktail party problem. A specific number of people, 4 in this case, are all talking in a room with an equal number of microphones placed randomly throughout the room. Each microphone picks up a

different mixture of the source voices. This can be described mathematically by a series of equations:

$$\begin{aligned}
\boldsymbol{m}_1 &= \boldsymbol{a}_1\boldsymbol{s}_1 + \boldsymbol{b}_1\boldsymbol{s}_2 + \boldsymbol{c}_1\boldsymbol{s}_3 + \boldsymbol{d}_1\boldsymbol{s}_4 \\
\boldsymbol{m}_2 &= \boldsymbol{a}_2\boldsymbol{s}_1 + \boldsymbol{b}_2\boldsymbol{s}_2 + \boldsymbol{c}_2\boldsymbol{s}_3 + \boldsymbol{d}_2\boldsymbol{s}_4 \\
\boldsymbol{m}_3 &= \boldsymbol{a}_3\boldsymbol{s}_1 + \boldsymbol{b}_3\boldsymbol{s}_2 + \boldsymbol{c}_3\boldsymbol{s}_3 + \boldsymbol{d}_3\boldsymbol{s}_4 \\
\boldsymbol{m}_4 &= \boldsymbol{a}_4\boldsymbol{s}_1 + \boldsymbol{b}_4\boldsymbol{s}_2 + \boldsymbol{c}_4\boldsymbol{s}_3 + \boldsymbol{d}_4\boldsymbol{s}_4
\end{aligned}$$

where $\boldsymbol{m}_i$ is the *i*th mixture; $\boldsymbol{a}_i, \boldsymbol{b}_i, \boldsymbol{c}_i, \boldsymbol{d}_i$ are weighting factors (i.e. distance between a source and *i*th microphone); and $\boldsymbol{s}_i$ is the *i*th source signal (person speaking).We can write this in matrix form as:

$$\boldsymbol{M} = \boldsymbol{A}\boldsymbol{S}$$

ICA attempts to reverse this process by estimating the unmixing matrix; matrix $\boldsymbol{W}$ in the following equation:

$$\boldsymbol{S} = \boldsymbol{W}\boldsymbol{M}$$

To estimate the unmixing matrix, ICA attempts to extract maximally independent sources algorithmically. Two sources (*x*,*y*) are independent only if their joint probability density function (pdf or $\boldsymbol{p}$ in the equation below) is equal to the product of the marginal pdf's:

$$\boldsymbol{p}_{xy}(\boldsymbol{x}, \boldsymbol{y}) = \boldsymbol{p}_x(\boldsymbol{x})\boldsymbol{p}_y(\boldsymbol{y})$$

In other words, at no time does the signal of *x*, give any information regarding the value of *y*. It is not possible to measure independence; however, we can minimize or maximize

some metric related to independence. ICA extracts sources based on three assumptions: (1) source signals are independent; mixtures are not; (2) source signals are less complex than mixture signals; (3) a histogram of a source is more non-Gaussian than a histogram of a mixture (Central Limit Theorem). Bell and Sejnowski (1997) demonstrated the effectiveness of an ICA algorithm based on entropy called Infomax. Entropy ($\boldsymbol{H}$) is a measure of the uniformity of a distribution and can be expressed by the following mathematical equation:

$$\boldsymbol{H}(\hat{\boldsymbol{S}}) = -\sum_{\boldsymbol{i}=1}^{\boldsymbol{N}} \boldsymbol{p}(\hat{\boldsymbol{S}}_{\boldsymbol{i}}) \log \boldsymbol{p}(\hat{\boldsymbol{S}}_{\boldsymbol{i}})$$

where $\hat{\boldsymbol{S}}$ is an estimated source signal extracted with an unmixing matrix. A rotation of axes can be iteratively performed on the multi-dimensional data set, where the rotation parameters are the unmixing matrix. Entropy is calculated for an extracted distribution at each iteration. At the point of maximal entropy, we assume we have extracted a source signal. This process is repeated until all sources are extracted.

Due to the multi-dimensionality and large volume of data, exhaustive search is not practical. Most ICA algorithms implement a gradient-ascent optimization technique to replace the exhaustive search. From an initial point, the rotation vector is moved along the direction where the absolute value of entropy is increasing most rapidly.

To speed up processing further, ICA algorithms often introduce preprocessing steps such as whitening and Principal Components Analysis (PCA) for decorrelation and data reduction. The number of components to extract is estimated using common information theoretic methods such as minimum description length (MDL) [Rissanen, 1983] or can be chosen to keep a specified proportion of the variance.

In the case of fMRI data, each image voxel is analogous to a microphone in the cocktail party example above and contains some weighted amount of each source signal. Sources are made up of coherent signal changes related to underlying activity of neural networks, artifacts caused by physiological phenomena, head motion, or equipment. One can generally assume there are fewer sources than time points. Thus, temporal PCA can be performed on the raw data that results in *N* decorrelated mixtures of *N* sources. ICA is then performed in the spatial dimension to extract a set of spatially independent components consisting of set of voxels that exhibit an associated time course. Voxels are typically converted to z-scores and the resulting spatial maps from the independent components can then be tested with a random effects analysis as described above. For an in-depth explanation of group ICA of fMRI data see Calhoun (2001).

Eye-tracking in fMRI

Recently, eye-tracking has been integrated into fMRI setups at many institutions. A number of eye-trackers based on in-magnet [Kimming et al., 1999; Kanowski et al., 2007] and long range optics [Gitelman et al., 2000] have been developed specifically for the unique MRI environment. At St. Jude Children's Research Hospital we use eye-tracking on several different functional imaging protocols.

Performing eye-tracking during fMRI serves a number of purposes. Foremost, it is essential for brain activation to be representative of the task conditions under investigation. Eye-tracking systems often provide a method for real-time monitoring of participant compliance during an fMRI exam. Should an fMRI researcher notice an individual not participating completely in task, the fMRI scan can be stopped and the

subject can be corrected and given the instructions again, or the individual's data can be justifiably excluded from group analysis.

Analysis of eye-track data can quantify a participant's time-on-task. For example, the majority of our fMRI tasks involve serially presented stimuli that are displayed in the center of the projection screen. We can define some area of interest around the center of the screen and calculate the percentage of time an individual's gaze was contained within that area. These values can then be entered as behavioral covariate in fMRI analysis.

We are also using eye-tracking to gather behavioral data on more visually complex fMRI tasks. The Rapid Automatized Naming (RAN) task presents subjects with a 2-dimensional array of stimuli, typically letters, numbers, colors or objects. Individuals are instructed to go across each row naming each stimulus as quickly as possible without making mistakes [Denckla & Rudel, 1974]. The primary variable of interest is the time it takes to accurately name every stimulus in the array. MR imaging requires patients or volunteers to remain as still as possible during scanning. This requirement precludes overt speech during the RAN task in an fMRI setting. Eye-tracking provides a method of determining performance during a covert version of the RAN task (Figure 3-3). Further examination of this eye-tracking data can provide us with derived behavioral measures such as average dwell-time-per-stimulus and might allow the detection self-corrections during the task.

Furthermore, analysis of eye-tracking data can provide insights into types of performance errors during an fMRI task. For example, in 0-back version of the N-Back task for fMRI, participants are instructed to squeeze a button every time the letter 'X' appears on the screen. Stimuli appear on the screen for 500 milliseconds. Examination of

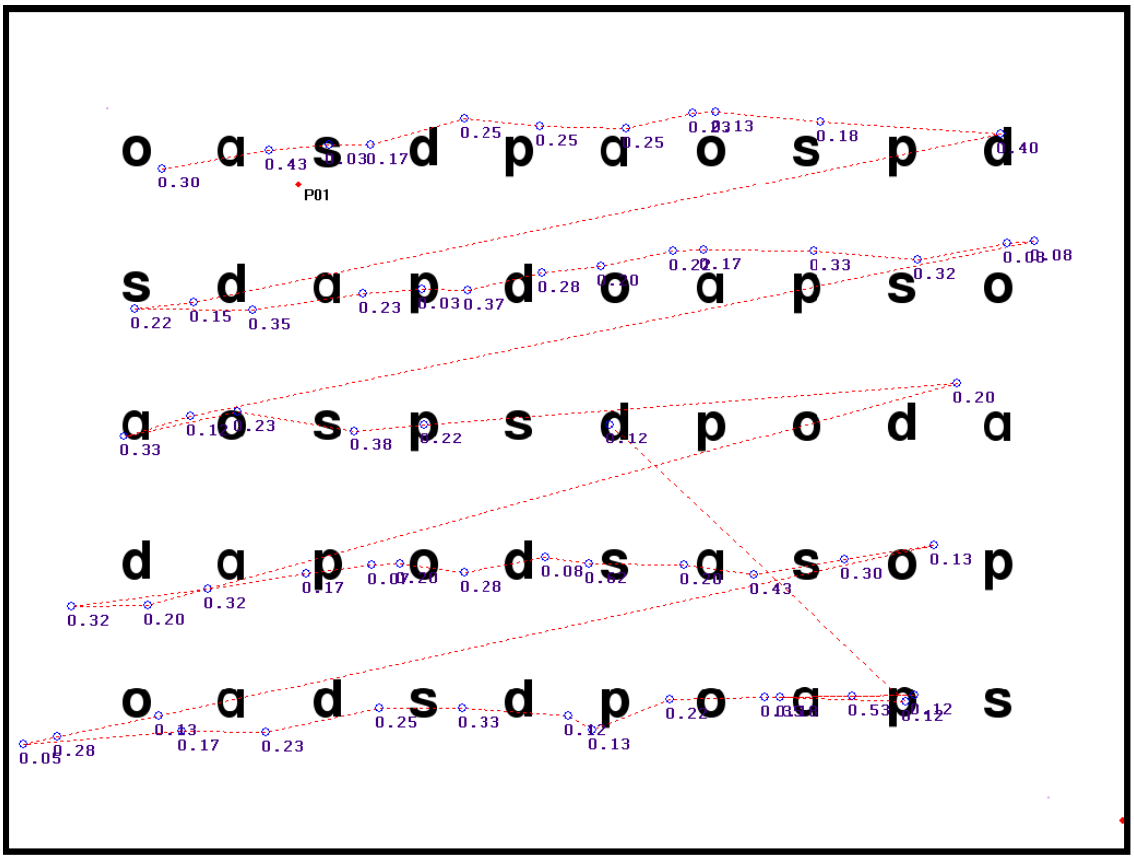

Figure 3-3. Eye-tracking in a Rapid Automatized Naming (RAN) task. The participant was instructed to go across each row, say each letter covertly as quickly as possible without making a mistake. The participant's gaze path is traced in red. Fixation points are noted with blue circles with an associated dwell time given in seconds. The eye-tracker operates at 60Hz.

eye-track data can provide evidence that missed button presses were due to the individual looking away from the stimuli at time of presentation (attentional error) versus a recognition error. In this case, an event-related analysis investigating brain activation related to errors, separating attentional errors from true mistakes increases sensitivity to brain patterns involved in making a true error.

For this project, we develop a novel use for eye-tracking in fMRI. Eye-tracking provides an "out of the way" interface that allows fMRI tasks to become more interactive. In the case of the SOS, an individual is able to select a single object or word from a set of stimuli by fixating on the desired stimulus and squeezing a pneumatic MRI-safe response bulb. Implementation of the eye-tracking based SOS task is discussed in Chapter 4.

Researchers have developed any number of MR-compatible response devices such as keyboards [James et al., 2005], mice, and game controllers (www.magconcept.com). Using eye-tracking as our interface has several advantages over these other interface methods. The eye-tracking system is already implemented in our standard fMRI setup. We only need to facilitate real-time communications between the eye-tracker and our stimulus delivery software. Using response devices such as mice or key-boards induces patient motion during the fMRI task. If this motion is task correlated, it can result in lost sensitivity to true activation and detection of false activation patterns because of motion correction of the functional images. Compared to MR-compatible game controllers, eye-tracking introduces no additional cognitive demands for motor planning. Also, the use of complicated response devices potentially introduce

performance confounds between participants familiar with game controllers and those unfamiliar with computers or game-consoles.

Chapter 4: General Methods

Functional-MRI Equipment setup

Functional-MRI is performed on a standard clinical MRI scanner. We used a Siemens' Trio 3T MRI scanner with standard receive-only array head coil for experiments in this project. In addition to the MRI, a few extra pieces of equipment are needed to perform functional experiments.

Figure 4-1 provides a diagram of the scanner and additional equipment used in our functional experiments. Visual stimuli are projected onto a screen at the back of the magnet via a digital projector. The projector is connected to a personal computer outside the scanner room that is running Presentation software. Individuals are positioned head-first supine in the magnet and view the screen via a mirror attached to the head coil. The visible area of the projection subtends a visual angle of approximately 30 x 40 degrees. Participant responses are recorded using a squeeze bulb interfaced with the Presentation PC. Using a trigger pulse from the MRI controller, image acquisition was coordinated with stimulus presentation.

Eye-tracking was performed using an LRO-6000 eye-tracking system from Applied Science Laboratories (www.asleyetracking.com, Bedford, MA). The eye-tracker was positioned at the back of the magnet near the projector and was positioned such that it had an unobstructed view of an average individual's right eye in the mirror attached to the head coil (Figure 4-1). The LRO-6000 system operates at a 60 Hz data acquisition rate.

To facilitate communications between the MRI controller, response button, ASL eye-tracker control unit, and the PC running Presentation software, we constructed a

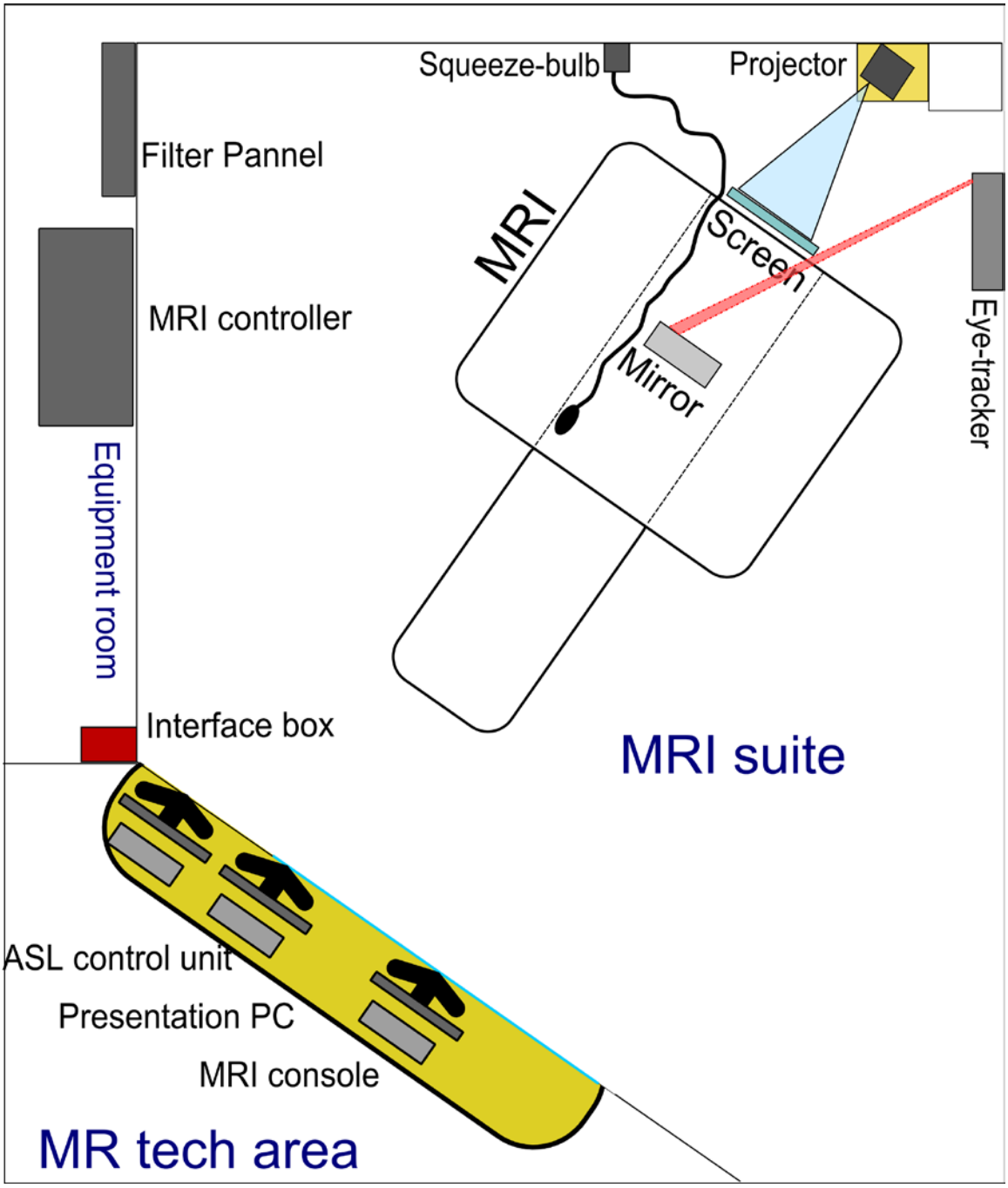

Figure 4-1. Functional-MRI equipment layout. (Not to scale.) Video signal is sent from the Presentation PC through the filter plate, to the projector. Signals from the squeeze-bulb and MR-controller are sent through the interface box and redirected to the Presentation PC. The eye-tracker optics unit communicates with the ASL control unit via an optical fiber. Presentation and the ASL control unit communicate via the interface box and serial connection.

custom interface box (Appendix E). Figure 4-2 shows a communications diagram. The signal from the MRI trigger line is passed through a pulse-shaping circuit to insure accurate pulse counts. Responses from the squeeze bulb are converted to electrical signals using a pneumatic switch and are input to the interface box and shaped before being rerouted to the Presentation PC. Presentation software sends event flags to the ASL control unit via the interface box. The ASL control unit sends position data to the Presentation PC via a direct serial port connection.

Presentation

Presentation is a neurocognitive stimulus delivery and experimental control software package available from Neurobehavioral Systems, Inc. (www.neurobs.com, Albany, NY). Presentation serves as a foundation for delivering visual and auditory stimuli with millisecond timing, interfacing with response devices, and programming neurocognitive tasks with built in event logging. Presentation provides 2 innate programming languages for developing neurocognitive tasks, called scenarios. Scenario Description Language (SDL) is a high-level language that can be used to specify simple stimuli or sequences of stimuli, and their associated properties. While it is possible to develop simple neurocognitive tasks entirely in SDL, scenarios often require complex control of stimulus presentation. Presentation Control Language (PCL) is an interpreted programming language that facilitates data manipulation, logic, and flow control found in typical computer programming languages. For this project, we developed several scenarios to control calibration of the eye-tracker, the N-back task, and the SOS task.

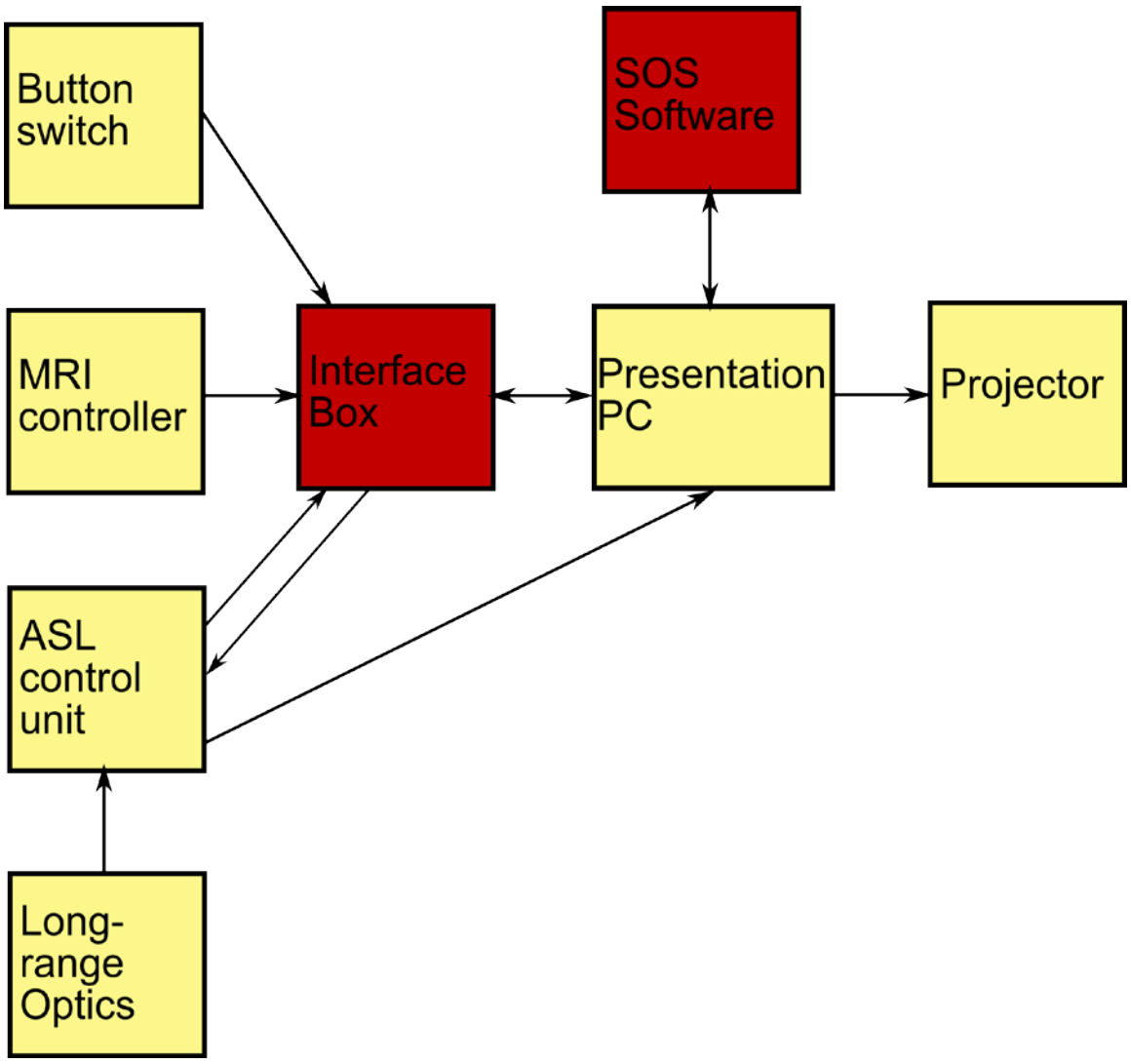

Figure 4-2. Communications diagram. Panel shows communications between the various system components. Red boxes denote custom components.

Eye-tracker Calibration

The ASL eye-tracking system requires calibration before standard operation. An individual is asked to look at a minimum of 9 points that typically define the center and outer boundaries of the experimental display space. ASL provides a static image containing the 9 points that can be displayed on the computer monitor or projection screen. We used Presentation to replace the static image with an animated eye (Appendix A). The spinning eye moves sequentially to each of the 9 calibration points in order. The animation provides visual interest to help keep an individual's attention during calibration. More importantly, using Presentation to handle the calibration routine provides an opportunity to handle an additional part of the setup process.

Following display of the initial 9 points, the ASL system is ready for standard visual tracking. However, to use this system interactively an extra calibration step is required. The output coordinates from the ASL system must be mapped to Presentation display space (VGA coordinates). To accomplish this, the custom calibration scenario repeats the sequential display of the 9 points as in the initial calibration step. This provides an opportunity to verify a good calibration. More importantly, during this second run-through Presentation records the *x,y* output from the ASL control unit. When a calibration point is displayed, the first 166 milliseconds of fixation data are thrown away to allow an individual to fixate on the new point. The remaining coordinate data is stored in a memory buffer. The mean *x,y* coordinates are calculated for each of the 9 points and are written to a text file that the SOS scenario will use later for real-time mapping and participant feedback.

N-Back

The N-back task (Figure 4-3) is a proto-typical WM measure that has been widely used in neuroimaging studies [Owen, 2005]. N-back requires a participant to respond to a presented stimulus (either letters or objects in our implementation) only when it is the same as the one presented on a trial at a predetermined number (N) prior to the current trial. For example, in the letter-identification N-back task, participants view a continuous stream of single, phonologically distinct, letters. For each letter, participants need to squeeze the response bulb when the letter is identical to the letter presented one or two back in the sequence for the 1-back and 2-back trials respectively. A control condition (0-back trial) is used during which the same continuous stream of single letters is presented but the participant need only decide whether each letter matches a single target communicated at the start of the task. Behavioral measures include reaction time, omissions and commissions.

For this study, we implemented the 0-, 1- and 2-back variations of N-back task with both letter and object stimuli. For the verbal task, the stimuli comprised the set of phonologically distinct letters: X, N, C, A and Q. For the object identification task, 5 novel objects were created (Figure 4-4). Each task block consisted of 16 stimuli (letters or objects) presented serially. Block order was: 0, 1, 2, 0, 1, 2, 0, 1, 2. Stimuli were displayed for 500 ms, with an inter-stimulus interval of 1500 ms. Each block has a total of 4 (25%) N-back targets. Before each task block, instructions were displayed on the screen for 2 seconds corresponding to task-level, and fixation cross was presented for 5 seconds. The targets for the 0-back condition were ‘X’ and the first object in Figure 4-4.

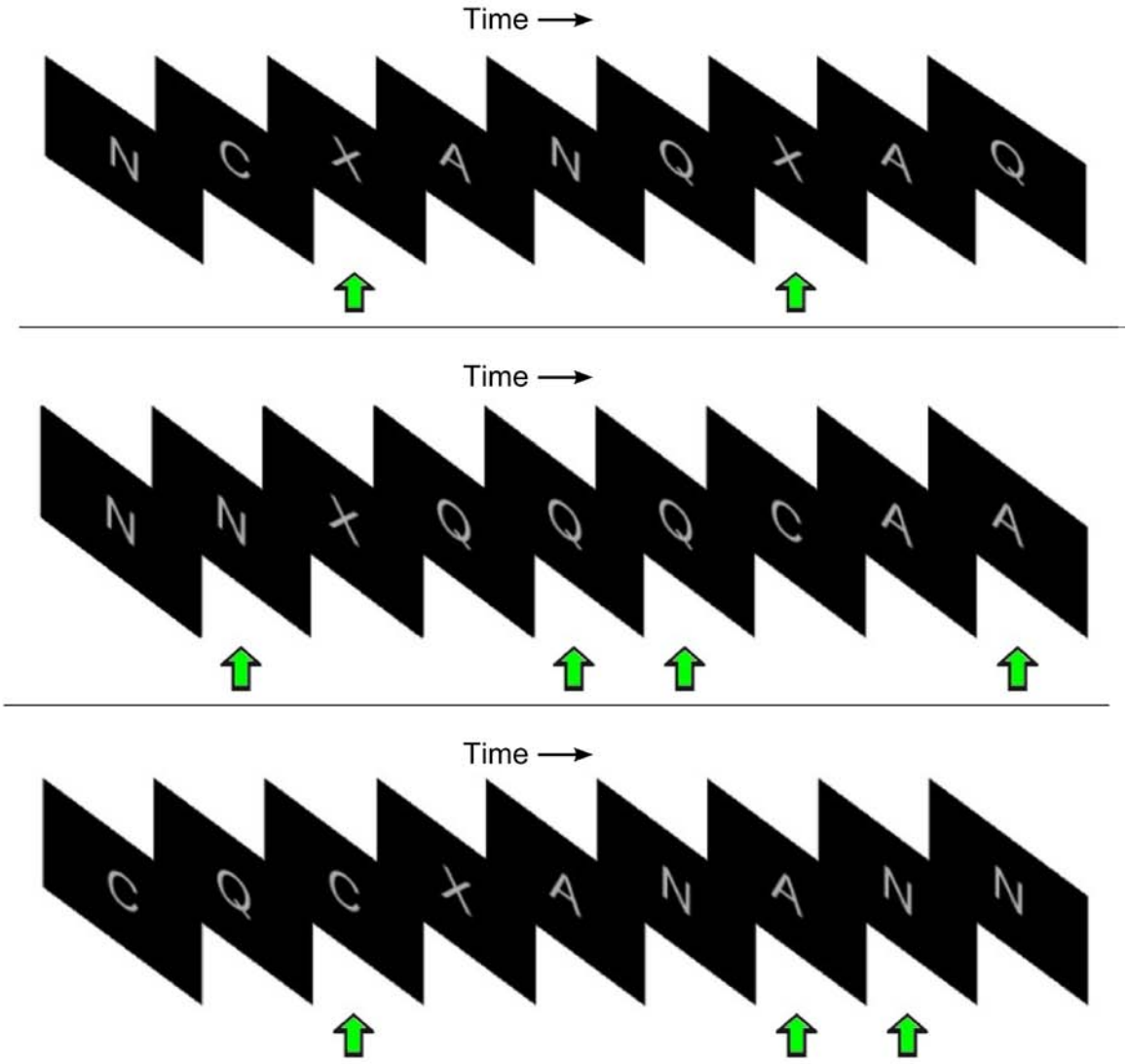

Figure 4-3. N-back task. 0-back task (top): respond for target letter ‘X’. 1-back task (middle): respond for repeating letters. 2-back task (bottom): respond when stimuli are the same as 2 previous. Stimuli are display for 500 ms. Inter-stimulus interval was 2500 ms. An 2 second instruction screen, followed by 5 seconds of rest occurs before each block.

Figure 4-4. N-back objects. Object stimuli created for the object variation of the N-back task.

The Presentation scenario for the N-back task contains a mixture of SDL and PCL code (Appendix C). The SDL section contains definitions for our stimuli (letters or bitmaps), picture objects, and simple trials to handle fixation, instruction, and stimulus events. As with the SOS, the task is controlled in the PCL section of the scenario file. A top-level loop executes each task block. The task level is determined by the values 0, 1 or 2 that are defined in the *num_blocks* variable. Upon entering a task block, the appropriate instructions trial is chosen and executed. We then have to randomize positioning of N-back events in the up-coming task block. To insure that there are only 4 N-back targets per block, we defined an array of 16 integers called *stims* and initialize all elements to 0. N-back events cannot occur before N stimuli have been displayed. To account for this, we ignore the first N elements, the next 4 array elements are set to a value of 1, leaving the remaining elements 0. Fortunately, Presentation provides a function that will randomize a sub-set of elements in an array. We exploit this functionality and randomize elements N+1 to 16 in the *stims* array and proceed to loop through it. To assure the correct stimuli are presented for N-back events and to prevent any accidental N-back events we record the identity of last N stimuli presented. When an N-back event occurs (a value of 1 in the *stims* array) we look up the last N-stimuli and display the appropriate stimulus. In the case of a non-N-back event, we randomly choose any other stimulus that does not match the stimulus present N-back.

Self-ordered Search

The SOS was introduced in Chapter 1 and 2 as a neuropsychological task developed to study WM. It engages WM by requiring on-line maintenance and monitoring of information. For the SOS task, participants view a 2-dimensional array of words or geometric objects on a computer, or projection screen. Participants are asked to select each item in the array once and only once, in any order. After a selection has been made, the array rearranges in random (verbal implementation) or pseudo-random order (objects implementation). A trial ends when all words or objects have been selected, or 3 × N responses have been made, where N is the total number of stimuli. The size of the array is modified to vary the difficulty of different trails. For the verbal and object versions we use the following array sizes: 3 × 2, 3 × 3, and 4 × 3 for 6, 9 and 12 words, or 5, 8, and 11 objects respectively. One array location in the object version of the task is filled with a blank square for reasons explained below. The participant must maintain a growing list of selected words or objects in working memory. The goal of this task is to select all items in as few responses as possible. Behavioral measures include the number of responses to completion and the time to completion for each level.

To insure the use of WM we implemented several safeguards in the SOS program. In the verbal version of the SOS task, the program will display a warning message when 3 words have been selected in alphabetical order. Similarly, in an effort to preclude spatial strategies in the verbal-SOS, the program will display a warning message when the same location in the array has been selected for three consecutive trials. The participant will be asked to select a different stimulus in another location. The object

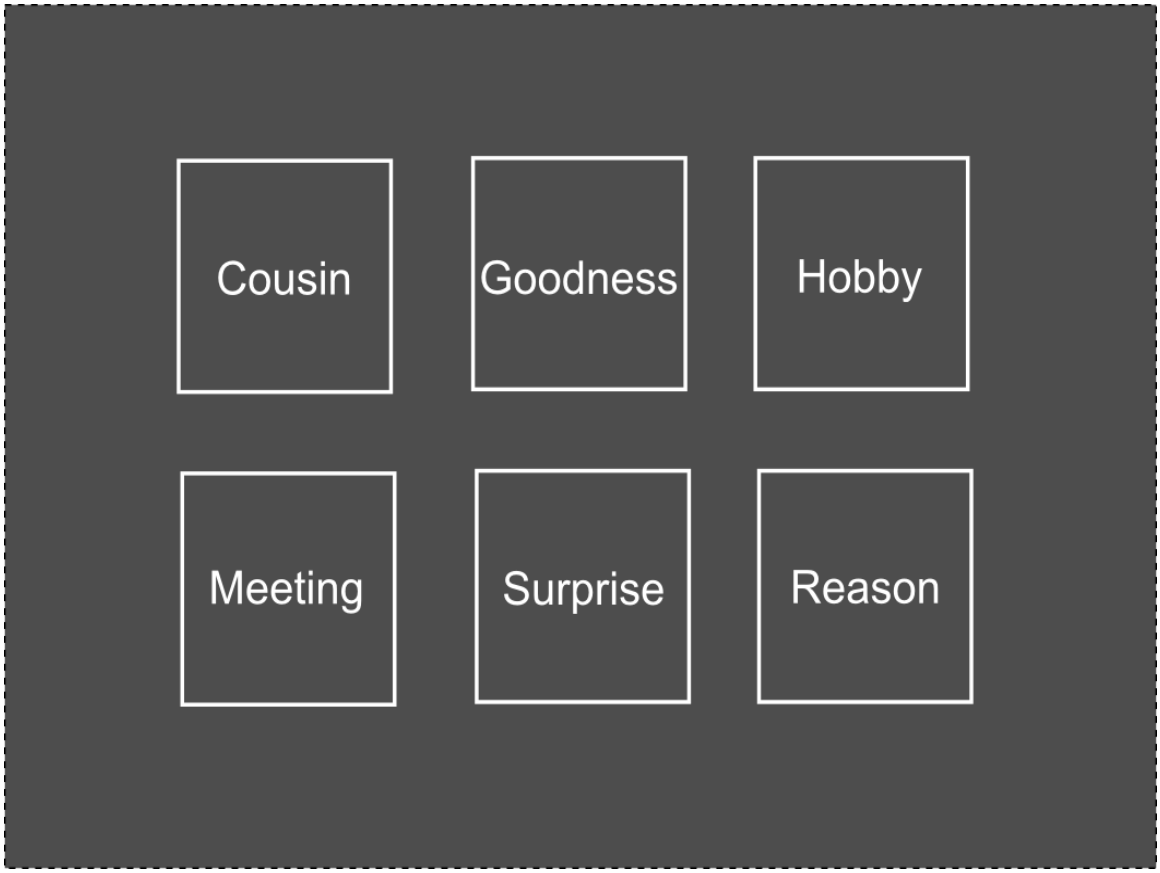

Figure 4-5. 6-word level SOS task. Words are chosen to be difficult to visualize. Words shuffle after each selection.

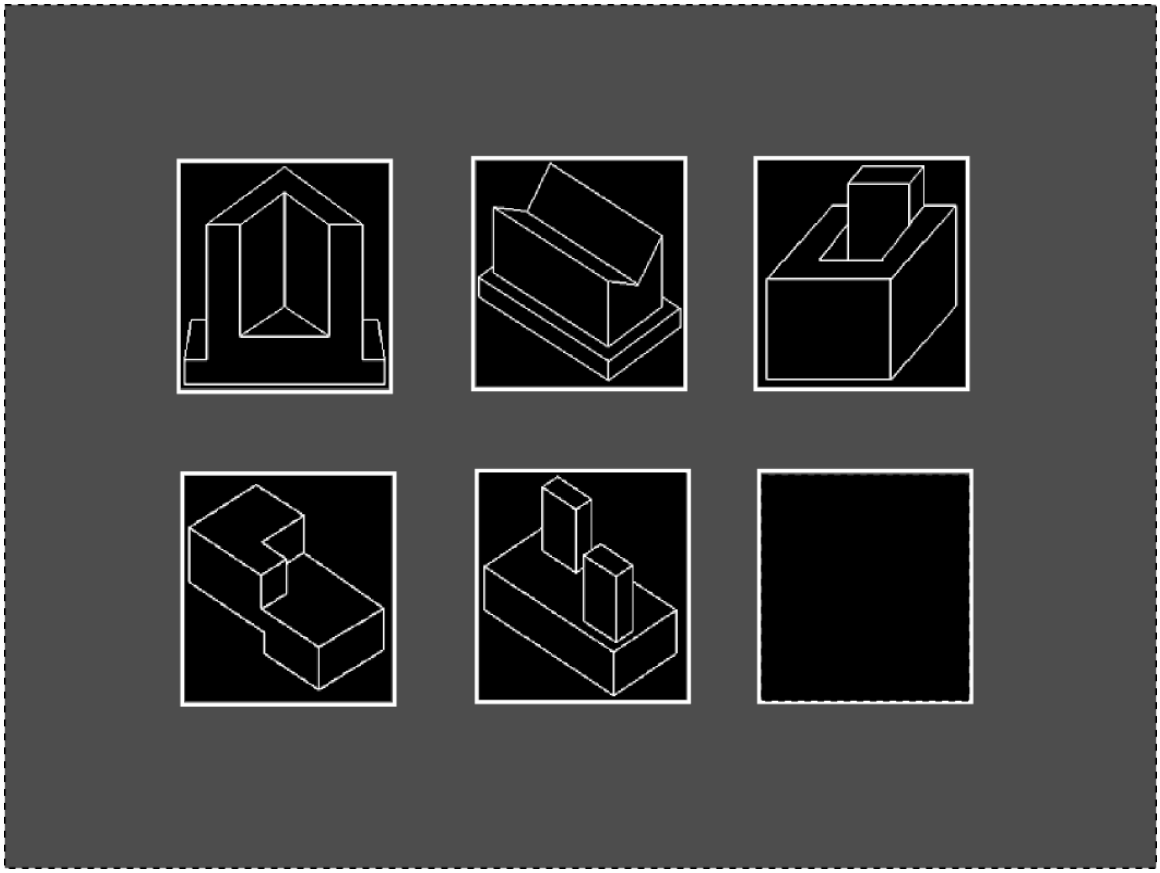

Figure 4-6. 5-object level SOS task. The geometric shapes are difficult to name. The black square is placed at the location of the previously selected stimulus.

version of the SOS uses a different method to prevent spatial strategies. As previously mentioned, the object-SOS incorporates a blank square to fill one of the array locations. This blank square is placed at the last selected location to force selection of a new position in the array.

Before each trial, the participant will perform a control task in which the goal is to select the one word or object that is marked with an asterisk. The asterisk will be placed on each of the stimuli in random order and the control task ends when N stimuli have been selected. The control tasks maintain the same randomization mechanics, visual stimuli, visual search and motor selection mechanics as in the actual SOS WM trials.

Eye-tracking along with a pneumatic squeeze ball serves as our interface for stimulus selection. Gaze coordinates are sent from the ASL eye-tracking control unit to the PC running the SOS scenario in Presentation via a serial connection. As the SOS scenario initializes, it opens the coordinate file generated by the eye calibration scenario discussed previously. The coordinates in the file are read and parameters for a transform matrix are calculated. The transform is used in the real-time mapping from ASL coordinate space to Presentation display space which is specified at a resolution of 1024 × 768 (XGA). The visual screen is divided into active stimuli locations and dead space (Figure 4-7). Gaze coordinates are continually monitored and a pink border is placed around the stimulus location when a participant's gaze falls in the specified area of the screen containing the object or word. The border highlighting of an array location gives feedback to the participant to confirm that eye tracking is working accurately and the selected stimulus matches the desired stimulus. An array location remains active (pink highlight) until a participant's gaze falls into a different stimulus area, not when gaze

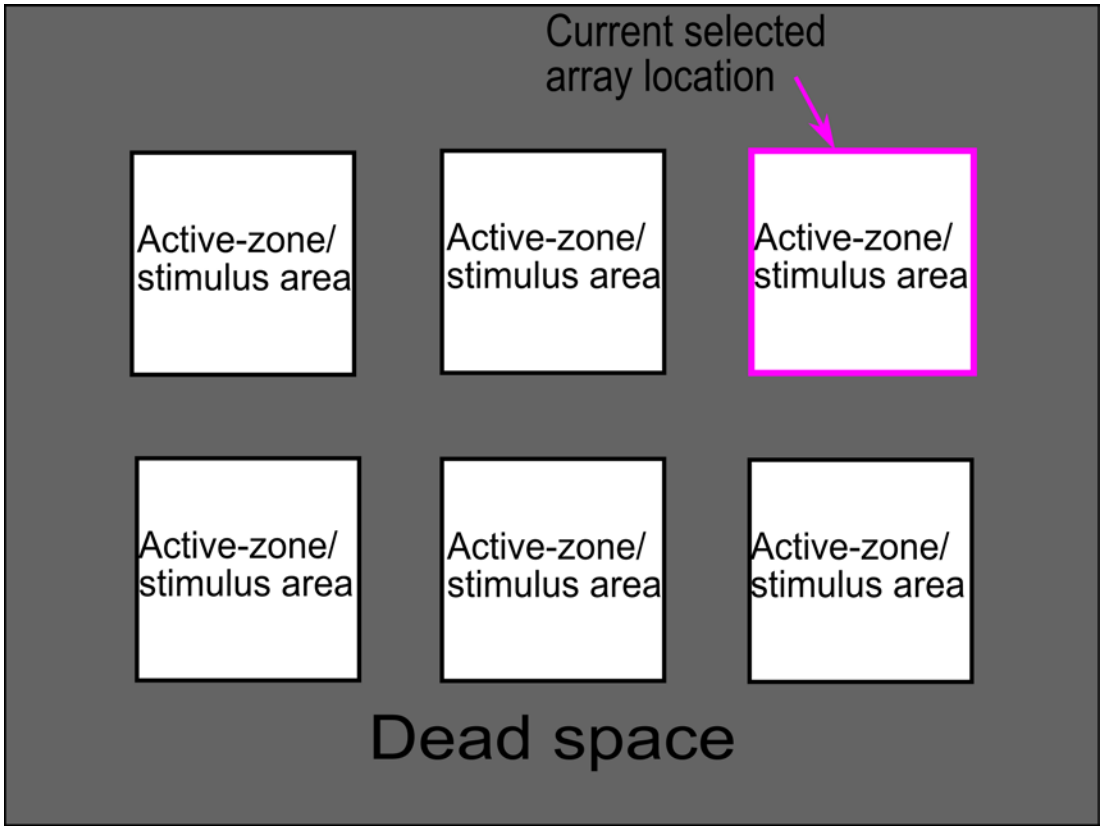

Figure 4-7. Layout of the 6-word (or 5-object) SOS task. An array location stays selected until participant's gaze enters a new active-zone. A pink square highlighted the current selected stimulus for participant feedback. Stimulus areas were 210 × 210 pixels for 6-words, 200 × 200 pixels for 9-words, and 190 × 190 pixels for 12-words. Screen resolution was 1024 × 768.

enters dead space. Selection of an object or word is made by squeezing the pneumatic bulb. The border color is changed to blue and the scenario pauses for 1500 ms, during which eye-tracking coordinates and additional squeeze-bulb responses are ignored.

The SOS task was implemented using a mixture of SDL and PCL code in Presentation (Appendix B). The SDL section defines all of the SOS stimuli, along with additional text objects. Top-level picture objects are specified for each level of the SOS task (2 × 3, 3 × 3, 4 × 3) to define stimuli placement during the task. Each position in the 2D array is surrounded by a border that will change colors for participant feedback during the task as previously mentioned. Three simple trials are defined to handle an initial period of fixation and presentation of instructions for both the control tasks and working memory tasks. The majority of SOS code was written in PCL and is built around multi-dimensional arrays that define parameters of each task level, as PCL does not implement data structures. During initialization the PCL code performs several important operations such as: calculating our coordinate transform, establishing a connection with the ASL control unit, and opening various log files for recording performance data and debugging information. When the SOS scenario receives the first pulse from the MRI a fixation screen is displayed for 10 seconds. Following fixation, we enter control/task pair blocks.

An important part of the SOS task is that stimuli rearrange after a selection has been made. Rearranging stimuli positions was implemented differently in the object and verbal versions of the SOS. For the verbal version, new placements were chosen randomly by executing the *shuffle()* function on an array that contains location indices. The object SOS has an additional requirement that the blank square be placed at the last selected position. To accomplish this, we set the black square to each location in the array

and generated 3 permutations of stimuli locations for the object stimuli. The permutations are stored in a multi-dimensional array. Upon participant selection of a location, one of the three permutations for the selected location was randomly chosen for the next trial.

For testing outside of the fMRI setting, a mouse-based version was created. The participant selects a stimulus by point-and-click. For the fMRI exam we introduced a 10 minute timer. If the participant has not finished the task at the end of the 10 minutes, the program exits and the MRI-scanner is stopped.

Behaviorally modified design matrices

As discussed in Chapter 3, fMRI task designs tend to follow a block design or event-related design. The self-ordered search task is a behaviorally driven task, i.e., progression through the task is based on fulfilling some condition (selecting a proper stimulus) rather than reaching a fixed time limit of a certain condition. We introduce a variant of the standard block design, which we term *behaviorally modified block design*. A behaviorally driven task design preserves an important behavioral measure (time to completion) at the cost of complicating fMRI analysis. We extract timing variables (start time & duration of each condition) for each participant by parsing log files generated by the SOS scenario code. This was performed automatically during the batch processing by a combination of Matlab functions and the Linux/Unix scripting tools Bash, Sed and Awk (Appendix D). The statistical power for each individual's analysis varies, resulting in an unbalanced design. However, group analysis is still valid for sufficiently similar design matrices [Friston et al., 2007].

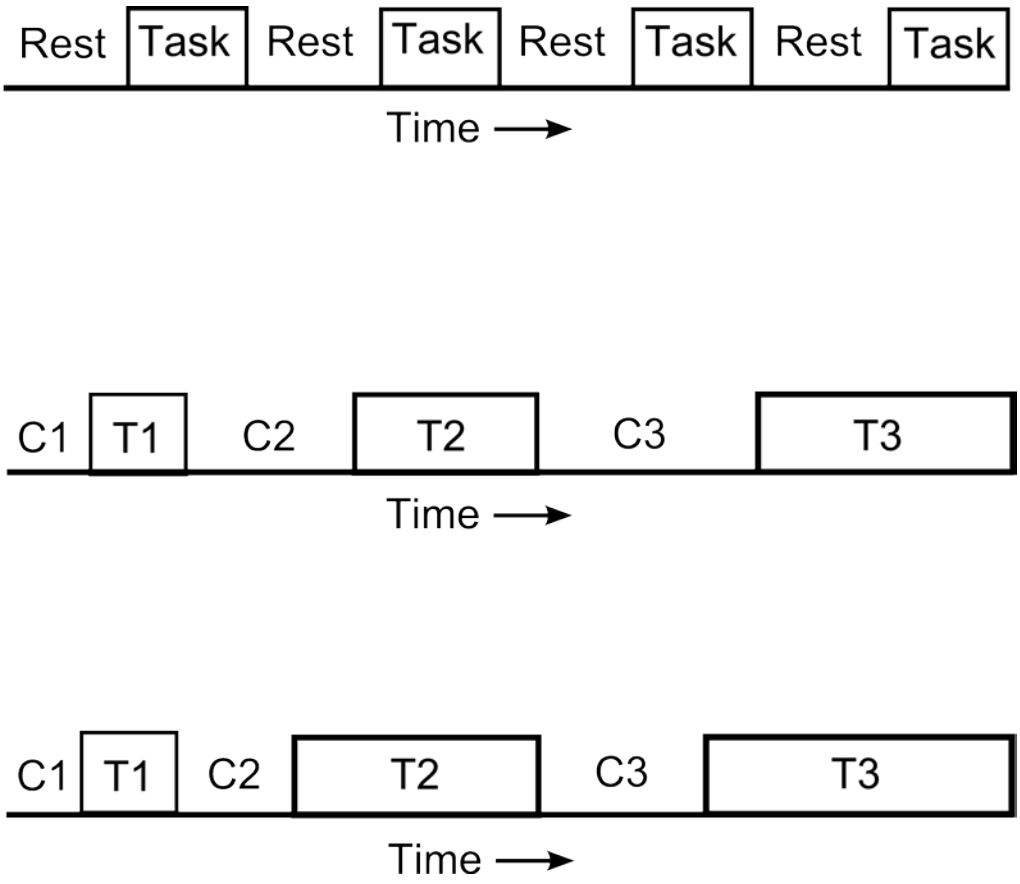

Figure 4-8 Behavioral modified block design for fMRI. A typical block design (top) consists of alternating epochs of fixed duration. Blocks of a behavioral modified block design (middle and bottom) will have different durations based on individual performance. Control conditions (e.g. Rest) are denoted by C. Task conditions are denoted by T.

Functional-MRI Image Acquisition

Functional images of the whole brain were acquired using a T2*-weighted Echo Planar Imaging (EPI) pulse sequence commonly chosen for fMRI and used in our previous studies [Ogg et al., 2008; Barb et al., 2010]. The EPI sequence was set up on the Siemens 3T Trio MRI scanner with the following parameters: field of view (FOV) = 192 mm; matrix = 64 × 64; slices = 32; slice thickness = 5 mm; TR = 2.06 s, TE = 30 ms. The resulting resolution in-plane is 3 mm × 3 mm. Bandwidth was 1953 Hz/pixel. Slices were acquired in planes parallel to the anterior and posterior commissures (AC-PC line) in subjects' brains.

All subjects participated in a video-based orientation and training program prior to the fMRI experiment. The material familiarized the subjects with the sights, sounds, and activities they would soon be experiencing during the fMRI session. The training also provided practice of the N-back and SOS tasks to ensure directions and expectations were understood. The practice effects of N-Back and SOS tasks are generally thought to have little impact on performance. All healthy volunteers and St. Jude patients received additional anatomic imaging to identify morphologic abnormalities (volunteers), or as part of routine protocol examination (patients). These images facilitate spatial normalization of brain images and visualization of functional imaging results.

Functional participants' heads were padded in the head-coil to restrict movement during imaging. In certain instances, subjects were placed slightly off-center in the head-coil to get an unobstructed view of the right eye. They were given a set of MR-compatible head-phones through which the examiner could deliver instructions before a

task and check on an individual's comfort level over the duration of the exam. The options of additional ear-plugs, blankets and padding were also made available.

SPM5

SPM5 is a freely available collection of Matlab (www.mathworks.com) scripts and compiled C code designed for the analysis of functional neuroimaging data. SPM is developed and distributed by the Functional Imaging Laboratory, Wellcome Trust Centre for Neuroimaging at University College London (http://www.fil.ion.ucl.ac.uk/spm/). SPM5 contains all the necessary methods for preprocessing and model driven statistical analysis of fMRI data. SPM5 is open source code, allowing modification and customization of processes to fit experimental specific requirements.

Functional data for this project were preprocessed using SPM5. Preprocessing included realignment using a 6-parameter rigid-body transform, spatial normalization to the Montreal Neurological Institute brain template [Mazziotta et al., 1995], and spatial smoothing using a Gaussian kernel (FWHM = 8mm). Preprocessed functional images were analyzed in SPM5 using a 2-level design as described previously. The first level consists of a fixed-effect general linear model analysis for each subject. Design matrices were created to model task conditions. For the SOS, behaviorally modified design matrices were generated as discussed above. The N-back model consists of the 0-back, 1-back, 2-back, and instructions conditions for both verbal and object versions. Activity for a specific condition is represented as a box-car function convolved with the canonical hemodynamic response function. After parameter estimation, contrast images were generated and used as variables in a 2^{nd}-level random effects analysis to identify group

patterns of activation and areas in which brain activity is related to behavioral performance.

GIFT

The Group ICA of fMRI Toolbox (GIFT) is a freely available software package designed for independent component analysis of fMRI data. GIFT is developed and distributed by Medical Image Analysis (MIA) Laboratory, University of New Mexico (mialab.mrn.org). Like SPM5, GIFT is a collection of open source Matlab scripts and compiled C code that allows for modification and customization of processes. GIFT implements data reduction processes and a number of different algorithms necessary for ICA of fMRI data.

For this project, data reduction was performed in 2 steps. Initially, individual subjects' time series were reduced to 50 temporal components via PCA. The individual results were then concatenated and reduced again to the estimated number of components. The number of estimated components was chosen by taking the mean of MDL estimation of every individual's data set. The entropy based Infomax algorithm was used for ICA analysis. The resulting independent components were scaled to Z-scores.

Chapter 5: SOS Validation in a Group of Healthy Individuals

Introduction

A group of healthy volunteers participated in a pilot study approved by the St. Jude Children's Research Hospital Institutional Review Board (IRB) called EXFXN2. The objectives of EXFXN2 were to investigate the feasibility and utility of the SOS as a measure of working memory in fMRI and establish and validate the neural correlates of the SOS task in healthy young adults.

Subjects

Participants from the local community were recruited through IRB approved advertisements posted in the St. Jude Today and newsletters of local universities. Written informed consent was given by each subject before testing. All volunteers were right-handed, between the age of 18-30, and had English as their primary language. Individuals were also excluded based on the following criteria:

- Significant impairment in global intellectual functioning (operationalized as a history of special education in a self-contained classroom)
- History of documented CNS injury or disease
- History of documented Attention Deficit Hyperactivity Disorder (must have been diagnosed by a physician with medication prescribed)
- History of a documented learning disability
- History of mental illness diagnosed by a psychiatrist or psychologist that is known to be associated with structural or functional brain changes (e.g., schizophrenia, obsessive-compulsive disorder)

- Treatment with psychostimulant or psychotropic medication within two weeks of study enrollment
- History of treatment for alcohol or substance abuse
- Sensory or motor impairment that would preclude valid cognitive testing

Inside- versus outside-MRI

Each participant performed the N-back and SOS tasks both in an fMRI setting and a typical clinical setting. In the fMRI setting, the SOS task used the eye-tracking/squeeze-bulb interface. The SOS in the clinical setting used a typical computer-mouse point-and-click interface. The order of tasks (SOS and N-back) and setting (inside/outside) were randomized. Statistical analysis was performed on the behavioral data to test for any effects of setting and task order on performance.

Additional Neuropsychological Testing

Assessment of neuropsychological abilities was derived from the Wechsler Abbreviated Scale of Intelligence (WASI) [Wechsler 1999a] and the Wechsler Digit Span task [Wechsler 1999b]. The WASI is an estimate of full-scale IQ. The digit span task is a measure of attention and working memory ability in particular. The scores from these tests were used as behavioral correlates in the fMRI analysis.

Functional-MRI Analysis

Functional data were acquired and preprocessed according to the methods discussed in Chapter 4.

Modeling the SOS

Both SOS task variants (object and verbal) were modeled with 7 conditions (Figure 5-1). Each condition was represented by a box-car function convolved with the

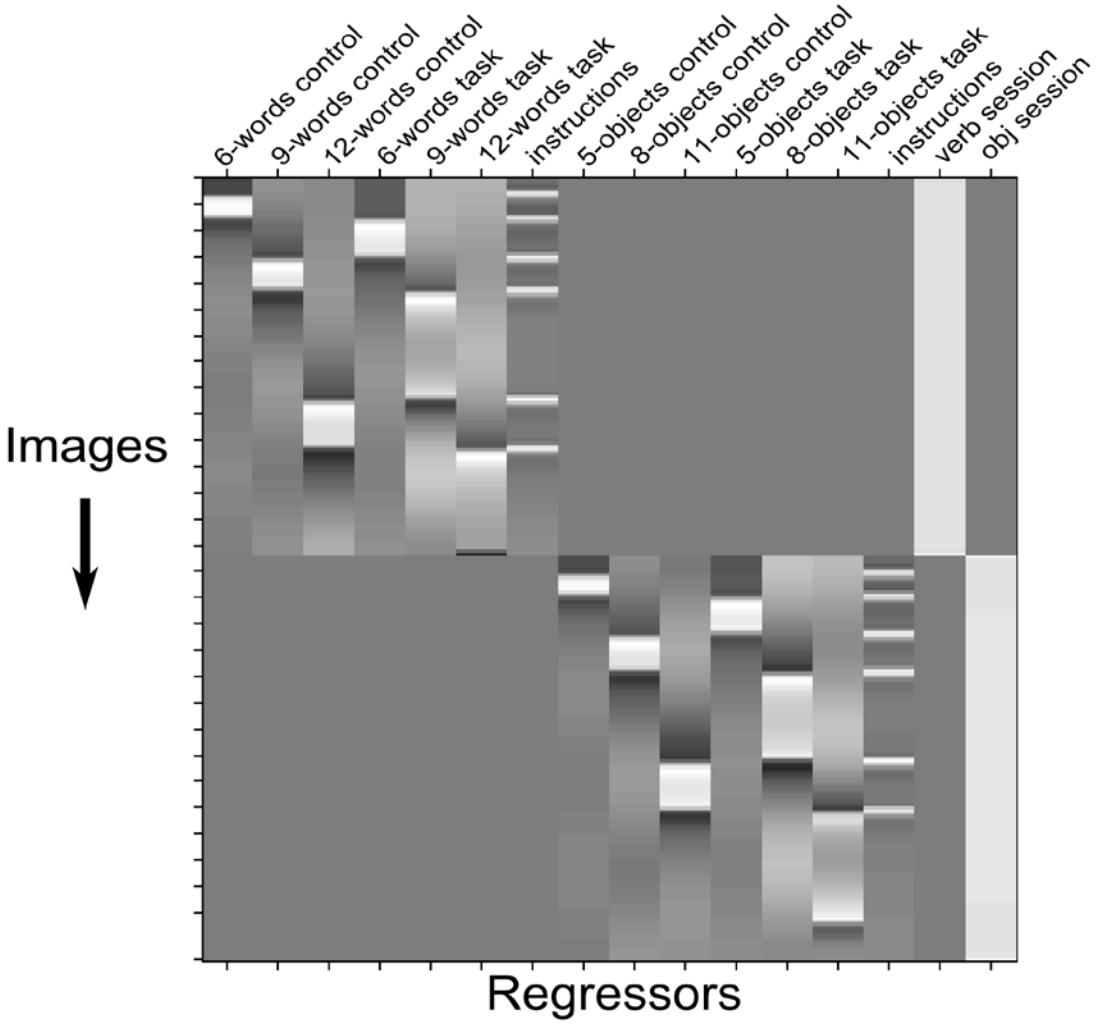

Figure 5-1. Modeling the SOS task. The model contains 7 regressors for each variant (verbal and object) of the task that include separated control-tasks, WM-tasks and instruction conditions. Regressors are represented by box-car functions convolved with the canonical hemodynamic response function. The duration of each condition is determined by individual performance.

canonical hemodynamic response function. The 7 conditions for the verbal task were: the 6-word control task, 6-word task, 9-word control task, 9-word task, 12-word control task, 12-word task, and presentation of the instruction screen. The 5-, 8- and 11-object conditions in the object-SOS were modeled similarly. The duration of each condition was determined by behavioral performance of each individual and extracted from the SOS logfiles generated by the Presentation stimulus delivery software. Functional data from both object and verbal sessions were concatenated in order to examine difference in activation between verbal and object tasks.

Modeling the N-back

The object and verbal N-back tasks were modeled (Figure 5-2) with 4 conditions as described above. The regressors represented the 0-back, 1-back, 2-back conditions and instruction screens. As with the SOS, the verbal and object N-back sessions were concatenated to investigate differences in activation due to the different stimuli.

Functional-MRI Fixed Effect Analysis

Functional-MRI data from each participant were entered into a 1st-level, fixed effect analysis. Fixed-effect analysis was performed in SPM5 using the GLM with the SOS and N-back models as design matrices. After parameter estimation, contrast images were generated to investigate activation effects between different task conditions. Contrasts for the SOS included, but were not limited to: mean task activation, 9-word task > 6-word task, 12-word task > 9-word task, object task > verbal task, etc… N-back contrasts included, but were not limited to: 1-back > 0-back, 2-back > 1-back and object > verbal.

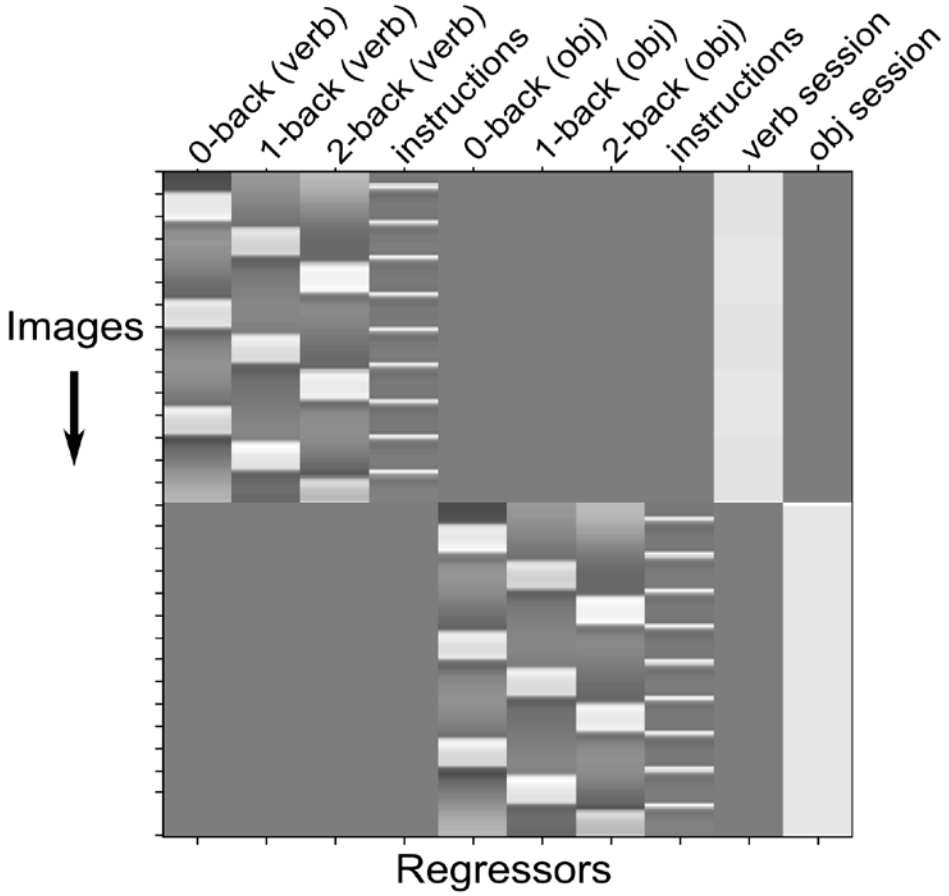

Figure 5-2. Modeling the N-back task. The model contains 4 regressors for each variant (verbal and object) of the task that include: 0-, 1-, 2-back and instruction conditions. Regressors are represented by box-car functions convolved with the canonical hemodynamic response function.

Functional-MRI Random Effects Analysis

Contrast images for each participant were entered as variables in a random effects analysis to identify areas in which brain activity is related to behavioral performance. A random effects analysis was also used to compare activation during the SOS and N-back tasks. Clusters of activation were summarized by location, statistical significance and number of voxels.

Independent Component Analysis

ICA was performed using the GIFT toolbox for Matlab. ICA analyses were performed on the N-back and SOS data separately and combined. The number of estimated components was chosen by taking the mean of MDL estimation of every individual's data set. Components of interested were selected by inspection and entered into random effects analysis.

Statistical analysis of behavioral data

The effect of setting on performance and the relationships between behavioral measures were investigated using both T-tests and a linear mixed-effects model. For the mixed-effects model gender and setting were entered as fixed-effects. Random-effects included age, raw Digit Span score, IQ. Separate models were created to investigate SOS performance (combined, verbal, object; time to completion and trials to completion) and N-back performance (combined, verbal, object; reaction time, omissions, commissions and combined error-rate).

Results

Forty-five individuals between 18 – 30 years of age were recruited to obtain 25 complete data sets free of exclusionary incidental findings. Twenty participants were

replaced due to log data over written (N = 1), poor brain coverage during imaging (N = 4), exclusionary or medically significant findings (N = 7), difficulties with eye-tracking equipment (N = 4), or poor-tracking (N = 4). Demographic data and neuropsychological testing results of the final 25 healthy participants (age: 25.2, 18.11 – 30.51; IQ: 120.12, stdev = 7.3) are listed in Table 5-1.

N-back

Figure 5-3 shows the mean pattern of activation for the combined verbal and object N-back task ($p < 0.05$, FWE corrected for multiple comparison). Task activation was robust and included the dorsolateral PFC, ventral PFC, dorsal cingulate, frontal poles, parietal, ventral visual and cerebellar areas (Table 5-2). Activation maps were generated for verbal and object conditions separately (Figures 5-4 and 5-5, Tables 5-3). Activation in the DLPFC, parietal, dorsal cingulate and lateral premotor areas increased with WM load (Figure 5-6). Bilateral activation in the ventral PFC region was detected only in the high demand 2-back condition. No significant differences between verbal and object versions of the N-back were detected. Figure 5-7 shows areas of brain that experience greater activation in the control condition (i.e.: 0-back > 1- and 2-back).

The mean MDL for the functional data was calculated to be 32. The mean value was used in all ICA analyses. Resulting spatial maps and associated time courses are shown in Figure 5-8. Of the 32 extracted components, 4 exhibited WM task related signal changes that are consistent with the GLM analysis (Figure 5-9). These four networks include the left and right executive networks [Cole et al., 2010] (components 16 and 18), a component containing bilateral DLPFC (component 8) and a component containing the ventral PFC, dorsal cingulate and lateral premotor areas (component 21). Components of

Table 5-1. Demographic data and neuropsychological testing results for EXFXN2 healthy participants.

ID #	Gender	Race	Age	Estimated IQ	Total Digit Span Raw
1	Female	White	29.7	119	19
2	Female	White	25.8	120	15
3	Female	White	30.5	125	24
4	Male	White	26.3	108	21
5	Female	White	28.7	121	19
6	Female	White	23.8	125	23
7	Male	White	27.0	129	18
8	Male	White	30.3	123	23
9	Female	Black	30.0	121	24
10	Male	White	19.2	125	21
11	Male	White	23.7	134	23
12	Male	White	26.3	126	21
13	Female	White	18.8	119	20
14	Female	White	27.9	122	19
15	Male	White	20.1	101	23
16	Male	White	28.7	123	16
17	Male	White	24.5	121	23
18	Female	White	26.8	124	19
19	Female	White	18.1	120	17
20	Male	White	27.4	128	23
21	Female	White	25.0	117	18
22	Male	White	24.3	115	16
23	Female	White	28.0	111	23
24	Male	White	21.2	107	21
25	Female	White	23.0	119	16
Mean			25.42	120.12	20.2
StDev			3.71	7.32	2.83
Max			30.5	134	24
Min			18.1	101	15

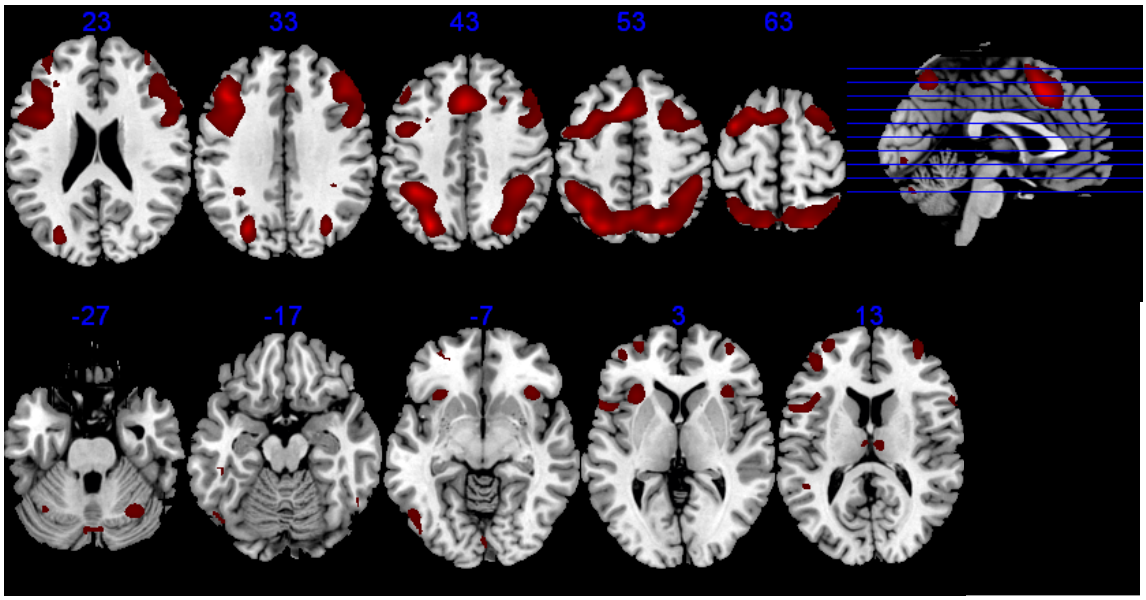

Figure 5-3. Pattern of mean activation in the N-back task in a group of 25 healthy young adults. Panel shows random effects group analysis ($p < 0.05$, FWE corrected for multiple comparisons).

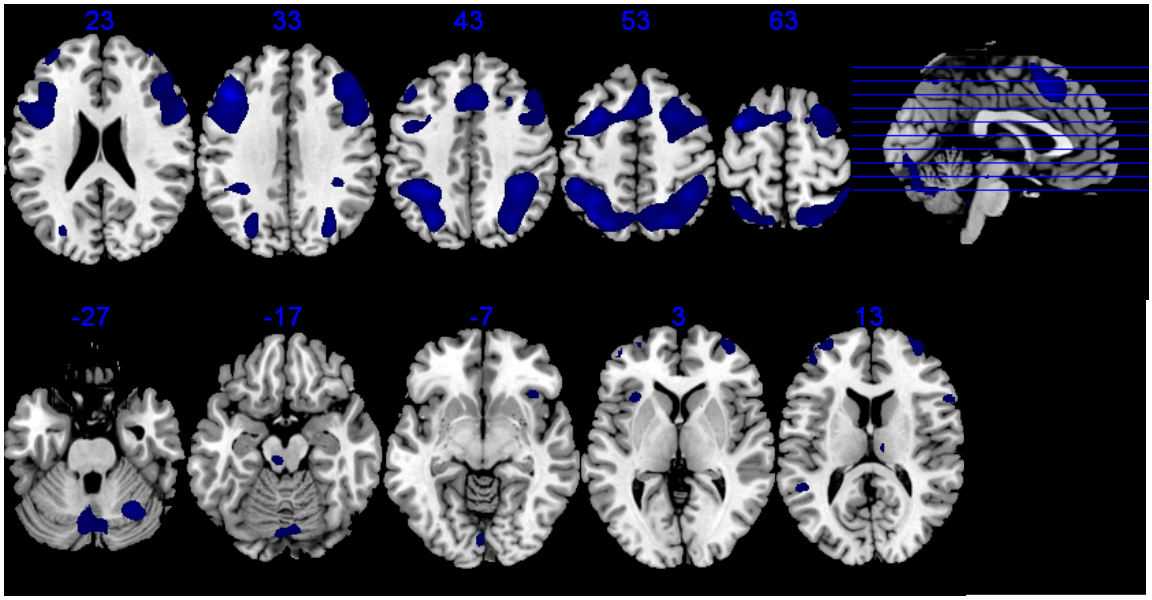

Figure 5-4. Pattern of mean activation in the N-back verbal task in a group of 25 healthy young adults. Panel shows random effects group analysis ($p < 0.05$, FWE corrected for multiple comparisons).

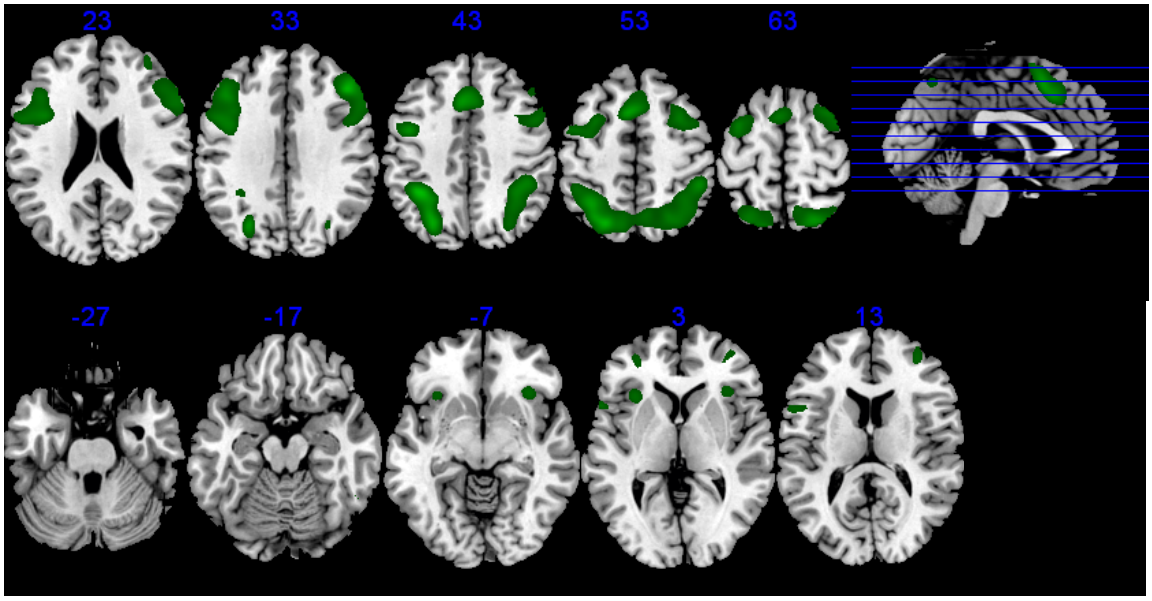

Figure 5-5. Pattern of mean activation in the N-back object task in a group of 25 healthy young adults. Panel shows random effects group analysis ($p < 0.05$, FWE corrected for multiple comparisons).

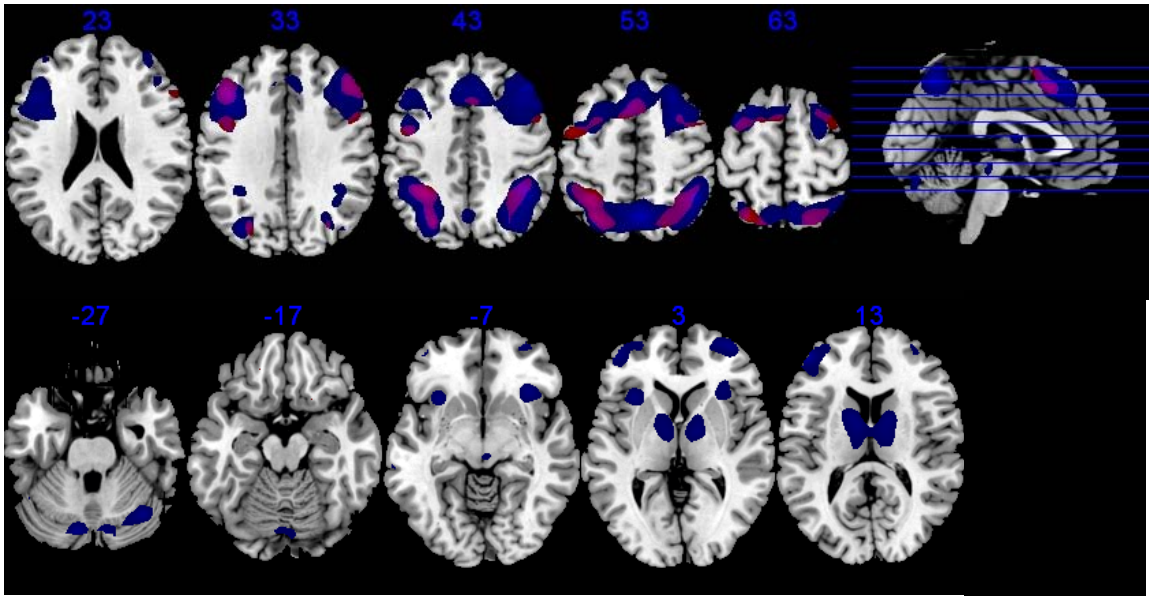

Figure 5-6. Pattern of parametric activation in the N-back task in a group of 25 healthy young adults. Panel shows random effects group analysis ($p < 0.05$, FWE corrected for multiple comparisons). Red denotes the contrast 1-back > 0-back while blue denotes the contrast 2-back > 1-back. Activation in the right frontal-parietal network increased linearly with working memory load, while activation in the bilateral ventral prefrontal area was detected only in the high-load 2-back condition.

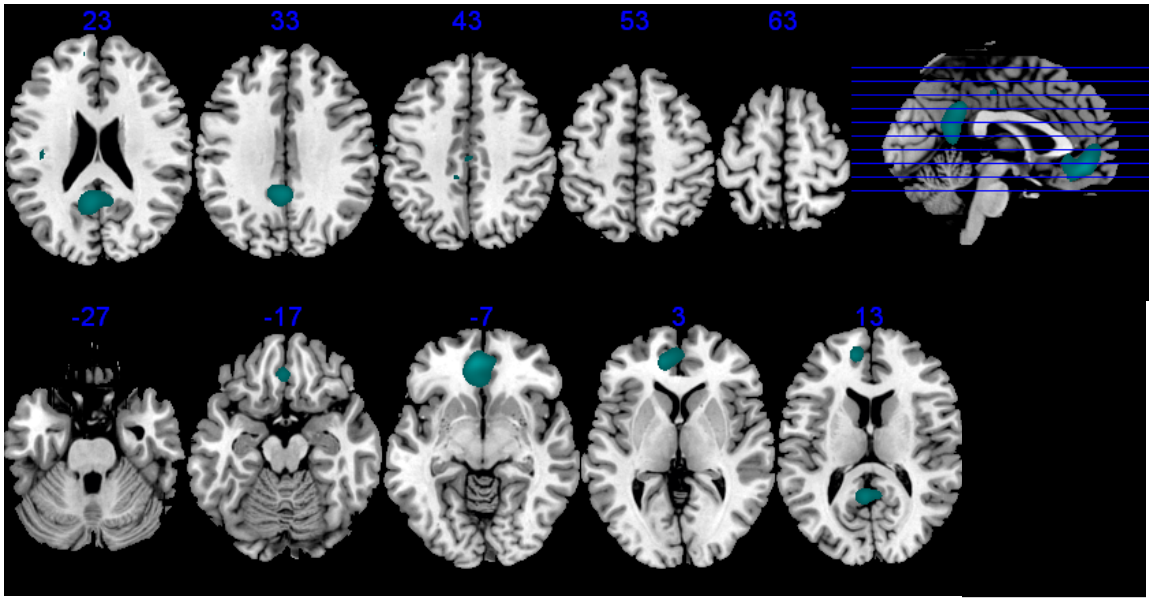

Figure 5-7. Pattern of negative activation in the N-back task in a group of 25 healthy young adults. Panel shows random effects group analysis ($p < 0.05$, FWE corrected for multiple comparisons).

interest were identified by inspection. Four components exhibit a signal change inversely related to the task demand that included: frontal medial (component 4), medial motor cortex/cingulate (component 7), temporal poles (component 15), and auditory cortex (component 14). Component 5 corresponds to anterior visual cortex and spikes in relation to the presentation of instruction screens before each task block. The Default Mode network loaded onto 3 components (medial frontal dominant, 4; retrosplenial dominant, 24; parietal dominant, 31) with the retrosplenial activation peaking during the 5 second rest before each task block. Two-sample T-tests revealed no significant differences in component maps between verbal and object N-back. Random-effects analysis revealed no areas that demonstrated significant changes in coherence associated to behavioral variables.

Table 5-2. Clusters of positive activation during the N-back task for a group of 25 healthy young adults. Coordinates are given in MNI space. Positive X denotes right hemisphere.

Area	**X**	**Y**	**Z**	**T-value**
N-back (Verbal and Object)				
Dorsolateral PFC	44	30	30	14.76
	-44	28	32	13.23
Ventral PFC	34	24	-4	9.44
	-32	20	0	10.14
Dorsal cingulate	-4	14	50	16.22
Lateral premotor	-32	4	60	15.10
	30	12	60	10.53
Parietal	-26	70	44	19.89
	24	-66	58	13.68
Frontal pole	36	54	8	8.72
	-28	52	-4	7.73
Ventral visual	-50	-66	-12	8.55
	56	-54	-16	8.42
Cerebellum	28	-62	-34	9.87
	6	-78	-28	8.75
	-30	-62	-32	

Table 5-3. Clusters of positive activation during the N-back verbal and object task for a group of 25 healthy young adults. Coordinates are given in MNI space. Positive X denotes right hemisphere.

Area	**X**	**Y**	**Z**	**T-value**
N-back Verbal				
Dorsolateral PFC	44	32	30	14.38
	-44	28	32	13.72
Ventral PFC	-32	20	0	8.32
	34	24	-2	8.00
Dorsal cingulate	0	16	48	11.96
Lateral premotor	-30	6	58	15.83
	32	8	56	10.29
Parietal	-40	-44	46	16.49
Frontal pole	36	58	20	8.71
	-32	58	18	7.04
Ventral visual	-50	-66	-10	7.00
	58	-56	-14	8.17
Cerebellum	-28	-62	-32	9.91
	-6	-64	-28	8.87
	-30	-56	-34	8.35
N-back Object				
Dorsolateral PFC	-38	10	26	12.39
	36	28	32	11.44
Ventral PFC	-32	22	2	9.07
	34	24	-4	8.74
Dorsal cingulate	-4	12	54	12.81
Later premotor	-32	2	62	10.49
	30	12	60	8.88
Parietal	-32	-52	48	14.32
	26	-66	58	11.82
Frontal Pole	-30	54	-2	7.39

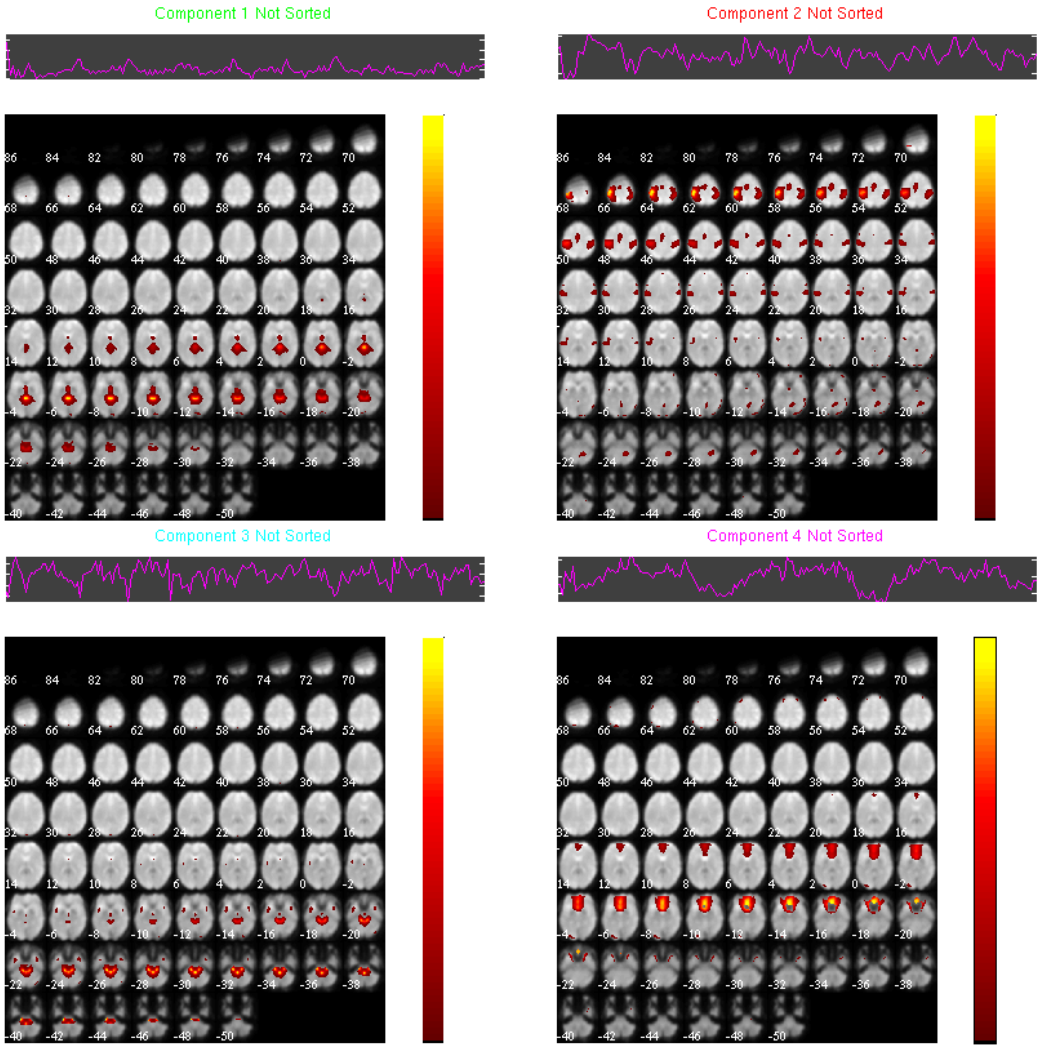

Figure 5-8. Spatially independent components extracted from the N-back task in a group of 25 healthy young adults. Panel shows spatial maps (z > 1) and associated time courses.

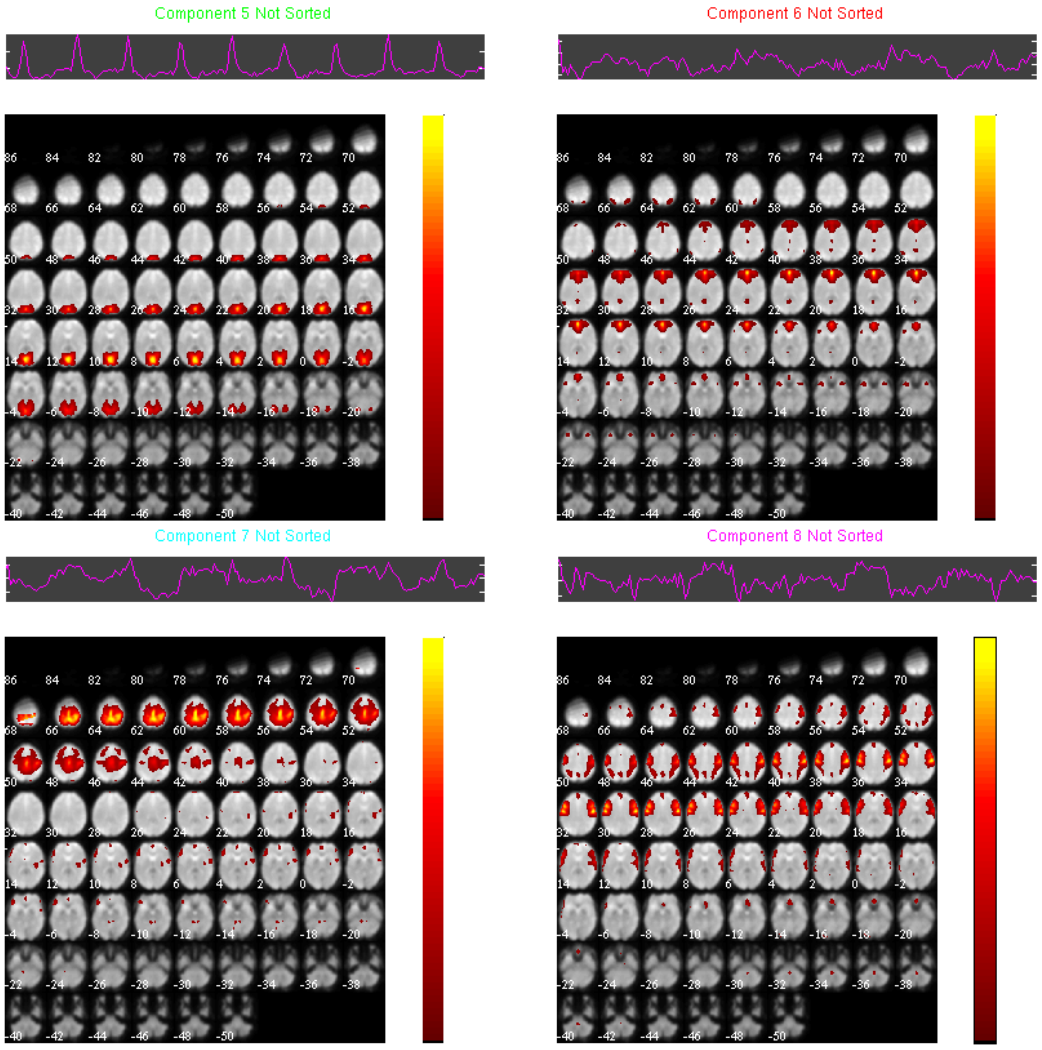

Figure 5-8 continued.

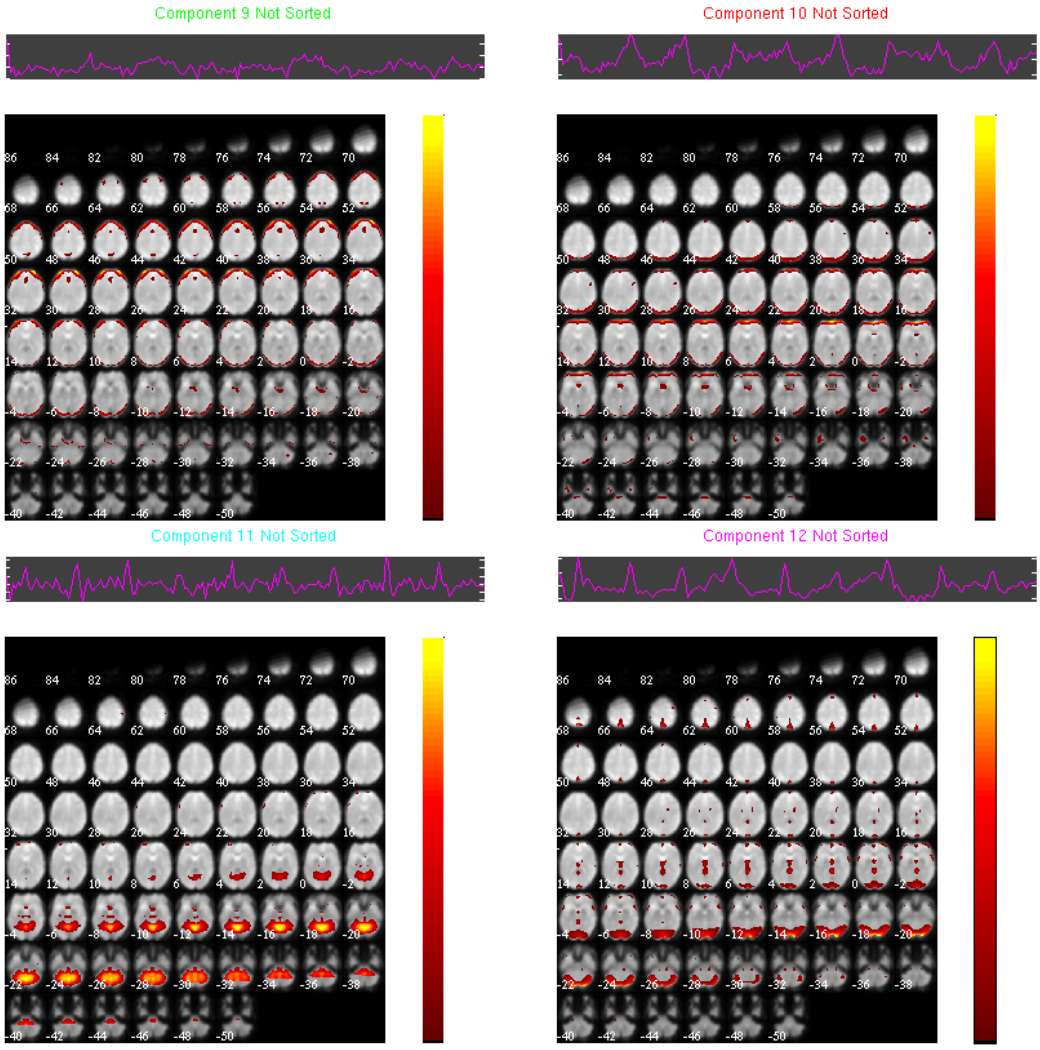

Figure 5-8 continued.

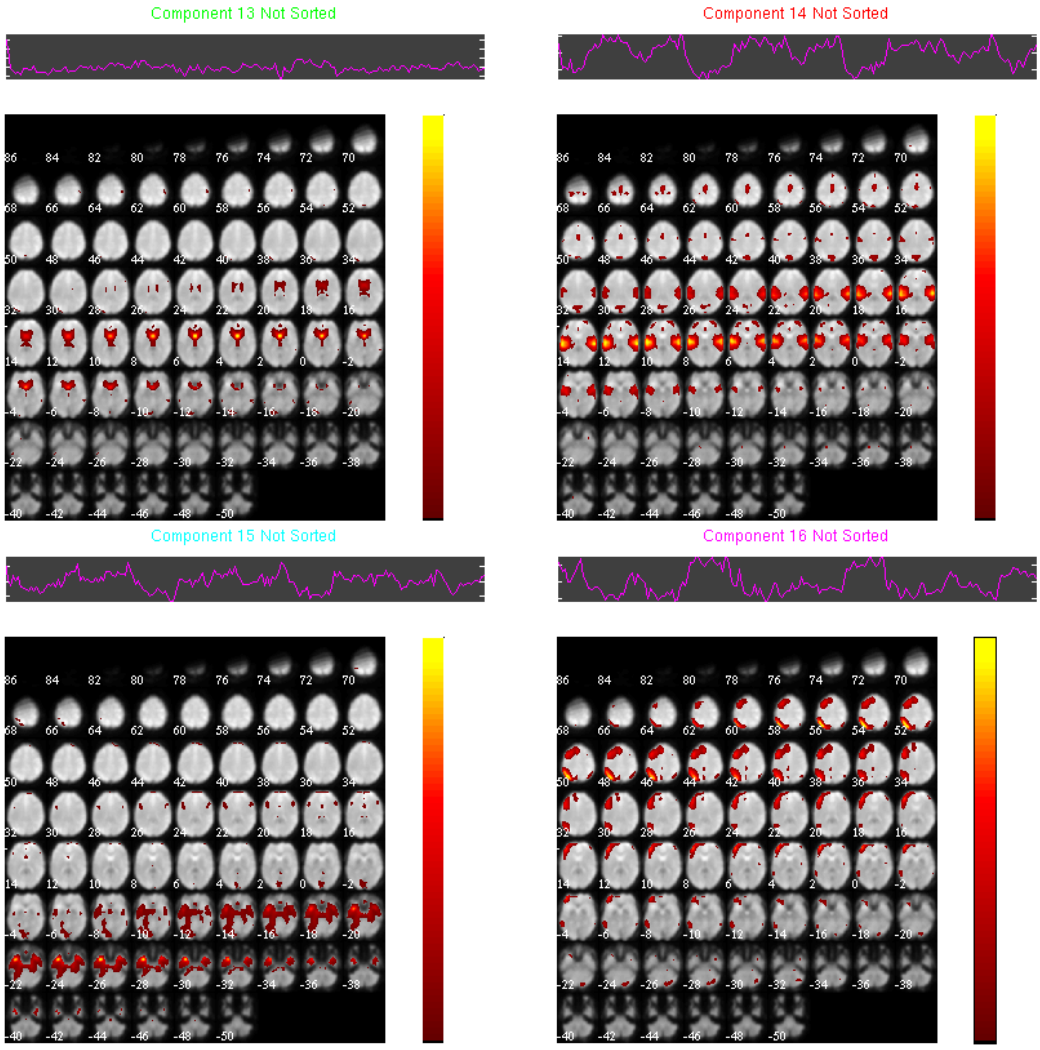

Figure 5-8 continued.

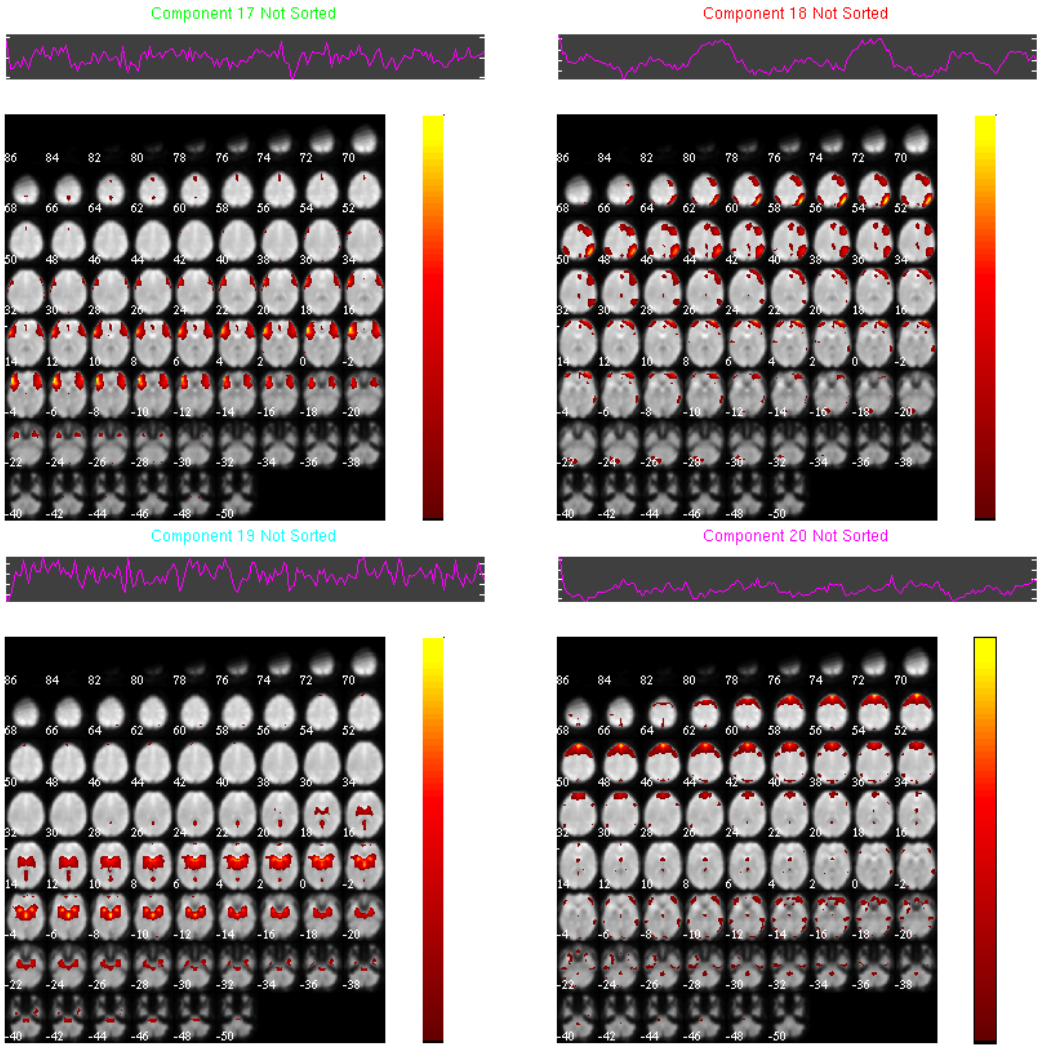

Figure 5-8 continued.

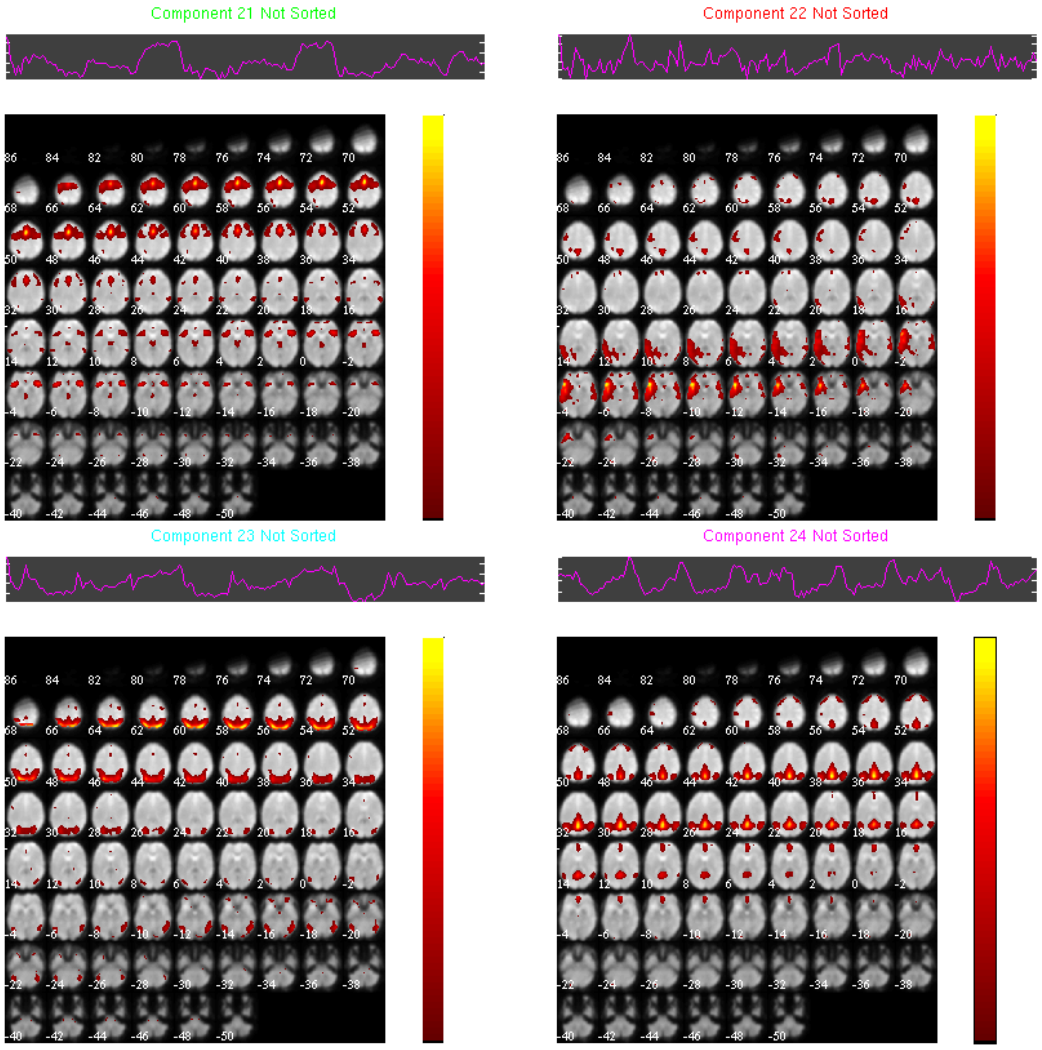

Figure 5-8 continued.

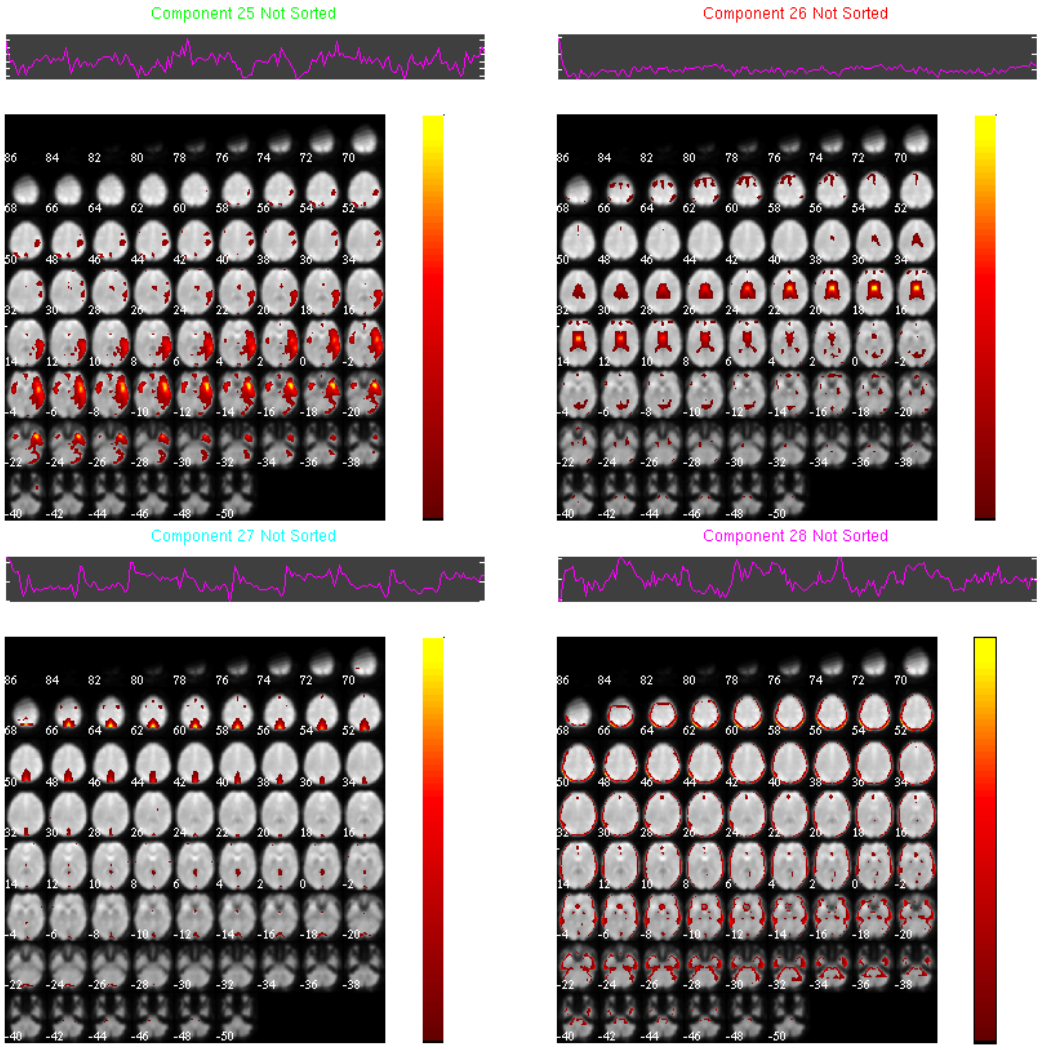

Figure 5-8 continued.

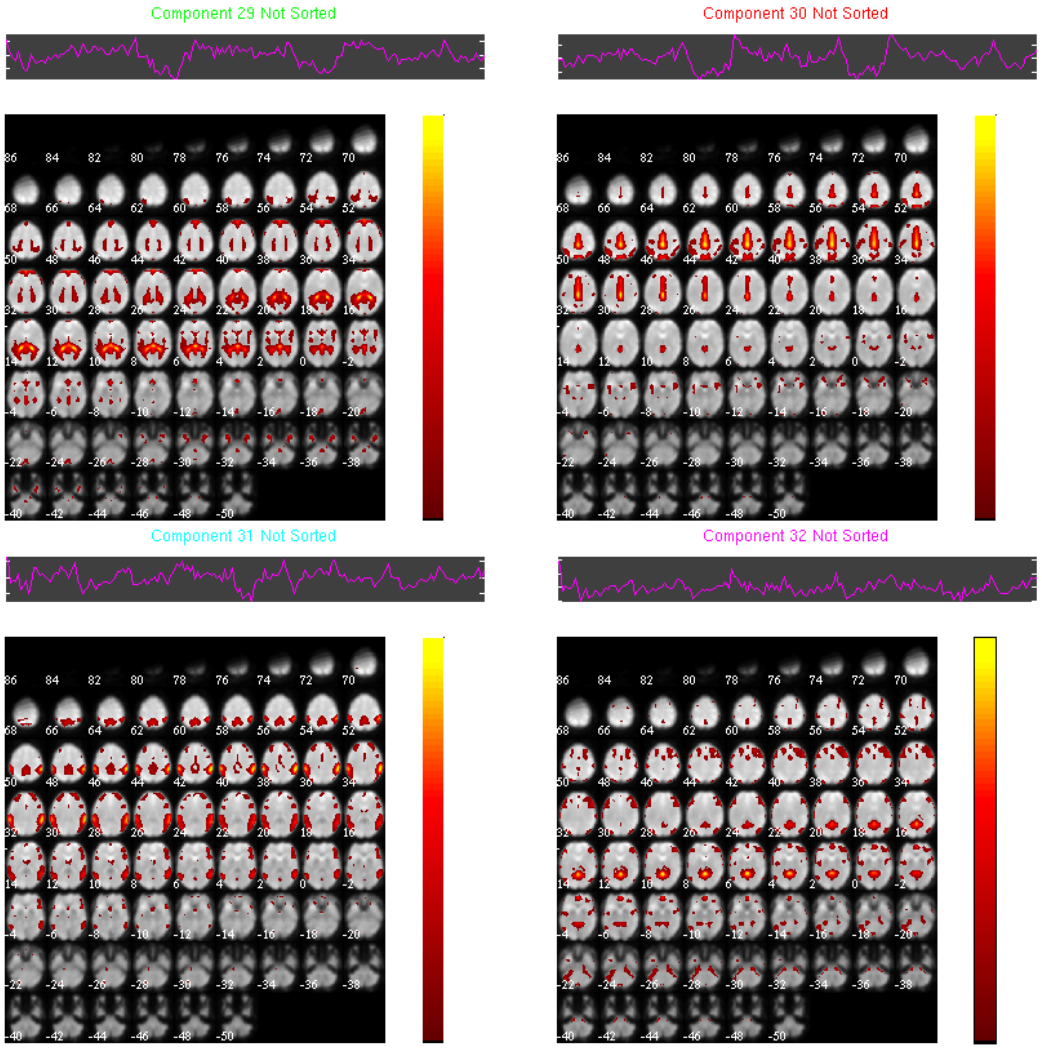

Figure 5-8 continued.

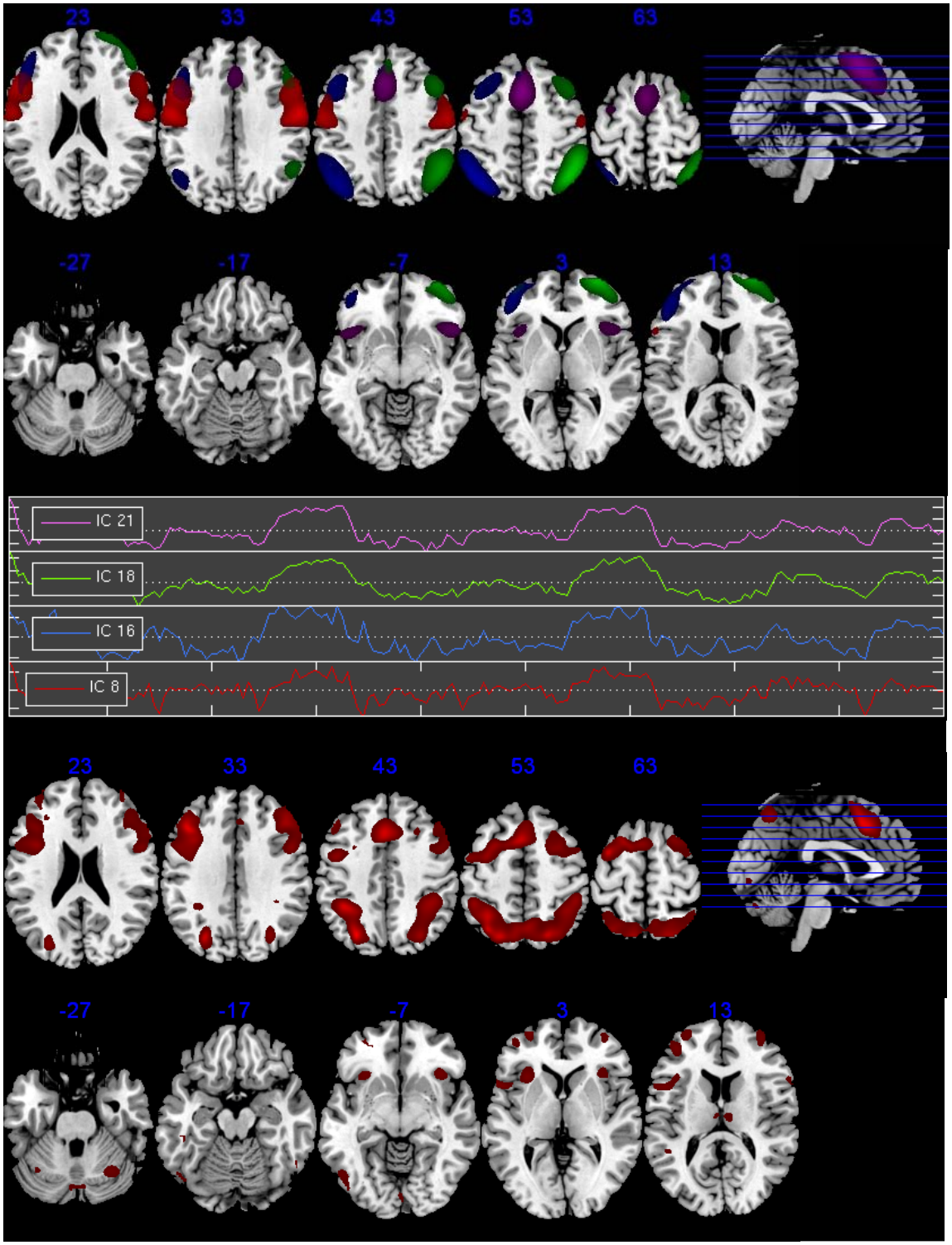

Figure 5-9. Consistency between ICA and GLM results. Top panel shows spatial maps (threshold: $z > 2$) of 4 independent components containing N-back task related time courses (middle panel). Spatial patterns are consistent with activation patterns in the lower panel that were identified by GLM analysis ($p < 0.05$, FWE corrected for multiple comparisons).

SOS

Table 5-9 contains the inside-MRI SOS performance of the study participants. The timing information was used to generate the design matrices for SOS fMRI analysis (Figure 5-10). Figure 5-11 shows the mean pattern of activation for the combined verbal and object SOS task ($p < 0.05$, FWE corrected for multiple comparisons). Task induced activation was present in the dorsolateral prefrontal cortex, ventral frontal, parietal, dorsal cingulate and lateral premotor areas (Table 5-4). Activation maps were also generated for the verbal and object tasks separately (Figures 5-12 and 5-13). For the verbal SOS, DLPFC and parietal activation are left lateralized. The object version of the SOS induces bilateral DLPFC and parietal activation, along with additional activation in the ventral visual system. No clusters were identified that exhibited activation related to performance, estimated IQ or age. Areas of brain that experience greater activation in the control condition (i.e.: control-task > WM-task) were similar to those in the N-back (Figure 5-14, Table 5-5).

ICA extracted 32 components. Task related components are not detectible by inspection due to the variability in task timing between individuals. However, ICA extracts the same networks identified in the N-back task (Figure 5-15) including: left and right executive networks, the bilateral DLPFC network, a network containing the ventral PFC with dorsal cingulate and lateral premotor, anterior visual cortex, and others. Two-sample T-test revealed no differences in components' spatial maps between verbal and object stimuli. Random effects analysis revealed no areas that demonstrated significant coherence changes associated with behavioral variables.

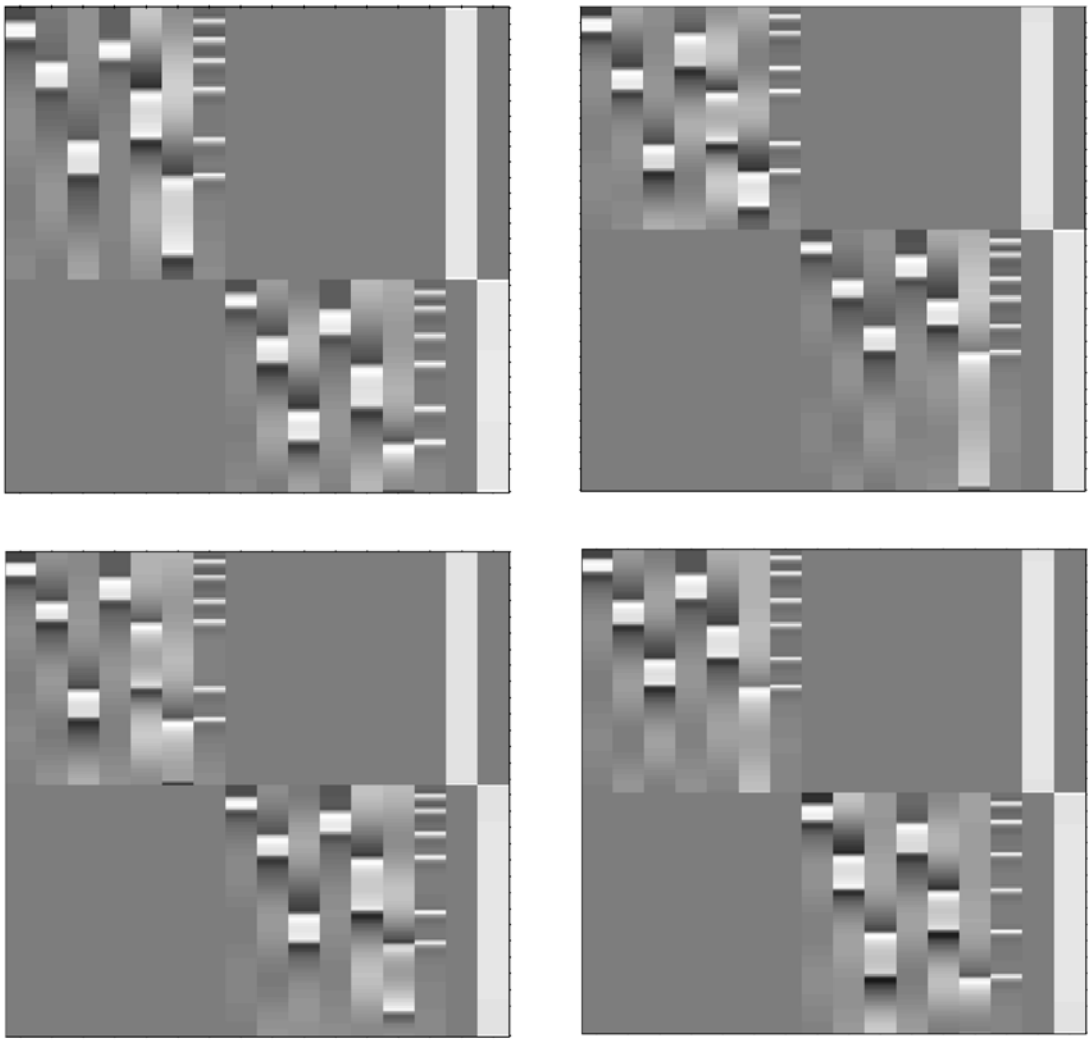

Figure 5-10. SOS behaviorally modified design matrices. Shown here are four representative design matrices for EXFXN2 participants.

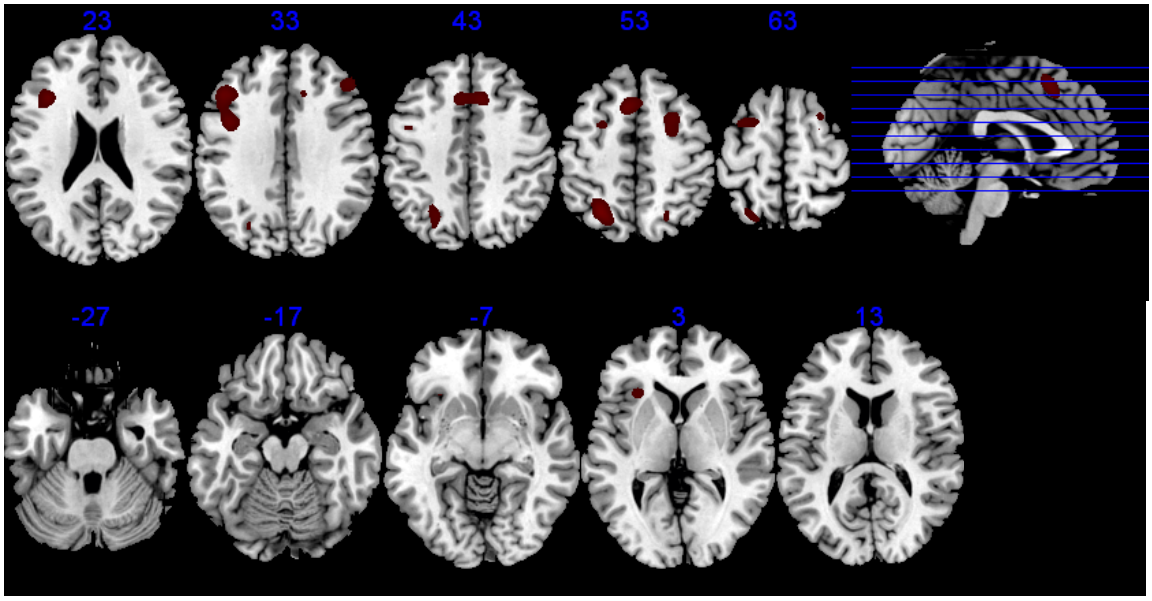

Figure 5-11. Pattern of mean activation in the SOS task in a group of 25 healthy young adults. Panel shows random effects group analysis ($p < 0.05$, FWE corrected for multiple comparisons).

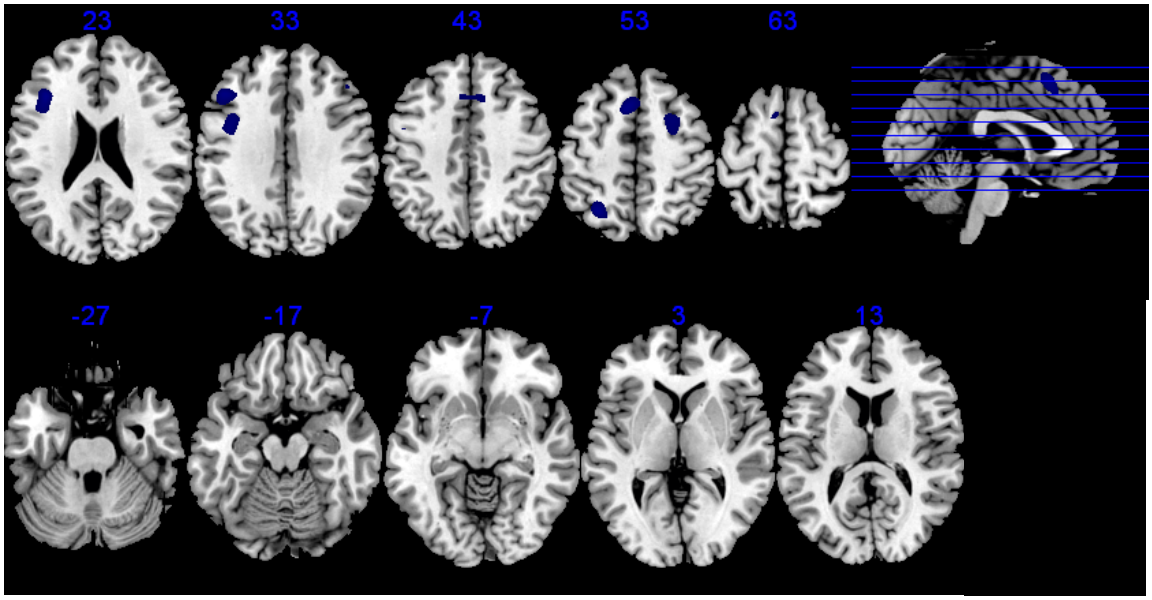

Figure 5-12. Pattern of mean activation in the SOS verbal task in a group of 25 healthy young adults. Panel shows random effects group analysis ($p < 0.05$, FWE corrected for multiple comparisons).

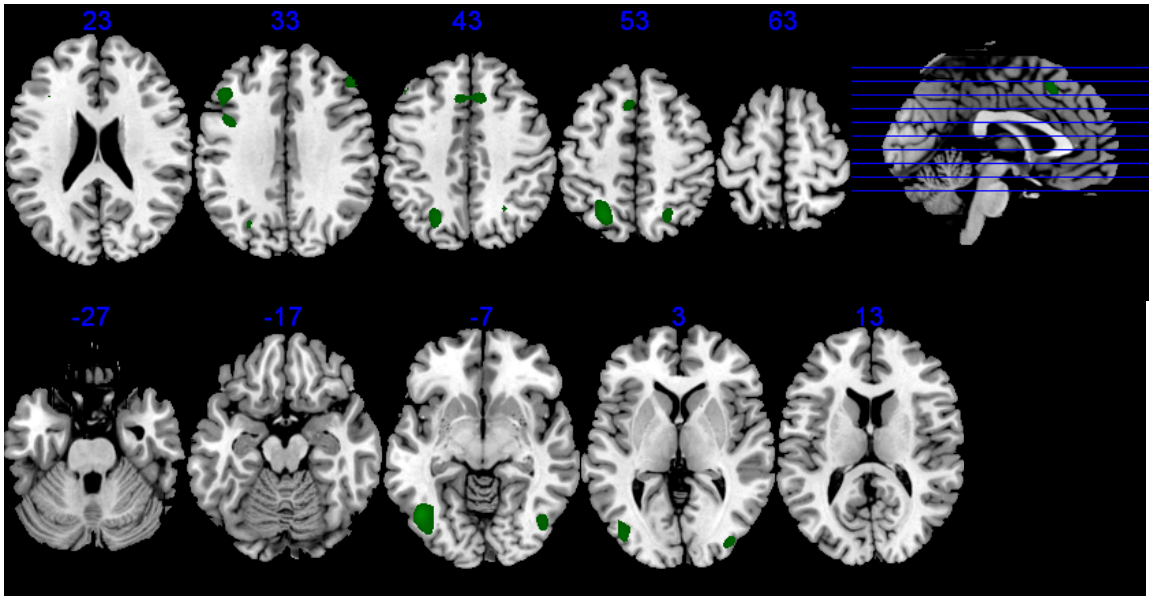

Figure 5-13. Pattern of mean activation in the SOS object task in a group of 25 healthy young adults. Panel shows random effects group analysis ($p < 0.05$, FWE corrected for multiple comparisons).

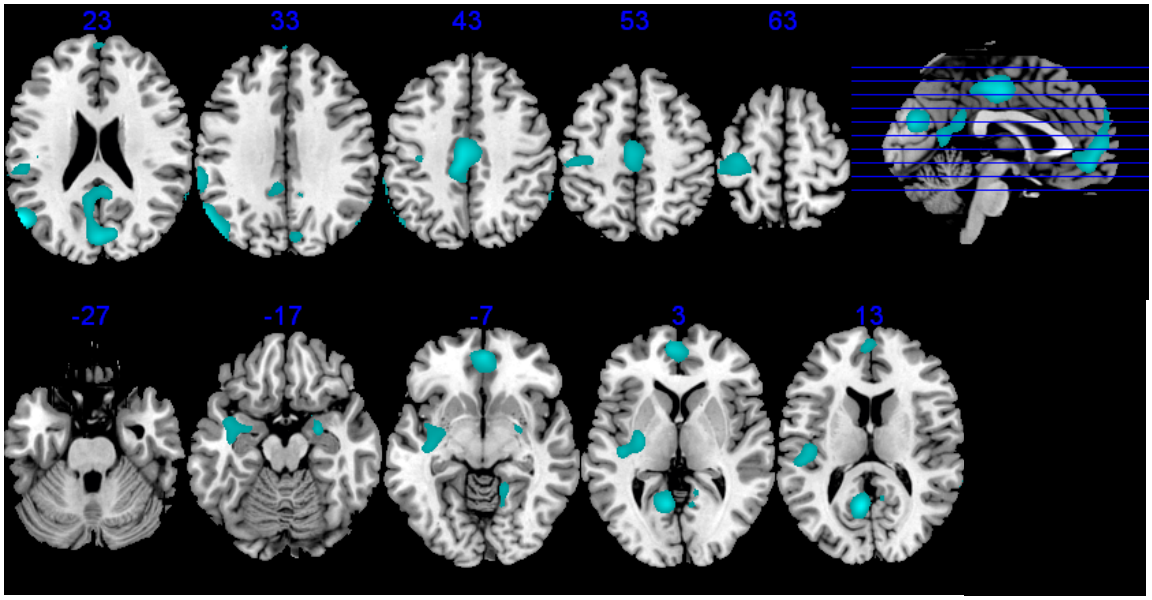

Figure 5-14. Pattern of negative activation in the SOS task in a group of 25 healthy young adults. Panel shows random effects group analysis ($p < 0.05$, FWE corrected for multiple comparisons).

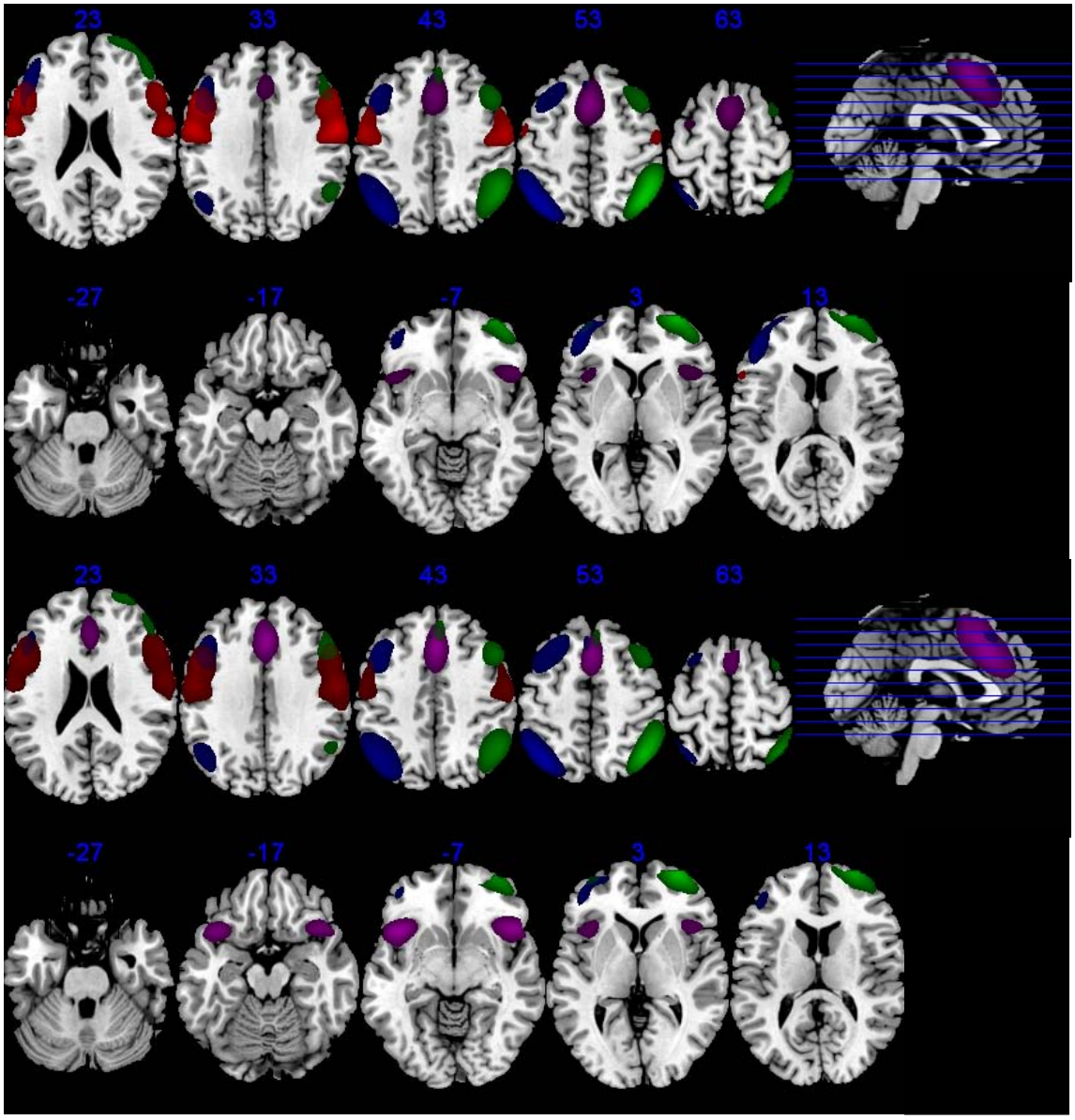

Figure 5-15. Similar components identified in the N-back and SOS tasks. Panel shows components that had time courses related to N-back task design (top). The same spatial patterns were identified in the SOS data (bottom) even though the behaviorally modified task designs obscure identification of task related time courses. Overlays are threshold: z > 2.

Table 5-4. Clusters of positive activation during the SOS tasks for a group of 25 healthy young adults. Coordinates are given in MNI space. Positive X denotes right hemisphere.

Area	**X**	**Y**	**Z**	**T-value**
SOS (Verbal and Object)				
Dorsolateral PFC	-36	22	36	8.44
	46	32	32	6.50
Ventral PFC	-30	22	-2	6.86
Dorsal cingulate	-6	18	50	8.09
Lateral premotor	28	8	56	6.90
	-24	4	58	6.43
Parietal	-26	60	50	8.76
	22	-64	54	5.90
SOS Verbal				
Dorsolateral PFC	-38	24	26	9.10
Dorsal cingulate	-6	16	52	7.72
Lateral premotor	26	8	58	6.96
Parietal	-28	60	52	7.96
SOS Object				
Dorsolateral PFC	-46	26	36	6.90
	48	36	36	6.19
	-42	6	32	6.09
Dorsal cingulate	-6	20	48	6.68
Parietal	-24	-62	50	7.51
	24	-62	50	5.91
Ventral visual	-46	-66	-6	7.95
	38	-86	2	6.06

Table 5-5. Clusters of negative activation during the SOS tasks for a group of 25 healthy young adults. Coordinates are given in MNI space. Positive X denotes right hemisphere.

Area	X	Y	Z	T-value
SOS (Verbal and Object)				
Retrosplenial	-2	-48	32	10.63
Medial frontal	2	26	-8	10.23
Hippocampus	-24	-2	-28	9.16
	22	-2	-26	8.83
Parietal	-46	-70	46	8.45
	64	-40	44	8.05
Temporal	-58	-8	-22	8.02
	62	02	4	6.62
Insular	-38	-14	-2	7.85
Cingulate	4	-18	46	6.37

Inside versus Outside

Performance results from the SOS and N-back tasks for both settings (inside-MRI/outside-MRI) were entered into a linear mixed-effects model to determine any effect of setting on performance. There was no significant difference in time to completion of the SOS ($p = 0.732$), number of trials to completion ($p = 0.561$), N-back reaction time ($p = 0.507$), N-back omissions ($p = 0.879$) or N-back commissions ($p = 0.904$). There were no significant interactions between any combinations of factors.

SOS versus N-back

Individuals' SOS and N-back contrast images were entered into a paired T-test to determine differences between SOS and N-back activation patterns (Figure 5-16). Ventral visual activation was increased in the SOS object task compared to the N-back. Posterior portions of the medial and superior temporal gyri, the medial temporal poles, and other areas are identified as more active during the N-back.

A joint ICA extracted networks similar to those in the individual task ICA's. Two-sample T-tests between SOS and N-back sessions revealed changes in signal

coherence in the visual cortex in two components. Figure 5-17 shows coherence between the DLPFC and Brodmann's area (BA) 19 in the left occipital lobe is increased in the SOS task ($p < 0.05$, FWE corrected for multiple comparisons).

Discussion and Conclusions

Eye-tracking as an interface for an fMRI task performed reasonably well. However, the success rate early on was hindered by a couple of factors (Figure 5-18). First, equipment malfunctions resulted in several unsuccessful experiments. Additionally, the original calibration routine we developed had a design flaw that was introducing error into the system and degrading eye-tracking performance. Poor performance led to the inability to select the desired stimulus, a distracting flutter of the highlighted border between 2 or more stimuli, or a failed exam. Adequate performance of the eye-tracking system requires accurate calibration for each participant. Our previous experiences using eye-tracking demonstrated that an accurate calibration can be difficult to achieve. The second step in the calibration routine maps coordinates from ASL space to visual display space, but it also provided us an opportunity to try to correct for an imperfect calibration. In the original version of the calibration routine, we recorded gaze coordinates during the entire time the spinning eye was at a calibration point, which could be on the order of seconds (the spinning eye is moved between calibration points by the person operating the eye-tracker and the Presentation program). During this time the participant would often anticipate movement of the spinning eye and look to the next location or gaze would begin to wander. The accumulation of "noisy coordinates" began to skew our calculated coefficients for our mapping matrix. The calibration program was modified to record only the first 10 gaze points after 166 ms when the spinning eye is moved to a new

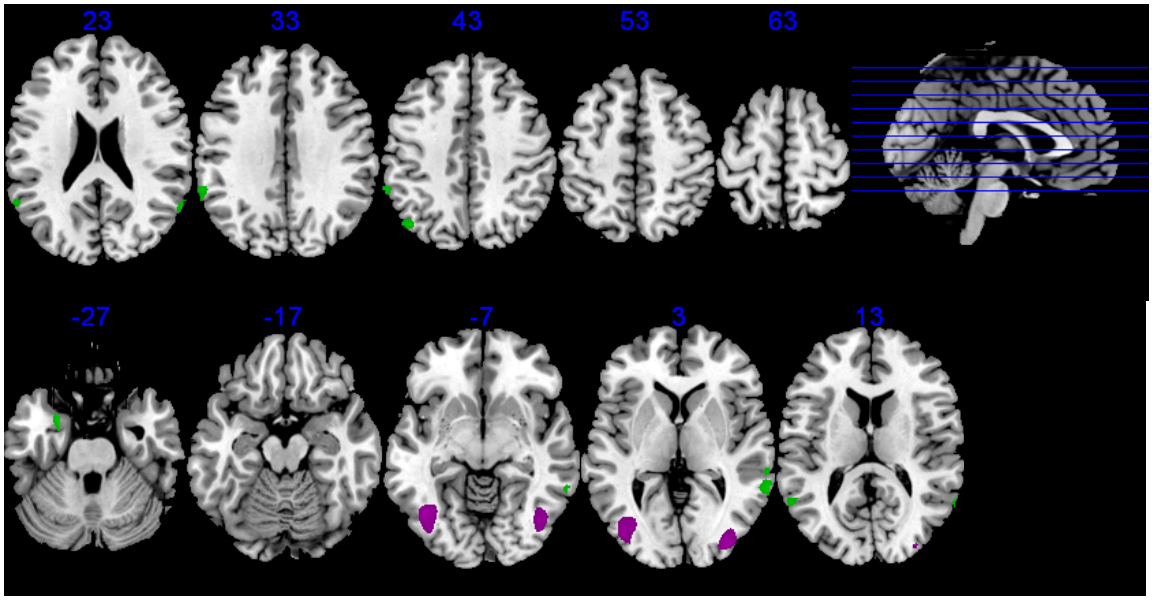

Figure 5-16. Differences in activation between the N-back and SOS tasks in a group of 25 healthy young adults. Panel shows random effects group analysis ($p < 0.05$, FWE corrected for multiple comparisons). Green denotes N-back > SOS. Violet denotes SOS > N-back.

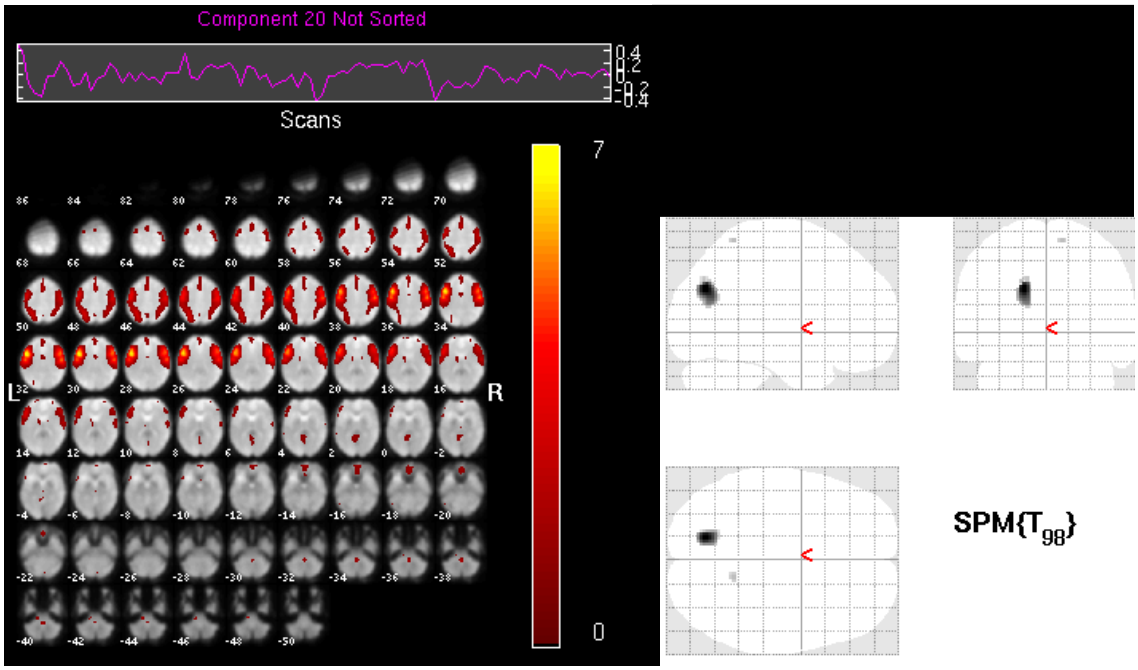

Figure 5-17. Changes in coherence between SOS and N-backs tasks. Left panel shows a component containing DLPFC (red, threshold: $z > 1$) from a joint N-back and SOS ICA. The right panel shows that BOLD signal coherence between the DLPFC and BA 19 was significantly increased in the SOS task compared to the N-back ($p < 0.05$, FWE corrected for multiple comparisons).

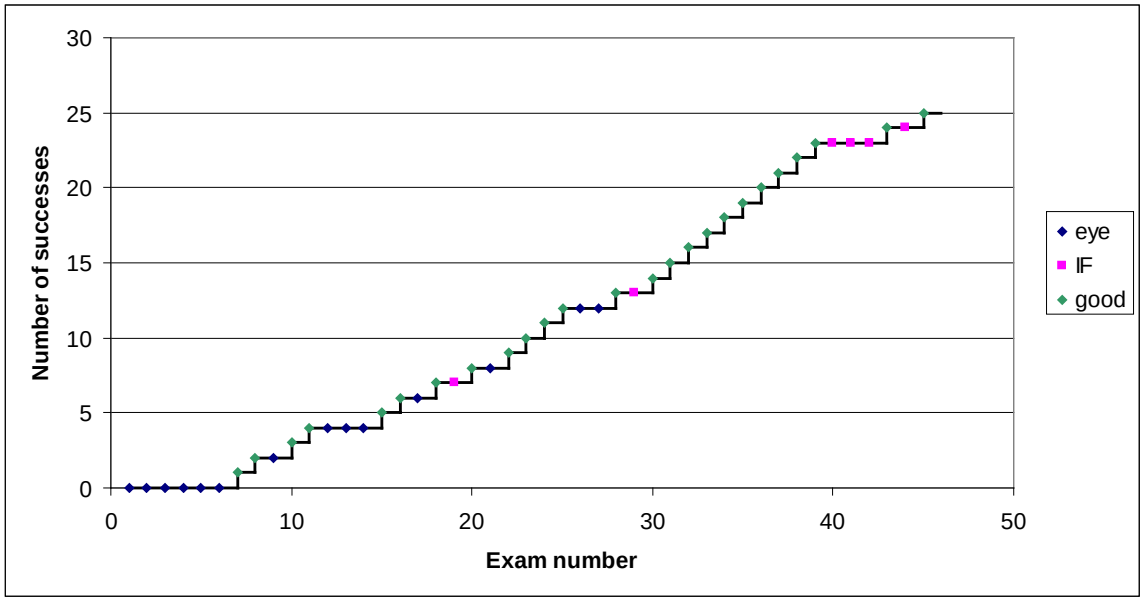

Figure 5-18. “Success plot” of SOS exams in EXFXN2. Successes were hindered early on by equipment malfunctions and a flaw in the calibration routine. Blue dots denote failures due to equipment or poor eye-tracking. Pink dots denote exclusionary incidental findings.

position. The delay allowed saccadic transition to the new location of the spinning eye. The shortened sampling resulted in the removal of confounding coordinate data and yielded a significant performance increase in the system.

However, resolving the equipment issues and modifying the calibration routine did not alleviate all eye-tracking difficulties. Generally, eye-tracking technology is based on identifying and monitoring the position of a pupil using a pattern recognition algorithm. The ASL eye-tracking system is based on a “light-pupil” technique in which near-infrared light is directed into the eye. The near-infrared light is reflected back from the retina resulting in a bright pupil amongst a dark background. The light also reflects back from the corneal surface of the eye, resulting in an additional smaller brighter reflection. The control unit attempts to discriminate the pupil and the corneal reflection from a video feed from an LCD camera, calculate the distance and angle between the

center of the pupil and the corneal reflection, and relate those values to gaze positions. But the variability in human anatomy and outside factors can present difficulties that lead to poor performance of the eye-tracking system. For example, in one case the participant's contact lenses created double reflections and the eye-tracker could not discriminate the real pupil and corneal reflection from the ghost reflections created by the contact lenses. Another case failed due to long eye-lashes obstructing a clear view of the pupil. Visual problems that result in a participant squinting also caused poor performance. The partial closing of an eyelid tends to cover the top part of the pupil, causing the center of the pupil to appear lower than actuality. This causes the estimated gaze coordinates to be below where the participant is actually looking. We did implement use of MR-compatible goggles with interchangeable corrective lenses to try to resolve vision problems which resolved some, but not all, cases.

Eye-tracking, however, was not the only factor influencing our replacement rate for study participants. Another factor in the high number of participants needed to get 25 complete data sets was an apparent high rate of exclusionary incidental findings. Previous studies have reported rates of incidental findings at 1.8% [Katzman et al., 1999], 4.6% [Illes et al., 2004] and 8% [Kim et al., 2002]. Five of our 45 recruits had exclusionary findings that did not require medical referral and two had medically significant findings that required medical referral. Together these combine for a rate of 13.3%. This may be due to a number of different potential factors. For example, the anatomical imaging in this study was higher resolution than the earlier studies which allows for better diagnosis. Additionally, the age of our cohort may also have had an effect, as previous studies

suggest incidence of pineal cysts peak within a specific age range for adults [Sawamura et al., 1995; Nolte et al., 2010].

Performance on the SOS and N-back tasks were consistent between fMRI and clinical settings. As such, one can be assured that activation patterns are representative of actual behaviors. Both the SOS and N-backs tasks induced activation in an extensive network of cortical areas. The patterns resemble those summarized in a meta-analysis of 24 studies using the N-back task [Owen et al., 2005]. Activation was primarily located in the dorsolateral and ventral PFC, dorsal cingulate, bilateral premotor, and parietal areas with activation extending into the ventral visual cortex and cerebellum. Negative activation was present in retrosplenial, frontomedial, bilateral parietal and hippocampal cortex; regions frequently termed the default mode network (DMN) [Ogg et al., 2008; Raichle et al., 2001; Fox et al., 2005; Thomason et al., 2008]. Evidence of demand modulated activation in DLPFC, dorsal cingulate, bilateral premotor and parietal cortex correspond to previous reports [Nelson et al., 2000; Ragland et al., 2002; Callicott et al., 1999] and provides further evidence that these areas are particularly involved in WM function. However, our results are not clear on how each area specifically participates in WM processes. For instance, activation in the ventral PFC was also modulated by the load. The general hypothesis is that ventral PFC participates primarily in maintaining information in WM. The 1-back condition of the N-back is primarily maintenance as opposed to manipulation; however we saw the ventral PFC activation primarily during the 2-back conditions in both GLM and ICA analyses.

Activation patterns identified by the model driven analysis were generally consistent between the SOS and N-back tasks, though N-back produced qualitatively

more robust activation. These similarities were expected, as both tests are WM tasks that involve intensive monitoring and updating of information. However, the SOS involves additional processes such as complex response selection, visual scanning, self-monitoring and development of cognitive strategies [Luciana et al., 2005]. As such, we hypothesized the SOS and N-back would induce slightly different patterns of brain activation. However, no significant differences were apparent in the prefrontal cortex in the SOS > N-back contrast. This may be due to a couple of reasons. The PFC is generally thought to contain modular circuits that participate in many cognitive processes and activity cannot be easily attributed to any specific cognitive process [D'Esposito et al., 2000]. The circuitry for these similar tasks may overlap. BOLD signal has been shown to associate most closely with local field potentials that result from integrated activity of groups of neurons [Raichle, 2009]. Additionally, the hemodynamic effect size is approximately 5 mm and subtle differences in the location of activation may be difficult to distinguish.

We would like to note, that although not explicitly significant, the SOS task is potentially more sensitive to laterality differences. Both the object and verbal N-back tasks consistently exhibited bilateral activation in the DLPFC under both 1-back and 2-back loads. The SOS verbal condition consistently activated left DLPFC, while the object SOS appeared bilateral in the 8-object task, and completely right lateralized in the 11-object task. However, the two tasks did not use the same set of stimuli. One could argue that the objects created for the N-back task are nameable, and as Nelson et al. (2000) has shown, use of nameable objects tends to induce bilateral activation for N-back tasks.

ICA of the fMRI data showed consistent results with the GLM analysis by detecting task related activation in cortical areas identified by the model driven analysis.

However, ICA also detected source networks with time courses seemingly unrelated to task design. ICA analysis of the SOS and N-backs tasks showed that ICA extracts meaningful networks even when task designs are different between individuals (i.e.: behavioral modified block designs of the SOS). T-tests of ICA components did detect one difference in neural networks between the N-back and SOS tasks. Signal coherence was increased between the DLPFC and BA 19 in the parietal cortex while performing the SOS task. BA 19 is known to be highly connected to neighboring visual areas, but also connects with an area of cortex called the frontal occulomotor area [Talaraich and Tournoux, 1988].

Unfortunately, both the SOS and N-back fMRI tasks failed to identify brain regions where activity was significantly associated with performance in the group of healthy volunteers. Several factors may have limited our ability to detect performance effects in patterns of activation during the WM tasks. It should be noted, previous studies are also inconclusive as to how activation is related to performance and conflicting results exist in the literature. D'Esposito et al. (2000) reported lesser extent of activation in DLPFC correlated with better performance on a WM task. Klingberg et al. (2002) and Curtis et al. (2000) report increased BOLD signal and relative cerebral blood flow that correlates positively with WM performance. The effect of interest may also be small and thus difficult to detect with our limited sample size of 25. For example, Nystrom et al. (2000), reports signal changes related to various conditions between of 0.1 – 0.3 %. As demonstrated by ICA, behavior may not be easily related to activation maps generated by a GLM analysis. Behavior and performance result from a complex interaction of the neural networks. The analysis methods implemented here may be insufficient to

adequately detect any real relationship between behavior and areas of activation identified by GLM or ICA analysis.

A quick examination of the behavioral results from our control group reveals another potential confound. The mean IQ for our control group was 120 (stdev = 7.3). The mean IQ of the normal population is 100 (stdev = 15). Comparatively, the majority of our healthy cohort is at least one standard deviation above normal intelligence. Similarly, the entire group performed reasonably well on the tasks and performance was tightly grouped (mean 34 trials, stdev of ~ 6 on verbal and object SOS; mean 7 N-back errors, stdev ~ 5). For example, our cohort had a mean trials-to-completion of 15.9 (stdev 4.0) on the 11-object version of the SOS. Conklin et al. (2005) reported a mean trials-to-completion of 56 healthy individuals on the 11-object SOS task at 16.6 (stdev 4.6). The PET study of 8 healthy individuals by Curtis et al. (2000) reported the mean number of trials to completion for the 11-object task was 20.5 (stdev = 8.8). Combine this limited dynamic range with a potentially small effect and it may explain why no areas of BOLD activation were found to correlate with performance.

Chapter 6: SOS in Children Treated with Radiation Therapy for Brain Tumors

Introduction

Children who undergo treatment for brain tumors are at a significant risk for developing cognitive deficits. Having established neural substrates of the SOS task in a group of healthy controls, we conducted a study to explore how neural networks are altered in children treated for brain tumors. A group of children enrolled on the RT1 protocol at St. Jude Children's Research Hospital performed the fMRI SOS and N-back tasks. Patient recruitment and study procedures were approved by the St. Jude IRB.

Subjects

Table 6-1 contains demographic data for the patient group (24 male and 21 female) with an average age of 15.3 years (range 9.8 - 24.4). All but 2 patients were right handed. The group comprised 15 survivors of ependymoma (EP), 15 survivors of craniopharyngioma (CRAN), and 15 survivors of low-grade astrocytoma (LGA). All patients were treated with conformal radiation as per RT1 protocol and were at least 2 years out from completing RT. As part of the RT1 protocol, patients receive neuropsychological testing, the results of which were used as variables in the subsequent analyses.

Functional-MRI studies

Patients performed the object and verbal versions of the SOS and N-back tasks in an fMRI setting. Functional data was acquired, preprocessed and analyzed as discussed previously. Random effects analysis was performed on the RT1 data group separately and in combination with the EXFXN2 cohort to examine differences between the two groups.

Table 6-1. Demographic, clinical and neuropsychological testing information for the RT1 patient group.

ID #	Gender	DX	Age at DX	Age at fMRI	Est. IQ	Handed-ness	Years from RT
1	M	LGA	10.6	20.7	128	L	10
2	M	EP	4.8	15.1	90	R	10
3	F	EP	3.3	13.4	78	R	10
4	F	LGA	6.4	14.0	114	R	8
5	M	EP	15.2	24.4	134	R	8
6	M	LGA	9.3	17.4	102	R	8
7	M	LGA	5.4	11.4	102	R	6
8	M	EP	8.3	16.2	118	R	8
9	F	LGA	6.6	14.9	94	R	8
10	M	LGA	5.6	14.9	142	R	10
11	M	CRAN	4.8	14.2	108	R	9
12	F	LGA	7.2	10.3	84	R	3
13	F	EP	2.0	15.4	116	R	9
14	F	EP	1.8	9.8	78	R	8
15	F	EP	5.4	14.5	92	R	9
16	M	EP	6.7	15.0	82	R	9
17	F	LGA	6.6	12.6	90	R	6
18	F	LGA	13.3	21.8	120	R	8
19	M	LGA	6.7	14.7	116	R	8
20	M	CRAN	7.2	15.4	130	R	8
21	M	CRAN	15.5	23.2	114	R	8
22	M	CRAN	11.8	19.4	118	R	7
23	M	CRAN	12.4	20.5	121	R	8
24	F	LGA	4.3	12.7	98	R	6
25	F	LGA	6.7	17.9	94	R	6
26	M	LGA	10.9	12.0	112	R	6
27	M	CRAN	7.9	14.8	142	L	4
28	F	CRAN	9.1	9.9	84	R	6
29	F	EP	4.6	10.4	84	R	4
30	F	CRAN	5.9	20.8	118	R	5
31	F	CRAN	14.7	13.8	82	R	6
32	F	CRAN	9.6	15.8	82	R	4
33	M	EP	11.7	13.2	118	R	3
34	F	CRAN	9.7	13.7	98	R	3
35	M	EP	8.7	17.2	104	R	5
36	M	EP	12.1	20.5	114	R	5
37	F	EP	16.9	10.9	112	R	4
38	F	LGA	6.4	14.9	96	R	5
39	M	CRAN	10.3	11.7	88	R	4
40	M	EP	8.1	17.2	100	R	3
41	F	CRAN	13.7	14.4	88	R	3

Table 6-1 (continued). Demographic, clinical and neuropsychological testing information for RT1 patient group.

ID #	Gender	DX	Age at DX	Age at fMRI	Est. IQ	Handed-ness	Years from RT
42	M	LGA	10.6	20.7	128	R	3
43	M	CRAN	13.1	16.1	98	R	3
44	M	CRAN	15.0	18.0	106	R	3
45	M	EP	14.4	16.9	92	R	3
$\bar{x}$			8.9	15.5	104.1		6.2
s			3.85	3.56	17.2		2.37

Statistical analysis of behavioral data

Group differences were investigated using T-tests and linear mixed-effects model. For the mixed-effects model gender, group (control/patient) and tumor type were entered as fixed-effects. Random-effects included age and IQ. Separate models were created to investigate SOS performance (combined, verbal, object; time to completion and trials to completion) and N-back performance (combined, verbal, object; reaction time, omissions, commissions and combined error-rate).

Results

Neuropsychological testing results for the RT1 patient group can be found in Table 6-1. Average IQ was 102 (stdev = 18.5, range 78 – 142) as estimated by either the WASI or Wechsler Intelligence Scale for Children (WISC III). Out of the 45 patients recruited, 44 patients completed the N-back and 29 patients completed the SOS task. Several data sets were excluded from analysis due to: poor brain coverage during imaging (4), response device not working (1), problems with spatial normalization (3), artifacts due to clips, shunts or dental implants (5), vision problems interfering with eye-tracking (3), difficulties with eye-tracking equipment (3), patient positioning and size preventing eye-tracking (3). The final number of fMRI data sets used in analysis were N = 24 for SOS and N = 34 for N-back.

N-back

Figure 6-1 shows the mean pattern of activation for the combined verbal and object N-back task ($p < 0.05$, FWE corrected for multiple comparison). Task activation was robust and included the dorsolateral PFC, ventral PFC, dorsal cingulate, frontal poles, parietal, ventral visual and cerebellar areas (Table 6-2). Activation maps were

generated for verbal and object conditions separately (Figures 6-2 and 6-3, Table 6-3). Activation in the DLPFC, parietal, dorsal cingulate and lateral premotor areas increased with WM load (Figure 6-4). Bilateral activation in the ventral PFC region was detected only in the high demand 2-back condition. No significant differences between verbal and object versions of the N-back were detected.

The number of components extracted in all ICA analyses was 32. Resulting spatial maps and associated time courses (not shown) are similar to those of healthy cohort. Of the 32 extracted components, 5 exhibited WM task related signal changes that are consistent with the GLM analysis. These 5 networks include the same 4 extracted in the EXFXN2 group: left and right executive networks [Cole et al., 2010] (components 12 and 15), a component containing bilateral DLPFC (component 18) and a component containing the ventral PFC, dorsal cingulate and lateral premotor areas (component 7). Additionally a component containing the dorsal visual system (component 2) contained a positive task related time-course. Four components exhibit a signal change inversely related to the task demand that included: two frontal medial (component 4 and 6), mid-cingulate (component 17), temporal poles (component 15), and auditory cortex (component 29). Anterior visual cortex (component 1) and ventral and dorsal visual streams (component 23) spike in relation to the presentation of instruction screens before each task block. The default mode network loaded onto 3 components (medial frontal dominant, 4; retrosplenial dominant, 14; parietal dominant, 17), with the retrosplenial dominant component most active during the 5 second rest period before each task block. Two-sample T-tests revealed no significant differences in component maps between

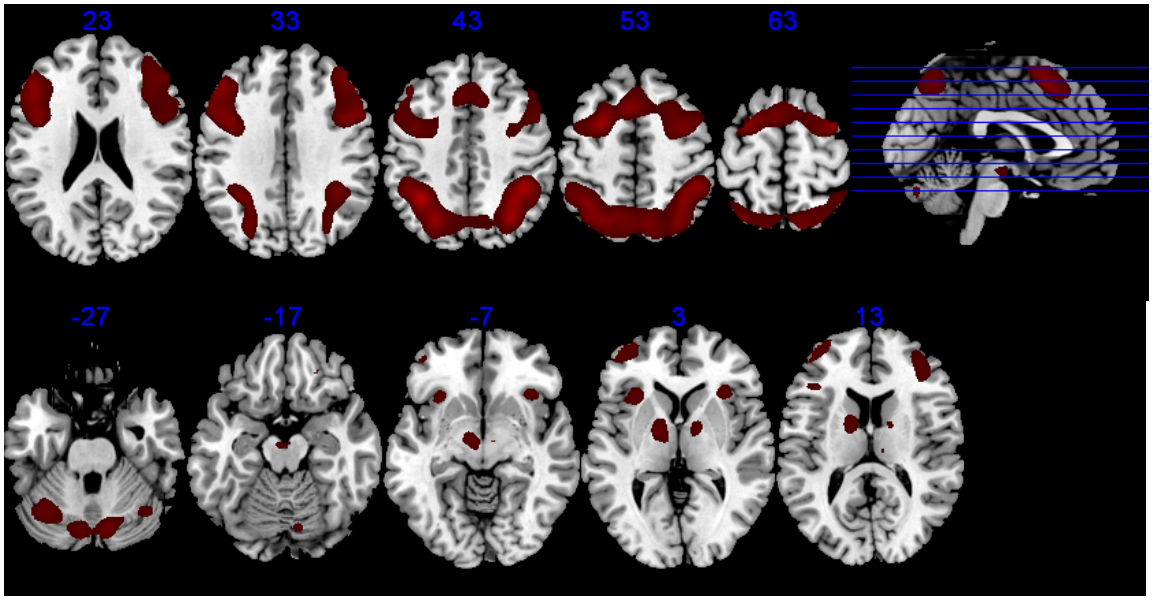

Figure 6-1. Pattern of mean activation in the N-back task in a group of children treated with conformal radiation therapy. Panel shows random effects group analysis ($p < 0.05$, FWE corrected for multiple comparisons).

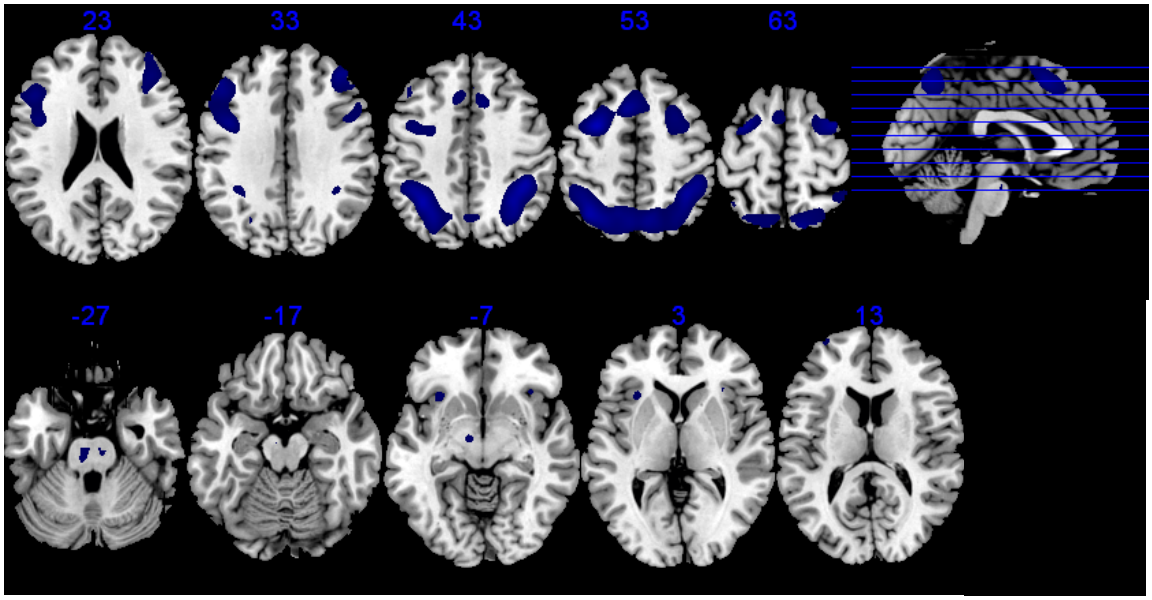

Figure 6-2. Pattern of mean activation in the N-back verbal task in a group of children treated with conformal radiation therapy. Panel shows random effects group analysis ($p < 0.05$, FWE corrected for multiple comparisons).

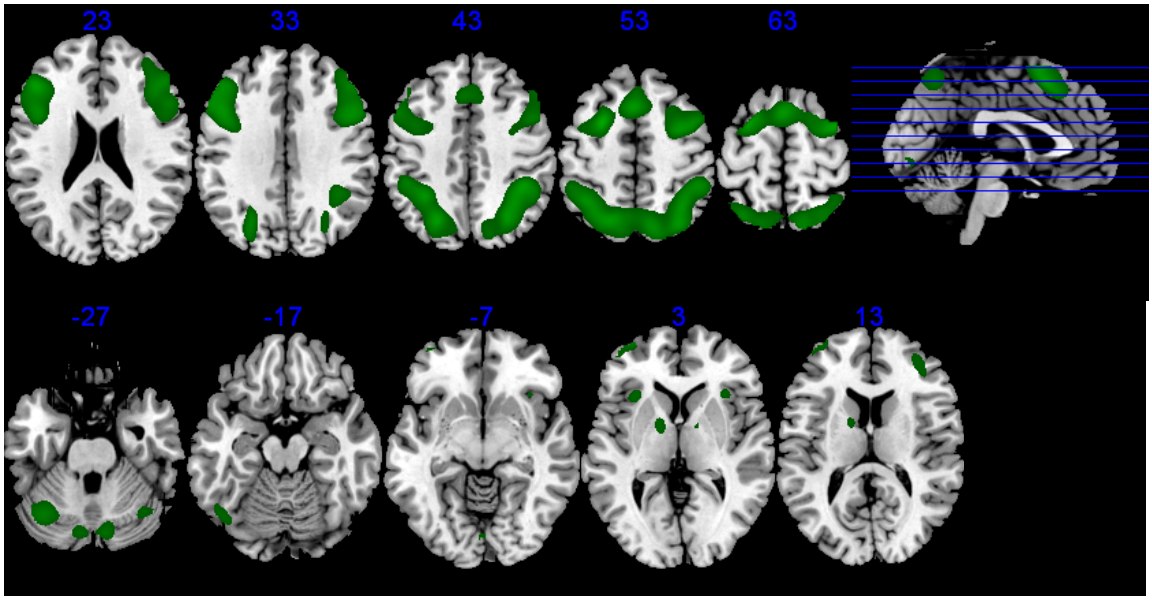

Figure 6-3. Pattern of mean activation in the N-back object task in a group of children treated with conformal radiation therapy. Panel shows random effects group analysis ($p < 0.05$, FWE corrected for multiple comparisons).

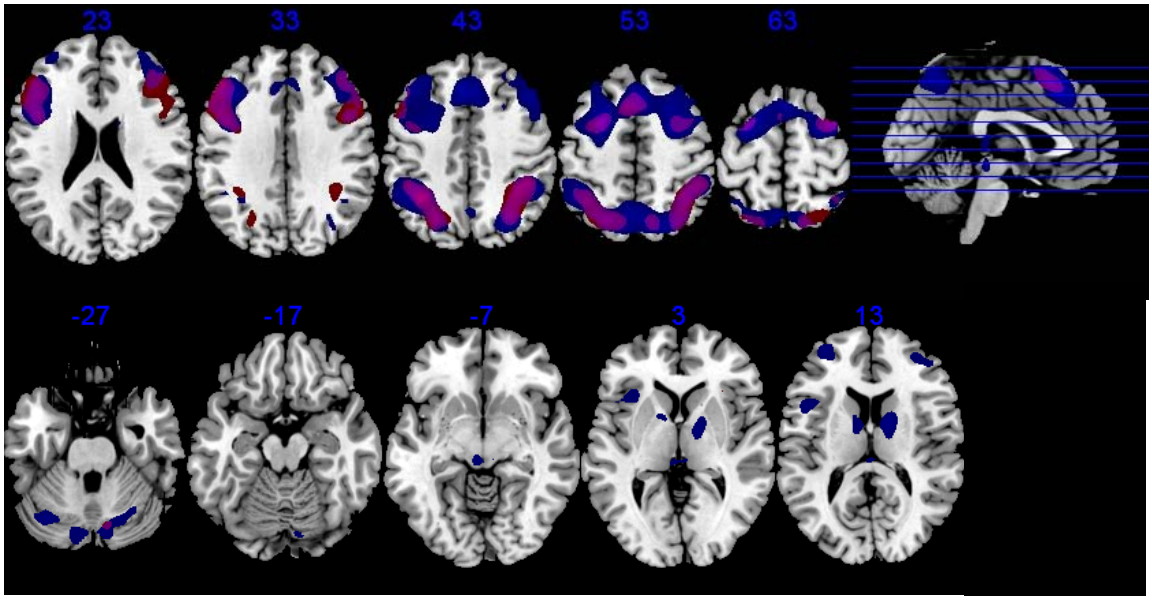

Figure 6-4. Pattern of parametric activation in the N-back task in a group of children treated with conformal radiation therapy. Panel shows random effects group analysis ($p < 0.05$, FWE corrected for multiple comparisons). Red denotes the contrast 1-back > 0-back while blue denotes the contrast 2-back > 1-back. Activation in the frontal-parietal areas increased linearly with working memory load, while activation in the bilateral ventral prefrontal area was detected only in the high-load 2-back condition.

Table 6-2. Clusters of positive activation during the N-back task for a group of patients treated with conformal radiation for childhood brain tumors. Coordinates are given in MNI space. Positive X denotes right hemisphere.

Area	**X**	**Y**	**Z**	**T-value**
N-back (Verbal and Object)				
Dorsolateral PFC	46	8	34	9.96
	46	38	30	9.08
	-48	34	28	13.28
	-44	8	28	10.44
Dorsal cingulate	-4	16	52	10.41
Lateral premotor	-26	4	56	13.28
	32	2	60	11.55
Parietal	-34	-52	42	14.36
	42	-43	44	13.47
	34	-54	46	12.46
Frontal pole	-44	52	10	7.68
Cerebellum	-36	-64	-32	8.90
	12	-76	-30	8.36

Table 6-3. Clusters of positive activation during the N-back task for a group of patients treated with conformal radiation for childhood brain tumors. Coordinates are given in MNI space. Positive X denotes right hemisphere.

Area	**X**	**Y**	**Z**	**T-value**
N-back Verbal				
Dorsolateral PFC	-42	4	30	8.06
	40	40	32	7.90
	46	8	32	6.17
Ventral PFC	-30	20	-4	6.53
	34	24	-2	5.97-32
Dorsal cingulate	-6	16	52	8.69
Lateral premotor	-28	2	54	11.02
	36	2	64	8.86
Parietal	-34	-54	46	10.83
	42	-42	44	9.87
Frontal pole	-32	60	16	5.92
N-back Object				
Dorsolateral PFC	-46	32	26	9.69
	46	32	28	8.15
Ventral PFC	-32	20	2	6.05
	34	22	0	5.97
Dorsal cingulate	-2	16	52	9.09
Later premotor	-24	6	58	10.96
	36	2	60	10.14
Parietal	-22	-66	48	9.28
	40	-42	44	9.21
Frontal pole	-34	60	6	7.32
	36	52	-14	5.90
Cerebellum	-36	-64	-30	7.52
	10	-78	-28	6.53
	38	-60	-34	6.08

verbal and object N-back. Random-effects analysis revealed no areas that demonstrated significant changes in coherence associated to behavioral variables.

SOS

Appendix F contains the inside-MRI SOS performance of the study participants. The timing information was used to generate the design matrices for SOS fMRI analysis. Figure 6-5 shows the mean pattern of activation for the combined verbal and object SOS task similar to the healthy cohort ($p < 0.05$, FWE corrected for multiple comparisons). Task induced activation was present in the dorsolateral prefrontal cortex, ventral frontal, parietal, dorsal cingulate and lateral premotor areas (Table 6-4). Activation maps were also generated for the verbal and object tasks separately (Figures 6-6 and 6-7). For the verbal SOS, activation in the parietal area is bilateral, while activation in the DLPFC is left lateralized. The object version of the SOS induces left dominated DLPFC and bilateral parietal activation, along with additional activation in the ventral visual system. Parametric activity related to task difficulty was only present in the ventral visual areas. No clusters were identified that exhibited activation related to performance, estimated IQ or age.

ICA extracted 32 components. Task related components are not detectible by inspection due to the variability in task timing between individuals. However, ICA extracted the same networks identified in the N-back task including: left and right executive networks, the bilateral DLPFC network, a network containing the ventral PFC with dorsal cingulate and lateral premotor, anterior visual cortex, and others. Two-sample T-test revealed no differences in component spatial maps between verbal and object

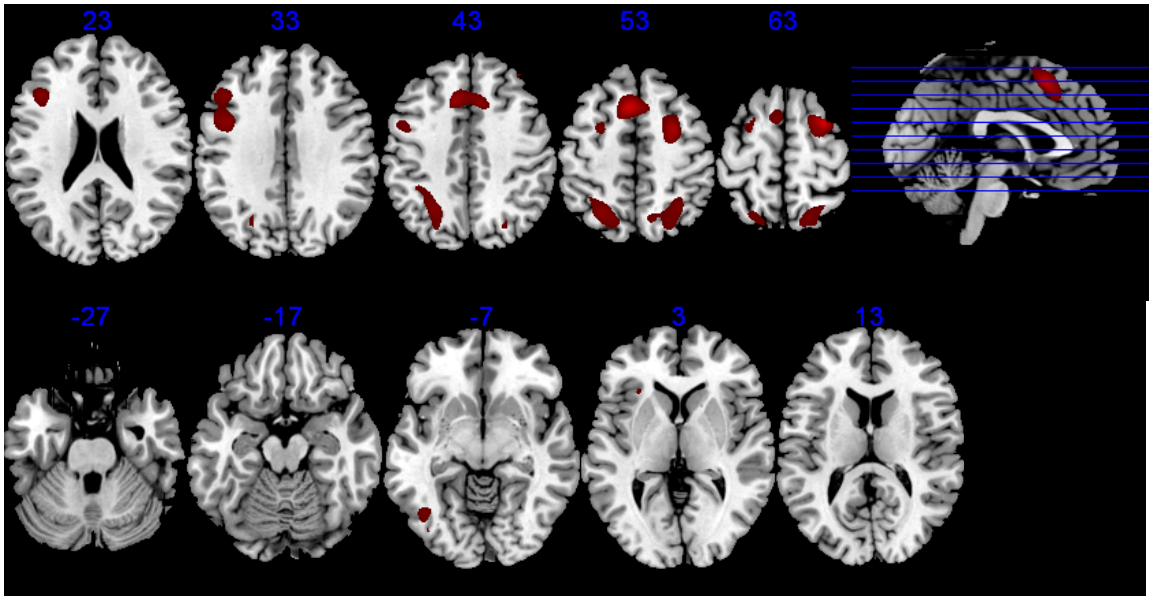

Figure 6-5. Pattern of mean activation in the SOS task in a group of children treated with conformal radiation therapy. Panel shows random effects group analysis ($p < 0.05$, FWE corrected for multiple comparisons).

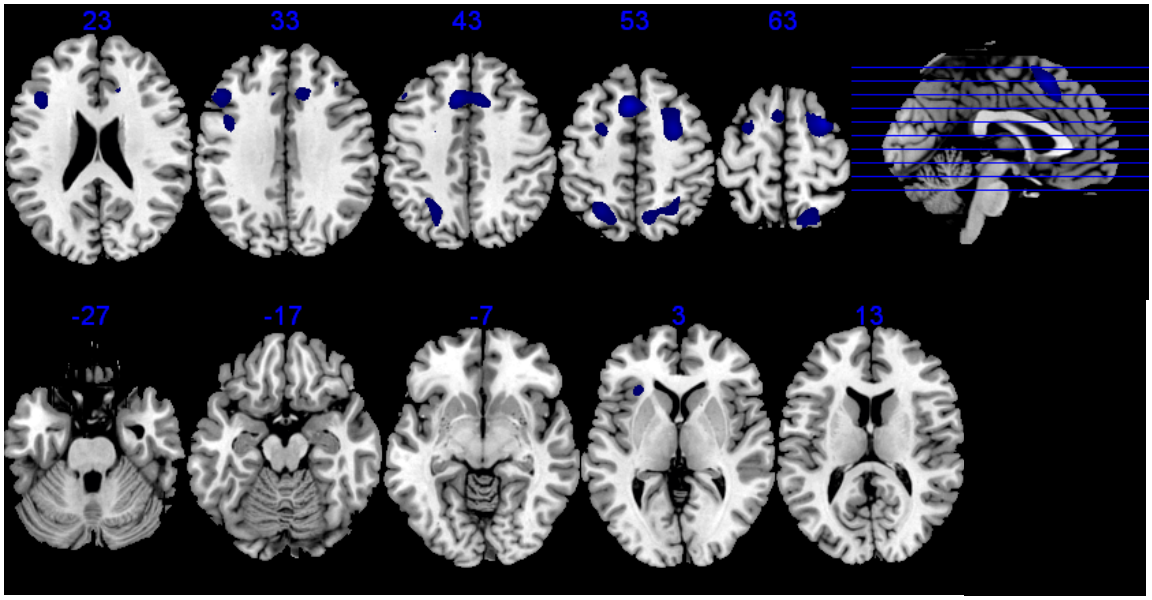

Figure 6-6. Pattern of mean activation in the SOS verbal task in a group of children treated with conformal radiation therapy. Panel shows random effects group analysis ($p < 0.05$, FWE corrected for multiple comparisons).

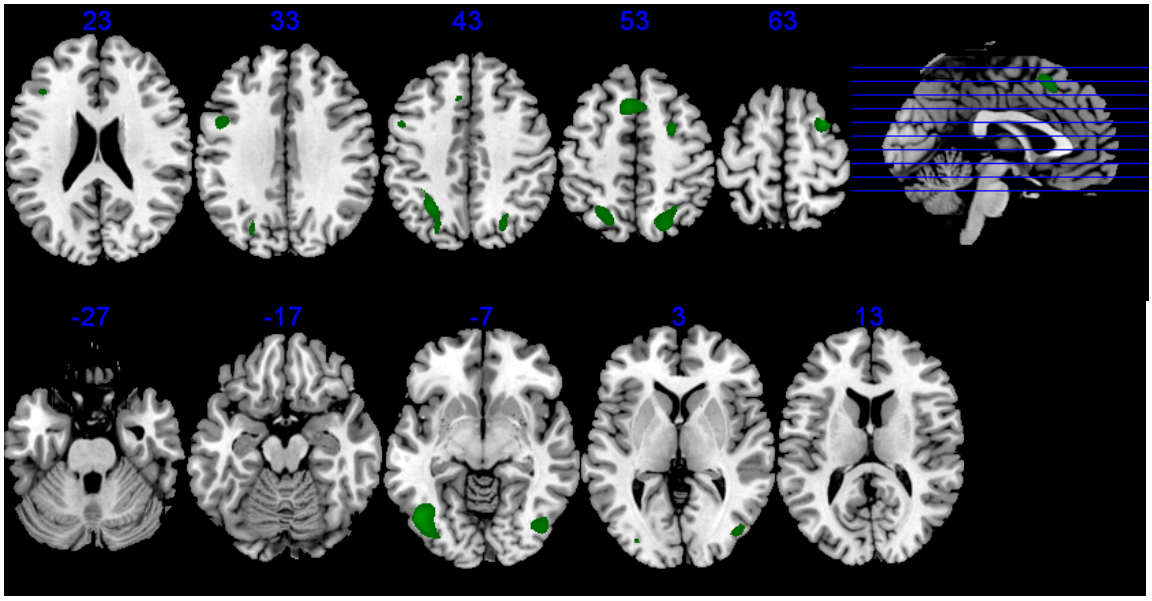

Figure 6-7. Pattern of mean activation in the SOS object task in a group of children treated with conformal radiation therapy. Panel shows random effects group analysis ($p < 0.05$, FWE corrected for multiple comparisons).

Table 6-4. Clusters of positive activation during the SOS tasks for a group of patients treated with conformal radiation for childhood brain tumors. Coordinates are given in MNI space. Positive X denotes right hemisphere.

Area	**X**	**Y**	**Z**	**T-value**
SOS (Verbal and Object)				
Dorsolateral PFC	-44	24	30	8.48
Ventral PFC	-30	24	0	6.15
Dorsal cingulate	-4	16	52	12.32
Lateral premotor	30	4	64	13.05
	-26	2	58	7.10
Parietal	-24	-58	48	8.60
	16	-64	58	7.39
SOS Verbal				
Dorsolateral PFC	-48	24	38	8.36
Ventral PFC	-30	24	2	6.94
Dorsal cingulate	-6	16	52	12.01
Lateral premotor	30	4	64	11.76
	-26	0	60	8.43
Parietal	-24	-60	50	8.87
	-16	64	58	8.33
SOS Object				
Dorsolateral PFC	-42	28	26	6.27
	-48	4	38	8.27
Dorsal cingulate	-4	18	52	7.82
Lateral premotor	30	4	64	8.51
Parietal	-28	-58	46	7.79
	22	-68	54	7.03
Ventral visual	-46	-68	-10	9.37
	44	-76	-4	7.40

stimuli. Random effects analysis revealed no areas that demonstrated significant coherence changes associated with behavioral variables.

EXFXN2 and RT1 analysis

Functional data from the EXFXN2 healthy participants and RT1 patients were entered into combined GLM and ICA analyses. Activation patterns from the GLM were similar to those in the analyses for individual groups (not shown). ICA extracted similar networks as previously described (not shown).

Figure 6-8 shows areas of activation correlated to performance variables among the combined data sets. Activation in the parietal area of the N-back activation map (Table 6-5) is significantly correlated (negatively; $p < 0.05$, FWE corrected for multiple comparisons) with N-back error rate. Additional negatively correlated clusters are identified in an examination of the Verbal N-back that include: dorsal cingulate, ventral visual cortex, parietal cortex and others (Table 6-5). One cluster in the medial motor cortex (BA 6) was positively correlated to the N-back error rate. There was no observed effect of age or IQ on activation patterns among the group.

A 2-sample T-test was performed between the two cohorts to examine group differences. Activation in the parietal cortex area identified in the previous analysis was significantly greater in the healthy young adults compared to the RT1 patient group (Figure 6-9; $p < 0.05$, FWE corrected for multiple comparisons). Increased activation in the retrosplenial area was marginally significant ($p = 0.068$, FWE corrected for multiple comparisons) in the patient population compared to the healthy population (Figure 6-9).

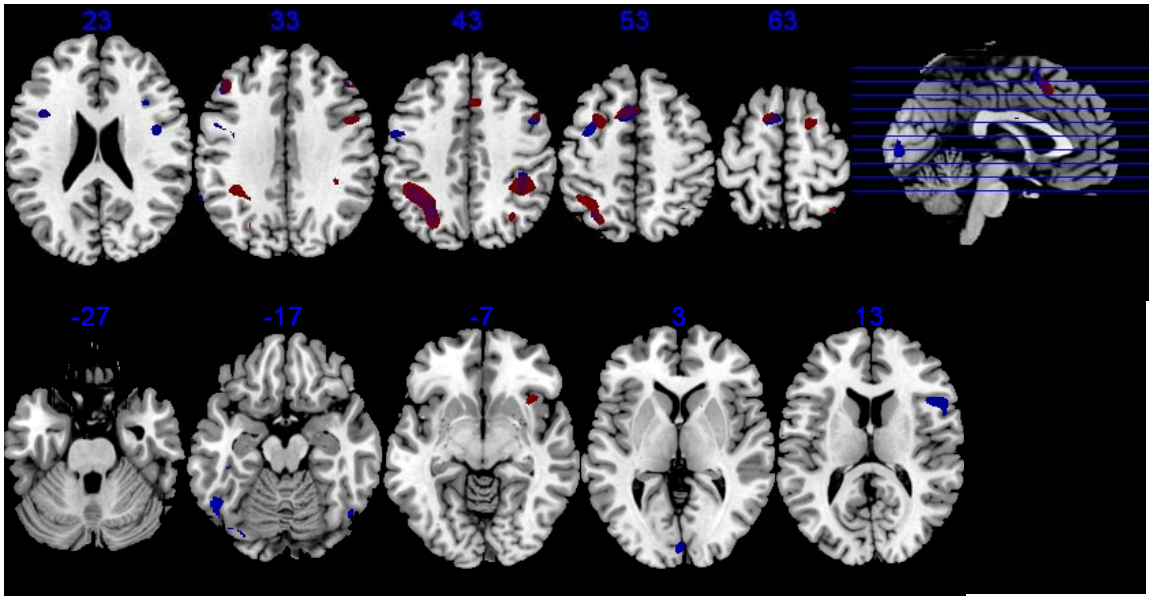

Figure 6-8. Areas of activation in the N-back task where activation was correlated to error rate. Higher activity was associated with fewer errors. Red denotes the combined object and verbal N-back tasks ($p < 0.05$, FDR corrected for multiple comparisons). Blue denotes areas correlated to performance for the verbal N-back task ($p < 0.05$, FWE corrected for multiple comparisons).

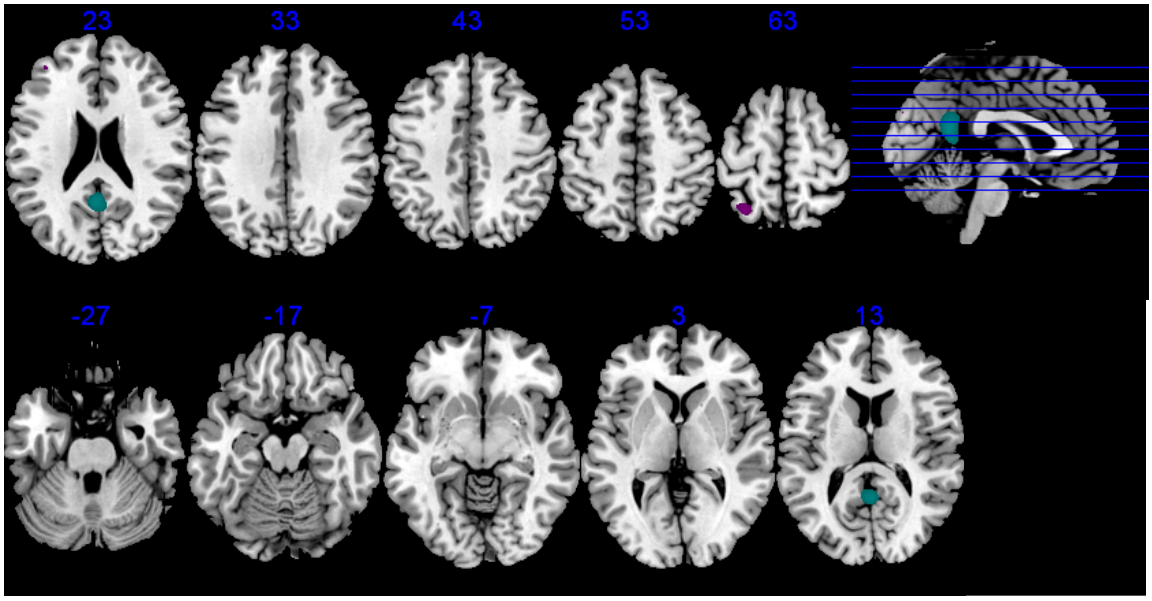

Figure 6-9. Differences in activation between a group healthy young adults and a group of children treated with conformal radiation therapy. Panel shows random effects group analysis ($p < 0.05$, FDR corrected for multiple comparisons). Violet denotes greater activation in the healthy group. Cyan denotes greater activation in the patient group.

Table 6-5. Clusters of activation associated with performance (error-rate) during the N-back tasks for a combined group of healthy young adults and RT1 patients. Coordinates are given in MNI space. Positive X denotes right hemisphere. Positive correlation suggests higher activity in the area is associated with more errors. Negative correlation suggests higher activity is associated with fewer errors (i.e., better performance).

Area	**X**	**Y**	**Z**	**T-value**	**Sign of Correlation**
N-back (Verbal and Object)					
Parietal	-36	50	44	5.18	Neg
N-back Verbal					
Dorsal cingulate	-6	12	52	5.63	Neg
Parietal	-38	-48	42	5.36	Neg
Ventral visual	-34	-82	-16	5.43	Neg
	-52	-58	-18	5.40	Neg
	50	-66	-18	5.26	Neg
Lateral premotor	-34	-2	50	4.89	Neg
Dorsolateral PFC	-44	32	32	4.87	Neg
	-50	4	30	4.86	Neg
N-back Object					
Medial motor/cingulate	0	-16	66	5.29	Pos

Behavioral analysis

Mean estimated IQ score for the patient group was 102 (σ = 18.5). T-tests suggest significant differences in the control group compared the patient group in SOS performance (Trials to completion) and N-back performance (Reaction-Time in 1- and 2-back conditions; Errors in 0-, 1- and 2-back conditions). However, when controlled for age and IQ effects in the linear mixed-effects model differences become non-significant.

Discussion and Conclusion

As previously discussed with the healthy group, eye-tracking problems hindered our success rate early on in the RT1 cohort as well (Figure 6-10). Equipment issues were resolved and the calibration procedure was modified (Chapter 5) which improved performance; however, this patient population presented further challenges for our eye-tracking based interface. Visual defects such as nystagmus, field cuts, and optic neuropathy are common in this population, particularly those children being treated for craniopharyngioma [Chen et al., 2003; Cavazzuti et al., 1983]. In certain cases, we could complete an exam by tracking the better functioning of the left- or right-eye or adjusting patient positioning. However, for some cases eye-tracking just would not function at an acceptable level and the exam was stopped. An additional complication arises with patients of petite stature. In 3 cases, the patient was unable to fit far enough into the head coil to allow a clear view of the patient's eyes. We implemented a screening procedure and began to screen candidates for vision deficits that would seriously hinder performance of the fMRI experiment.

GLM analysis and ICA yielded results remarkably similar to those of our healthy group, but yet again failed to detect any areas of activation that correlated to

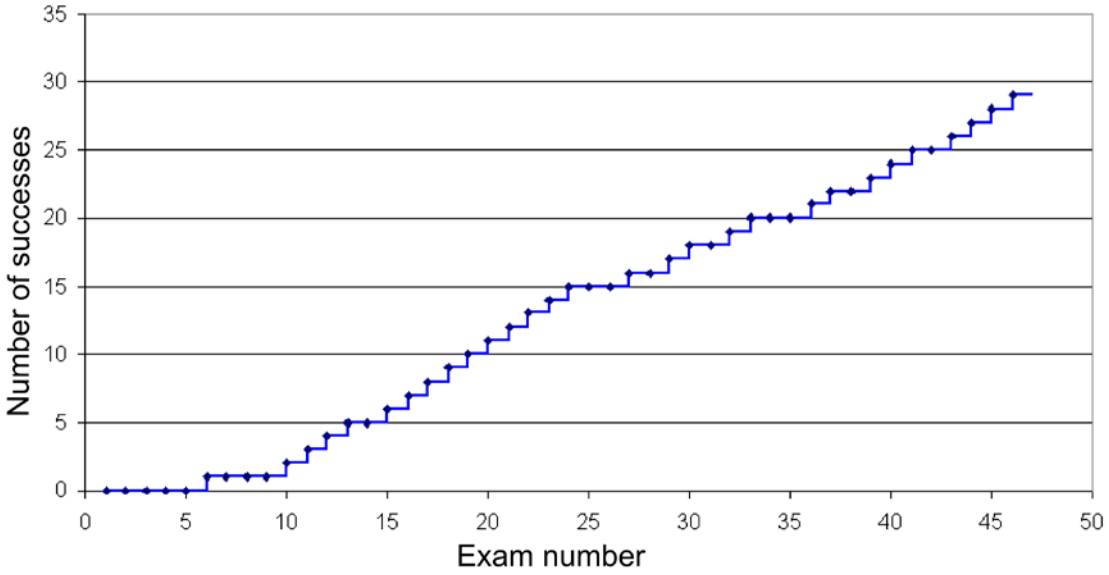

Figure 6-10. “Success plot” of SOS exams in the RT1 patient group. Successes were hindered early on by equipment malfunctions and a flaw in the calibration routine.

performance. As such, we combined the RT1 and EXFXN2 into a single analysis. The combined data did yield areas of cortex where activation was correlated with performance, particularly error-rate during the N-back task. The areas identified (DLPFC, ventral PFC, dorsal cingulate, bilateral premotor and parietal) encompass the primary areas of the WM network identified in the mean activation maps. Our data suggests that increased activation across the entire network is associated with fewer errors (i.e. better performance) and support the general conclusions of others showing a positive correlation between performance and activation [Klingberg et al., 2002; Curtis et al., 2000]. However, Klingberg et al. reported positive correlation in only 3 areas: left superior frontal sulcus (-26, 4, 60), left intraparietal (-36,-76, 44) and inferior parietal cortex (-50, -46, 56). Curtis et al. reported correlated signal changes only in the right DLPFC during the SOS object task. The fact that age and IQ did not significantly

associate to activation patterns, further supports our conclusion that this observed relationship activation is indeed related primarily to WM performance.

Children have been shown to have patterns of activation similar to adults while performing the N-back tasks [Nelson et al., 2000]. Based on this fact, similarities in our results from the individual analyses of healthy controls (Chapter 5) and the RT1 group, and the lack of effects between activation, age and IQ in the combination analysis, we entered the functional data into a between-groups analysis. A significant difference was found in the left parietal cortex (-28, -60, 66) that is part of the WM network. This area is one of the most active during WM tasks. However, we did not expect to see differences in activation between groups in this location. Our hypothesis was that the PFC, with its protracted development, is more vulnerable to damage by RT and thus any damage to neural networks would most likely be detected in the PFC. However, as ICA demonstrates behavior is related to complex interactions between neural networks. Each network may be made of up separated areas of cortex connected by white matter. Insult to one area, or the connections between separated areas may result in more distal effects.

The RT1 cohort was surprisingly normal on measures of IQ with a mean of 102 (stdev 18.5). This was unexpected, knowing that deficits in intellectual functioning are common in children treated with radiation to the CNS. However, it is possible that our group was biased by our screening processes and the requirement that patients be able to adequately participate in the fMRI experiments. In an examination of the behavioral data, T-tests suggested highly significant differences in performance between the RT1 group and healthy group. However, these differences must be interpreted with consideration of confounds such as age matching. Consequently, we entered the data into a linear mixed

effects model that accounted for age, IQ and gender. All significant differences disappeared. However, it should be noted IQ and WM are highly correlated [Wechsler D, 2003; Conklin et al., 2011] and entering IQ in the model potentially removes important variance. Our revised model included WM performance, age and sex and found significant differences in trials-to-completion of the SOS, and marginal ($0.05 < p < 0.1$) differences between omissions and commissions on the N-back. Finally, we suggest this answer is not accurate either and that the group differences are indeed significant. There was correlation between age and IQ in the RT1 group ($R^2 = 0.55$, $p < 0.001$) which should not be the case since IQ is already an age adjusted score. Upon further investigation we discovered a high correlation between age-at-diagnosis and age-at-testing for the RT1 group ($R^2 = 0.77$, $p < 0.001$). Earlier age at treatment has been linked to larger deficits in intellectual functioning (Chapter 1), and this phenomenon is systematically introducing confounding information into our behavioral analysis.

Chapter 7: Discussion and Conclusions

The previous chapters of this dissertation described the implementation, validation and application of a novel eye-tracking based Self-ordered Search task for fMRI. Here we provide a summary of the aims as discussed in Chapter 1.

SOS for fMRI

Eye-tracking based SOS

We have shown that an eye-tracking system can indeed be used as an interface for a neuropsychological test that requires interactivity in an fMRI environment. Generally, the system performed well after the initial problems with equipment and the calibration routine were solved (see Figures 5-18 and 6-10). However, performance of the system is inherently limited by current eye-tracking technology and incompatible of human features that are not easily solved (e.g.: squinting eyes, long eye-lashes, nystagmus, visual deficits, etc…). However, we believe the eye-tracking interface provides an "out of the way" system that controls for familiarity of using devices such as game controllers and minimizes artifacts from motion required to use complex hand-held devices for response.

Performance of the eye-tracking based SOS task could be improved in a number of ways. As was shown in Figure 4-7, the stimulus presentation for the SOS did not extend into the entire screen. A more maximal and effective use of the screen area could possibly yield better performance by allowing greater visual angle separation among the cells in the stimulus array. The original dimensions for stimuli presentation were taken from previous versions of the self-ordered tasks, but unlike some other neuropsychological tasks the SOS does not specify strict dimensions for stimulus size or

visual angle. Line of sight problems between the long-range optics unit and participant's eyes could be alleviated by another mirror andcamera arrangement. As mentioned in Chapter 3, a number of long-range and in-scanner cameras options are available.

SOS task design

We have shown that analyses using behaviorally modified design matrices produce results similar to block designs with fixed-timing. This design allowed us to collect important behavioral measures (trials to completion and time to completion) that could then be entered into the analysis to explore how performance relates to brain activation.

Generally, the SOS produced less robust activation then the N-back. This could be due to relative differences in the cognitive demands between the two tasks. Another possibility could lie in the task design itself. The behavioral modified design matrices introduce concerns about how the variation in block durations across subjects is related to peak BOLD signal. While peak BOLD signal change is related to stimulus duration, non-linear effects induce saturation resulting in a plateau effect after approximately 10 seconds (Figure 3-1). The average block time for the low-level (6-word, 5-objects) conditions was approximately 30 seconds, suggesting block duration did not have an effect on the peak BOLD signal. Also, the performance driven nature of the SOS entails task-blocks starting asynchronously with the start of image acquisition. However, the data were slice-time corrected for block onset to account for these timing differences. In fMRI image acquisition, the acquisition of image slices can vary by as much as the repition time (TR), 2 seconds in our case. Slice-time correction involves temporal interpolation of the data to account for the difference in acquisition times between images

slices [Friston et al., 2007]. In the case of the SOS, slice time correction was performed to start time of each block, rather than a certain image scan. Both of these concerns are also address by the use of ICA. ICA does not extract sources based on any expected signal.

Unfortunately, no relationship between SOS performance and activation was evident in this study. The lack of correlates between performance and activation could be due to a number of factors as discussed previously. One potential reason being the effect of interest may be too small to be detectable with our sample size. However, modification of the task design itself may improve detectability of the relationship between activation and performance. The SOS object and verbal designs consisted of 6 primary conditions (3 control tasks and 3 WM tasks) with 3 levels of demand (6-, 9, 12-word, or 5-, 8-, 11-objects). In actuality, this is a very sparse task design (1 control/task pair for each level of difficulty), though the individual conditions are of significant duration. One task modification that might increase sensitivity would be to repeat the conditions. However, average time to completion for the object and verbal SOS tasks were approximately 6.5 minutes. Repeating conditions significantly increases the length of the task, potentially decreasing participant performance due to loss of attention. Another option is to remove the behavioral modified component of the design and revert to a block design with fixed timing. We have shown performance of SOS was consistent inside and outside of the MRI. It is therefore justifiable to use outside-MRI performance as our regressors in the analysis of our functional data. Using outside performance data, removes the necessity for the participant to select all stimuli before proceeding to the next task level in the fMRI environment, which is similar to the experimental design used in the PET study by Curtis et al. (2000).

SOS for studying WM in fMRI

We have successfully used the eye-tracking based SOS task for fMRI in a group of healthy controls and group of patients being treated for childhood brain tumors. The SOS results were consistent with other neuroimaging studies of WM and were remarkably similar to the N-back results in this study. While this is not completely unexpected, we had hypothesized differences in activation due to the additional process involved in the SOS task such as response selection, visual search, self-monitoring and formation of strategies. Though differences in prefrontal activation were not identified between the tasks, it is still likely differences exist. As previously mentioned, we may be limited by the small sample size, sparse nature of the SOS task design, hidden age effects in the RT1 population or other unknown confounds. However, this research demonstrates that the SOS can be used to study WM performance in an fMRI setting and will give similar and reliable results of mean and demand modulated activation. Previous clinical research, suggests it is more sensitive to group differences than other measures of WM, as such we believe the potential of using the SOS in fMRI still remains.

Analysis of SOS and N-back fMRI data

The fMRI studies presented here used model-driven (GLM) and data-driven (ICA) methods of analysis. Results were generally consistent, in that ICA identified areas with task correlated signals that together resembled the GLM results, even with the behaviorally modified variability of the SOS task. GLM has been well established in the field of fMRI. Accordingly, the techniques provide tested and robust methods of statistical inference and hypothesis testing. However, GLM analysis is limited. In block designs, like the work presented here, GLM provides a static snapshot of accumulated

activity for specific conditions. Consequently, using other analysis methods, such as ICA, is important to further understand phenomena affecting the relationship between behavior and brain activation. What is active is important, but ICA suggests the complex interaction between networks may be as important if not more so. These analysis methods are complementary, not exclusionary. However, interpretation of ICA results is difficult, complicated by "data overload", and lack of established methods for component selection and statistical inference. ICA as applied to fMRI data is rapidly growing area of research. As time progresses, ICA methods will be refined and formalized.

In relation to our results, ICA may explain why detection of performance related effect in GLM analysis was not detected. ICA extracted multiple task related components of both positive and negative correlation, each with a unique time-course. The characteristics of the individual time-courses, or the interactions between these components may provide more information on how behavior relates to inter-network communication between intrinsic neural networks. However, temporal analysis of component time courses is beyond the scope of the work presented here. ICA did detect one interesting difference between the SOS task and N-back task that was not evident with GLM. Coherence between the DLPFC and BA 19 increased in the SOS task. One can hypothesize this is a form of neural recruitment or modulation where a higher order network influences activity in a different network responsible for sub-processes as described in Summerfield et al. (2006).

Working Memory in patients treated for childhood brain tumors

As described in Chapter 1, children treated for childhood brain tumors are at increased risk of developing cognitive deficits. The SOS for fMRI provides a new tool

that will allow us to further investigate deficits of WM in this patient population. Much of the fMRI research at St. Jude Children's Research Hospital is based on an over-arching hypothesis that cognitive deficits are related to altered neural networks. The RT1 pilot study is a first step in looking at how neural networks involved in WM processes differ between healthy controls and our patient population. In particular, our results identify an area in the left parietal cortex that was more active in the healthy group than the patient group. This area is part of the WM network as seen in the mean activation maps and is known to be highly connected with frontal areas. Discussions of neural substrates of WM typically involve the PFC, but it is important that we recognize the distributed nature of neural networks. The other interesting result from the fMRI studies suggest a greater disengagement of the default mode network in healthy controls compared with the RT1 group. We have seen evidence of this in other studies, including a longitudinal study of reading in medulloblastoma survivors and healthy controls (preliminary data).

The results presented support the argument for continued research of WM using fMRI in the St. Jude population. However, an appropriate longitudinal study would require several adjustments including recruitment of a properly aged matched group. Questions of task design optimization, and continued use of the eye-tracker interface to the SOS would have to be addressed. These could be investigated relatively quickly in short studies comparing the behaviorally modified design with fixed a design, and comparing results using the eye-tracker interface with a controller interface respectively.

List of References

Ayr LK, Yeates K, Enrile BG (2005): Arithmetic skills and their cognitive correlates in children with acquired and congenital brain disorder. Journal of the International Neuropsychology Society 11:249-262.

Baddeley A (1986): Working Memory. Oxford University Press. Oxford, England.

Baddeley A (1992): Working Memory. Science 255:556-559.

Baddeley AD, Hitch G (1974): Working Memory. In The Psychology of Learning and Motivation. Academic Press, New York.

Barb SM, Rodriguez-Galindo C, Wilson MW, Phillips NS, Zou P, Scoggins MA, Li Y, Qaddoumi, Helton KJ, Bikhazi G, Haik BG, Ogg RJ (2011): Functional neuroimaging to characterize visual system development in children with retinoblastoma. IOVS 10-5600.

Barnea-Goraly N, Menon V, Eckert M, Tamm L, Bammer R, Karchemskiy A, Dant CC, Reiss AL (2005): White matter development during childhood and adolescence: A cross-sectional diffusion tensor imaging study. Cerebral Cortex 15:1848-1854.

Bell AJ, Sejnowski TJ (1995): An information maximization approach to blind separation and blind deconvolution. Neural Computation 7:1129-1159.

Buxton RB, Uludag K, Dubowitz DJ, Liu TT (2004) Modeling the hemodynamic response to brain activation. Neuroimage 23S1:S220-S223.

Buxton RB, Wong EC, Frank LR (1999): The post-stimulus undershoot of the function MRI signal. In: Moonen CTW, Bandettini PA (eds) Functional MRI, pp 253-262.

Calhoun VD, Adali T, Pearlson GD, Pekar JJ (2001): A method for making group inferences from function MRI data using independent component analysis. Human Brain Mapping 14:140-151.

Callicott JH, Mattay VS, Bertolino A, Finn K, Coppola R, Frank JA, Goldberg TR, Weinberger DR (1999): Physiological characteristics of capacity constraints in working memory s revealed by functional MRI. Cerebral Cortex 9:20-26.

Casey BJ, Galvan A, Hare TA (2005): Changes in cerebral functional organization during cognitive development. J of Current Opinion in Neurobiology 15:239-244.

Casey BJ, Giedd JN, Thomas KM (2000): Structural and functional brain development and its relation to cognitive development. Biological Psychology 54:241-257.

Cavazzuti V, Fischer EG, Welch K, Belli JA, Winston KR (1983): Neurological and psychophysical sequelae following different treatments of craniopharyngioma in children. Journal of Neurosurgery 59:409-417.

Chen C, Okera S, Davies PE, Selva D, Crompton JL (2003): Craniopharyngioma: a review of long-term visual outcome. Clinical and Experimental Ophthalmology 31:220:228.

Cole DM, Smoth SM, Beckmann CF (2010): Advances and pitfalls in the analysis and interpretation of resting-state fMRI data. Frontiers in Systems Neuroscience 4(8):1-15.

Comon P (1994): Independent component analysis, a new concept? Signal Processing 36:287-314.

Conklin HM, Ashfold JM, Skinner, TN, Merchant TE, Ogg RJ, Santana V, Reddick WE, Wu S, Xiong X (2011): Working memory performance among childhood brain tumor survivors treated with conformal radiation therapy: behavioral evidence for pre-frontal cortex vulnerability. Neuropsychology, Submitted.

Conklin HM, Curtis CE, Calkins ME, Iacono WG (2005): Working memory functioning in schizophrenia patients and their first-degree relatives: cognitive functioning shedding light on etiology. Neuropsychologia 43:930-942.

Conklin HM, Luciana M, Hooper CJ, Yarger, RS (2007): Working memory performance in typically developing children and adolescents: Behavioral evidence of protracted frontal lobe development. Developmental Neuropsychology 31:103-128.

Curtis CE, Zald DH, Pardo JB (2000): Organization of working memory within the human prefrontal cortex: A PET study of self-ordered object working memory. Neuropsychologia 38:1503-1510.

De Jonge P (1996): Working memory, intelligence and reading ability and reading ability in children. Personality and Individual Differences 21:1007-1020.

Denckla MB, Rudel R (1974): Rapid automatized naming of pictured objects, colors, letters and numbers by normal children. Cortex 10(2):186-202.

D'Esposito M, Postle BR, Rypma B (2000): Prefrontal cortical contributions to working memory: evidence from event-related fMRI studies. Exp Brain Research 133:3-11.

Duffner PK, Cohen ME, Parker MS (1988): Prospective Intellectual Testing in Children with Brain-Tumors. Annals of Neurology 23:575-579.

Fox MD, Snyder AZ, Vincent JL, Corbetta M, Van Essen DX, Raichle ME (2005): The human brain is intrinsically organized into dynamic, anticorrelated functional networks. Proc Acad Sci USA 102(27)9673-9678.

Friston KJ, Mechelli A, Turner R, Price CJ (2000): Nonlinear responses in fMRI: The balloon model, volterra kernels, and other hemodynamics. Neuroimage 12:466-477.

Friston K, Holmes AP, Worsley KJ, Poline JB, Frith CD, Frackowiak RS (1995): Statistical parametric maps in functional imaging: A general linear model approach. Human Brain Mapping 2:189-210.

Friston KJ, Ashburner JT, Kiebel SJ, Nichols TE, Penny WD (2007): Statistical Parametric Mapping: The Analysis of Functional Brain Images. Elsevier, Boston.

Friston KJ, Zarahn E, Josephs O, Henson RN, Dale AM (1999): Stochastic designs in event-related fMRI. Neuroimage 10:607-619.

Friston K, Worsley KJ, Frackowiak RSJ, Mazziota JC, Evans AC (1994): Assessing the Significance of Focal Activations Using their Spatial Extent. Human Brain Mapping 1:214-220.

Fry AS, Hale S (1996): Processing speed, working memory, and fluid intelligence: evidence for a developmental cascade. Psychological Science 4:237-241.

Gitelman DR, Parrish TB, LaBar KS, Mesulam MM (2000): Real-time monitoring of eye movements using infrared video-oculography during functional magnetic resonance imaging of the frontal eye fields. NeuroImage 11:58-65.

Gogtay N, Geidd JN, Lusk L, Hayashi KM, Greenstein D, Vaituzis AC, Nugent TF, Herman DH, Clasen LS, Toga AW, Rapoport JL, Thompson PM (2004): Dynamic mapping of human cortical development during childhood through early adulthood. PNAS 101:8174-8179.

Goldman-Rakic P. (1987): Development of cortical circuitry and cognitive functions. Child Development 58:642-691.

Goldman-Rakic PS (1995): Cellular basis of working memory. Neuron 14:477-485

Hanten G, Levin HS, Song JX (1999): Working memory and metacognition in sentence comprehension by severely head injured children: A preliminary study with implications for rehabilitation. Developmental Neuropsychology 16:393-414.

Holmes AP, Friston KJ (1998): Generalisability, random effects, and population inference. Neuroimage 7:s754.

James GA, He G, Liu Y (2005): A full-size MRI-compatible keyboard response system. NeuroImage 25:328-331.

Kanowski M, Rieger JW, Noesselt T, Tempelmann C, Hinrichs H (2007): Endoscopic eye tracking system for fMRI. Journal of Neuroscience Methods 160:10-15.

Katzman GL, Dagher AP, Patronas NJ (1999): Incidental findings on brain magnetic resonance imaging from 1000 asymptomatic volunteers. JAMA 281:36-39.

Kim BS, Illes J, Kaplan RT, Reiss A, Atlas SW (2002): Incidental findings on pediatric MR images of the brain. AJ NeuroRadiology 23:1674-1677.

Kimming H, Greenlee MW, Huethe F, Mergner T (1999): MR-Eyetracker: a new method for eye movement recording in functional magnetic resonance imaging. Exp Brain Res 126:443-449.

Klingberg T, Forssberg H, Westerberg H (2002): Increased brain activity in frontal and parietal cortex underlies the development of visuospatial working memory capacity during childhood. J of Cognitive Neuroscience 14:1-10.

Kruger G, Kastrup A, Glover G (2001): Neuroimaging at 1.5 T and 3.0 T: Comparison of oxygenation-sensitive magnetic resonance imaging. Magnetic Resonance in Medicine 45:595-604.

Kruggel F, Cramon DY (1999): Temporal properties of the hemodynamic response in functional MRI. Human Brain Mapping 8:259-271.

Linaberry AM, Ross JA (2008): Childhood and adolescent cancer survival in the US by race and ethnicity for the diagnostic period 1975-1999. Cancer 3:2575-2596.

Logothetis NK, Pfeuffer J (2004): On the nature of the BOLD fMRI contrast mechanism. Magnetic Resonance Imaging 22:1517-1531.

Luciana M, Conklin HM, Hooper CJ, Yarger, RS (2005): The development of nonverbal working memory and executive control processes in adolescents. Child Development 76:697-712.

Luciana M, Nelson CA (1998): The functional emergence of prefrontally-guided working memory systems in four- to eight-year-old children. Neuropsychologia 36:273-293.

Mazziotta JC, Toga AW, Evans A, Fox P, Lancaster J (1995): A probabilistic atlas of the human brain: theory and rationale for its development. The International Consortium for Brain Mapping (ICBM). Neuroimage 2:89-101.

McKeown MJ, Sejnowski TJ (1998): Independent component analysis of fMRI data: examining the assumptions. Human Brain Mapping 6:368-372.

Mulhern RK, Merchant TE, Gajjar A, Reddick WE, Kun L (2004): Late neurocognitive sequelae in survivors of brain tumors in childhood. Lancet Oncology 5:399-408.

Mulhern RK, Palmer SL, Merchant TE, Wallace D, Kocak M, Brouwers P, Krull K, Chintagumpala M, Stargatt R, Ashley DM, Tyc VL, Kun L, Boyett J, Gajjar A (2005): Neurocognitive consequences of risk-adapted therapy for childhood medulloblastoma. Journal of Clinical Oncology 23:5511-5519.

Nelson CA, Monk CS, Lin J, Carver LJ, Thomas KM, Truwit CL (2000): Functional neuroanatomy of spatial working memory in children. Developmental psychology 36:109-116.

Nolte I, Brockmann MA, Gerigk L, Groden C, Schaf J (2010): TrueFISP imaging of the pineal gland: more cysts and more abnormalities. Clin Neurol Neurosurg 112(3):204-208.

Ogawa S, Lee TM, Kay AR, Tank DW (1990): Brain magnetic resonance imaging with contrast dependent on blood oxygenation. Proc Natl Acad Sci 87:5951-5955.

Ogg RJ, Zou P, Allen DN, Hutchins SB, Dutkiewicz RM, Mulhern RK (2008): Neural correlates of a clinical continuous performance test. Magnetic Resonance Imaging 26:504-512.

Owen AM, McMillan KM, Laird AR, Bullmore E (2005): N-back working memory paradigm: A meta-analysis of normative functional neuroimaging studies. Human Brain Mapping 25:46-59.

Packer RJ, Sutton LN, Atkins TE, Radcliffe J, Bunin GR, D'Angio G, Siegal KR, Schut L (1989): A prospective study of cognitive function in children receiving whole-brain radiotherapy and chemotherapy: 2-year results. Journal of Neurosurgery 70:707-713.

Palmer SL, Goloubeva O, Reddick WE, Glass JO, Gajjar A, Kun L, Merchant TW, Mulhern R (2001): Patterns of intellectual development among survivors of pediatric medulloblastoma: a longitudinal analysis. Journal of Clinical Oncology19:2302-2308.

Palmer SL, Reddick WE, Gajjar A (2007): Understanding the cognitive impact on children who are treated for medulloblastoma. Journal of Pediatric Psychology 32:1040-1049.

Palmer SL, Reddick WE, Glass JO, Gajjar A, Goloubeva O, Mulhern RK (2002): Decline in corpus collosum volume among pediatric patients with medulloblastoma: longitudinal MR imaging study. Am J Neuroradiology 23:1088-1094.

Parker GJ, Luzzi S, Alexander DC, Wheeler-Kingshot CA, Ciccarelli O, Ralph MAL (2005): Lateralization of ventral and dorsal auditory-language pathways in the human brain. Neuroimage 24:656-666.

Pauling L, Coryell CD (1936): The magnetic properties and structure of hemoglobin, oxyhemoglobin and carbonmonoxyhemoglobin. Proc Natl Acad Sci 22(4):210-216.

Paus T (2005): Mapping brain maturation and cognitive development during adolescence. Trends in Cognitive Sciences 9:60-68.

Petrides M, Alivisatos B, Meyer E, Evans AC (1992): Functional activation of the human frontal cortex during the performance of verbal working memory tasks. Proc. Natl. Acad. Sci. 90:878-882.

Petrides M, Milner B. (1982): Deficits on subject ordered tasks after frontal- and temporal-lobe lesions in man. Neuropsychologia 20:249-262.

Poldrack RA (2000): Imaging brain plasticity: conceptual and methodological issues – a theoretical review. NeuroImage 12:1-13.

Raichle ME (2009): A paradigm shift in functional brain imaging. Journal of Neuroscience 29:12729-12734.

Raichle ME, MacLeod AM, Snyder AZ, Powers WJ, Gusnard DA, Shulman GL (2001): Inaugural article: a default mode of brain function. Proc Natl Acad Sci USA 98(2):676-682.

Reddick WE, Glass JO, Palmer SL, Wu S, Gajjar A, Langston JW, Kun L, Xiong X, Mulhern RK (2005): Atypical white matter volume development in children following craniospinal irradiation. Neuro-Oncology 7:12-19.

Reddick WE, Russell JM, Glass JO, Xiong X, Mulhern RK, Langston JW, Merchant TE, Kun L, Gajjar A (2000): Subtle white matter volume differences in children treated for medulloblastoma with conventional or reduced dose craniospinal radiation. Magnetic Resonance Imaging 18:787-793.

Reeves CB, Palmer SL, Reddick WE, Merchant TE, Buchanan GM, Gajjar A, Mulhern RK (2006): Attention and memory function among pediatric patients with medulloblastoma. Journal of Pediatric Psychology 31:272-280.

Rissanen J (1983): A universal prior for integers and estimation by minimum description length. Ann Statistics 11:416-431.

Sawamura T, Ikeda J, Ozawa M, Minoshima T, Saito H, Abe H (1995): Magnetic resonance images reveal a high incidence of asymptomatic pineal cysts in young women. Neurosurgery 37(1):11-16.

Smith EE, Jonides J (1998): Neuroimaging analyses of human working memory. Proceedings of the National Academy of Science of the USA 95:12061-12068.

Spiegler BJ, Bouffet E, Greenberg ML, Rutka JT, Mabbot DJ (2004): Change in neurocognitive functioning after treatment with cranial radiation in childhood. Journal of Clinical Oncology 22:706-713.

Summerfield C, Egner T, Greene M, Koechlin E, Mangels J, Hirsch J (2006): Predictive codes for forthcoming perception in the frontal cortex. Science 314:1311-1314
Swanson HL (1999): What develops in working memory? A life span perspective. Developmental Psychology 35:986-1000.

Talairach J, Tournoux P (1988): Co-Planar Stereotraxic atlas of the human brain. Thieme Medical Publishers, Inc. New York.

Thomason ME, Chang CE, Glover GH, Gabrieli JDE, Greicius MD, Gotlib IH (2008): Default-mode function and task-induced deactivation have overlapping brain substrates in children. NeuroImage 41:1493-1503.

Vernooij MW, Ikram MA, Tanghe HL, Vincent AJPE, Hofman A, Krestin GP, Niessen WJ, Breteler MMB, ven der Lugt A (2007): Incidental findings on brain MRI in the general population. N Engl J Med 357:1821-1828.

Visscher KM, Miezin FM, Kelly JE, Buckner RL, Donaldson DI, McAvoy MP, Bhalodia VM, Peterson SE (2003): Mixed blocked/event-related designs separate transient and sustained activity in fMRI. Neuroimage 19:1694-1708.

Waber DP, Pomeroy SL, Chiverton AM, Kieran MW, Scott M, Goumnerova LC, Rivkin MJ (2006): Everyday cognitive function after craniopharyngioma in childhood. Pediatric Neurology 34:13-19.

Wechsler D (1999a): Wechsler abbreviated scale of intelligence. San Antonio, Texas: Harcourt Assessment.

Wechsler D (1999b): Wechsler adult intelligence scale, third edition. San Antonio, Texas. Harcourt Assessment.

Wechsler D (2003): Wechsler Intelligence Scale for Children- Fourth Edition, Integrated. San Antonio, TX: Psychological Corporation.

Zou P, Mulhern RK, Butler RW, Li C-S, Langston JW, Ogg RJ (2005): BOLD Responses to Visual Stimulation in Childhood Cancer Survivors. NeuroImage 24:61-69.

Appendix A: Eye-Calibration Scenario

This appendix contains the source code and associated images for the eye calibration task. The following is the scenario file for the eye-calibration task as described in Chapter 4:

```
# eye_calibrate.sce
#
# Matt Scoggins
# University of Memphis &
# St. Jude Children's Research Hospital
#
# A presentation file to use with eye-tracker calibration.
# Normally
# to calibrate the eye-tracker a screen with 9 points is shown,
# I thought we'd make it a little more enjoyable by throwing up
# a little animation and only showing the calibration points one
# at a time.
#
scenario = "eye_calibrate" ;
no_logfile = true ;
active_buttons = 1 ;
button_codes = 1 ; # left mouse button to proceed, for the
                   # instructor not the MRI-button

screen_width = 1024 ;
screen_height = 768 ;
screen_bit_depth = 16 ;

# background color for the presentation.
# This needs to approximately match the luminance of the
# actual presentation to be run following calibration.
$bg_color = "32,32,32" ;

# !!!
# The coordinates for the 9 calibration points are below at the
# beginning of the pcl section.
# !!!

begin ;

array {
   bitmap {
      filename = "images/eye1.bmp" ;
      trans_src_color = 0,255,0 ;
   } eye1 ;
   bitmap {
      filename = "images/eye2.bmp" ;
      trans_src_color = 0,255,0 ;
   } eye2 ;
   bitmap {
      filename = "images/eye3.bmp" ;
```

```
      trans_src_color = 0,255,0 ;
   } eye3 ;
   bitmap {
      filename = "images/eye4.bmp" ;
      trans_src_color = 0,255,0 ;
   } eye4 ;
   bitmap {
      filename = "images/eye5.bmp" ;
      trans_src_color = 0,255,0 ;
   } eye5 ;
   bitmap {
      filename = "images/eye6.bmp" ;
      trans_src_color = 0,255,0 ;
   } eye6 ;
   bitmap {
      filename = "images/eye7.bmp" ;
      trans_src_color = 0,255,0 ;
   } eye7 ;
   bitmap {
      filename = "images/eye8.bmp" ;
      trans_src_color = 0,255,0 ;
   } eye8 ;
   bitmap {
      filename = "images/eye9.bmp" ;
      trans_src_color = 0,255,0 ;
   } eye9 ;
} pics ;

picture {
   background_color = $bg_color ;
   bitmap eye1 ;
   x = 0 ; y = 0 ;
} bg ;

trial {
   trial_type = first_response ;
   trial_duration = 5000 ;

   picture {
      background_color = $bg_color ;
      text {
         caption = "Thank You!" ;
         font_size = 42 ;
         font_color = 175,175,175 ;
         background_color = $bg_color ;
      } ;
      x = 0 ; y = 0 ;
   } ;
   response_active = true ;
} thanks ;

trial {
   trial_type = first_response ;
   trial_duration = forever ;

   picture {
      background_color = $bg_color ;
```

```
      text {
         caption = "Please follow the spinning eye" ;
         font_size = 48 ;
         font_color = 175,175,175 ;
         background_color = $bg_color ;
      } ;
      x = 0 ; y = 0 ;
   } ;
   response_active = true ;
} instructions ;

trial {
   trial_type = first_response ;
   trial_duration = forever ;

   picture {
      background_color = $bg_color ;
      text {
         caption = "Please follow the spinning eye \none more time" ;
         font_size = 48 ;
         font_color = 175,175,175 ;
         background_color = $bg_color ;
      } ;
      x = 0 ; y = 0 ;
   } ;
   response_active = true ;
} instructions2 ;

########################################################################
begin_pcl ;

int npics = 9 ;
# center coordinates for the 9 points
# these coordinates are taken from the sample calibration bitmap
# from ASL. Why these points aren't symetric about 0,
# I don't know. ???
/*array <int> coords[9][2] = {
   { -416,  284 },
   {    0,  284 },
   {  450,  284 },
   { -416,  -26 },
   {    0,  -26 },
   {  450,  -26 },
   { -416, -332 },
   {    0, -332 },
   {  450, -332 }
} ; */
# changing the calibration points
array <int> coords[9][2] = {
   { -400,  284 },
   {    0,  284 },
   {  400,  284 },
   { -400,  0 },
   {    0,  0 },
   {  400,  0 },
   { -400, -284 },
   {    0, -284 },
```

```
   {  400, -284 }
} ;

array <double> pcoords[9][2] = {
   { 0.0, 0.0 },
   { 0.0, 0.0 },
   { 0.0, 0.0 },
   { 0.0, 0.0 },
   { 0.0, 0.0 },
   { 0.0, 0.0 },
   { 0.0, 0.0 },
   { 0.0, 0.0 },
   { 0.0, 0.0 }
} ;

# below taken from NBSDemo
sub wait (int wait_time)
begin
      loop int time = clock.time()
      until clock.time() > time + wait_time
      begin
      end;
end;
# end NBSDemo code

int response_count = 0 ;
int pic = 1 ;
int n = 1 ;

instructions.present() ;

# We go through the 9 points one time to calibrate
# the eye-tracker
response_count = response_manager.total_response_count() ;
loop until ( n > 9 )
begin
   bg.set_part_x( 1, coords[n][1] ) ;
   bg.set_part_y( 1, coords[n][2] ) ;
   loop until false
   begin
      bg.set_part( 1, pics[pic] ) ;
      bg.present() ;
      pic = pic + 1 ;
      if ( pic > 9 ) then
         pic = 1 ;
      end ;
      if ( response_manager.total_response_count() > response_count )
      then
         response_count = response_manager.total_response_count() ;
         break
      end ;
      wait(50) ;
   end ;
   n = n + 1 ;
end ;

# Eye tracker should be calibrated so we can now use it
```

```
eye_tracker tracker = new eye_tracker( "ASLEyeTracker" ) ;
tracker.send_string( "port=1" ) ;
tracker.start_tracking() ;
tracker.start_data( dt_position, false ) ;

eye_position_data edata ;
int position_count = 0 ;
int throw_away = 10 ;  # Throw away the first couple data points, to
account for
int pcount ;           # reaction time in fixating on the new point
position
double count ;
double x ;
double y ;

instructions2.present() ;

n = 1 ;
response_count = response_manager.total_response_count() ;
loop until ( n > 9 )
begin
   bg.set_part_x( 1, coords[n][1] ) ;
   bg.set_part_y( 1, coords[n][2] ) ;
   pcount = 0 ;
   count = 0.0 ;
   x = 0.0 ;
   y = 0.0 ;
   loop until false
   begin
      bg.set_part( 1, pics[pic] ) ;
      bg.present() ;
      pic = pic + 1 ;
      if ( pic > 9 ) then
         pic = 1 ;
      end ;
      if (tracker.event_count( dt_position ) > position_count)
      then
         position_count = tracker.event_count( dt_position );
         edata = tracker.last_position_data();
         if ( pcount > throw_away ) then
            x = x + edata.x() ;
            y = y + edata.y() ;
            count = count + 1.0 ;
         end ;
         pcount = pcount + 1 ;
      end ;
      if ( response_manager.total_response_count() > response_count )
      then
         response_count = response_manager.total_response_count() ;
         break
      end ;
      wait(50) ;
   end ;
   # gotta test for count = 0
   if ( count > 0.0 ) then
      pcoords[n][1] = x / count ;
      pcoords[n][2] = y / count ;
```

```
   end ;
   n = n + 1 ;
end ;
tracker.stop_data( dt_position ) ;

# Check our matrix points
loop int i = 1
until ( i > 9 )
begin
   if ( pcoords[i][1] == 0.0 || pcoords[i][2] == 0.0 )
   then
      exit( "Calibration Failed! 0's during the 2nd run. Check the
Serial cable. Rerun calibration." ) ;
   end ;
   i = i + 1 ;
end ;

# dump out our screen vs. eyetracker input coordinate data to a file


output_file of = new output_file ;
of.open( "coordinate_map_sub" ) ;
loop int i = 1
until ( i > 9 )
begin
   of.print( coords[i][1] ) ;
   of.print( "\t" ) ;
   of.print( coords[i][2] ) ;
   of.print( "\t" ) ;
   of.print( pcoords[i][1] ) ;
   of.print( "\t" ) ;
   of.print( pcoords[i][2] ) ;
   of.print( "\n" ) ;
   i = i + 1 ;
end ;
of.close() ;

thanks.present() ;
tracker.stop_tracking() ;
```

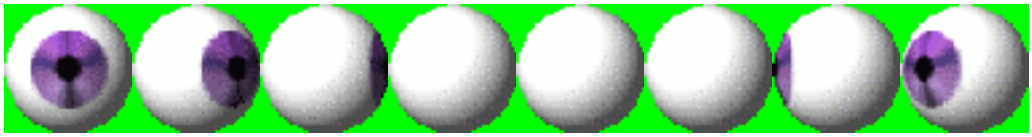

Figure A-1. The spinning eye. Panel shows the images created for the calibration scenario.

Appendix B: SOS Object Scenario

This appendix contains the source code and associated images for the eye-tracking based SOS object task. Additional scenario files (verbal versions, mouse version, etc…) are available by emailing the author at matthew.scoggins@stjude.org or Dr. Robert Ogg at Robert.Ogg@stjude.org.

SOS Object

What follows is entire Presentation scenario file for the eye-tracking based SOS (object task). The code contains a mix of SDL (primary for screen layout) and PCL code. These tasks were based on previous Delphi and E-Prime versions from Clay Curtis, PhD and Catalina Hooper, PhD.

```
# so_objects (Self-ordered Verbal)
#
# Matt Scoggins
# Radiological Sciences
# St. Jude Childrens Research Hospital
# University of Memphis
#
# Converting the self_ordered_objects2 task, originally done in
# E-prime.
#
scenario = "so_objects" ;

scenario_type = fMRI ;
#scenario_type = fMRI_emulation ;
#scan_period = 2000; # for emulation pulse only
pulses_per_scan = 1 ; #mri send 1 pulse per scan volum (TR)
pulse_code = 100 ;

no_logfile = false ;

screen_width = 1024 ;
screen_height = 768 ;
screen_bit_depth = 16 ;

active_buttons = 1 ; # currently only left mouse should be active
button_codes = 1 ;

default_background_color = 25,25,25 ;
default_text_color = 175,175,175 ;
default_font_size = 38 ;
```

```
begin ;

$instr_dur = 2500 ; # time duration instructions are displayed (ms)
$fix_dur = 5000 ;   # time duration fixation screen is displayed (ms)

# image sizes for the different levels
$image_size_3 = 230 ;
$image_size_5 = 210 ;
$image_size_8 = 200 ;
$image_size_11 = 190 ;

# Coordinates for the word picture layout
# I decided to calculate all these based on the desired
# spacing and images sizes, so I don't have to constantly tweak
# hardcoded coordinates for each image placement
$image_spacing = 20 ;  # pixels
# 3+1 level   (2x2 matrix)
$3x1 = '-($image_size_3 + $image_spacing) / 2' ;
$3x2 = '($image_size_3 + $image_spacing) / 2' ;
$3y1 = '($image_size_3 + $image_spacing) / 2' ;
$3y2 = '-($image_size_3 + $image_spacing) / 2' ;
# 5+1 level   (3x2 matrix)
$5x1 = '-($image_size_5 + $image_spacing)' ;
$5x2 = 0 ;
$5x3 = '$image_size_5 + $image_spacing' ;
$5y1 = '($image_size_5 + $image_spacing) / 2' ;
$5y2 = '-($image_size_5 + $image_spacing) / 2' ;
# 8+1 level   (3x3 matrix)
$8x1 = '-($image_size_8 + $image_spacing)' ;
$8x2 = 0 ;
$8x3 = '$image_size_8 + $image_spacing' ;
$8y1 = '$image_size_8 + $image_spacing' ;
$8y2 = 0 ;
$8y3 = '-($image_size_8 + $image_spacing)' ;
# 11+1 level  (4x3 matrix)
$11x1 = '-($image_size_11 + $image_spacing) * 3 / 2 ' ;
$11x2 = '-($image_size_11 + $image_spacing) / 2' ;
$11x3 = '($image_size_11 + $image_spacing) / 2' ;
$11x4 = '($image_size_11 + $image_spacing) * 3 / 2 ' ;
$11y1 = '$image_size_11 + $image_spacing' ;
$11y2 = 0 ;
$11y3 = '-($image_size_11 + $image_spacing)' ;

# our word stimuli
array {
   # objects for the 3-object task
   bitmap { filename = "images/22b.bmp" ; height = $image_size_3 ;
width = $image_size_3 ; } a3_bmp ;
   bitmap { filename = "images/34b.bmp" ; height = $image_size_3 ;
width = $image_size_3 ; } b3_bmp ;
   bitmap { filename = "images/84b.bmp" ; height = $image_size_3 ;
width = $image_size_3 ; } c3_bmp ;
   bitmap { filename = "images/blankc.bmp" ; height = $image_size_3 ;
width = $image_size_3 ; } blank3_bmp ;
   # objects for the 5-object task
   bitmap { filename = "images/29b.bmp" ; height = $image_size_5 ;
width = $image_size_5 ; } a5_bmp ;
```

```
   bitmap { filename = "images/15b.bmp" ; height = $image_size_5 ;
width = $image_size_5 ; } b5_bmp ;
   bitmap { filename = "images/05b.bmp" ; height = $image_size_5 ;
width = $image_size_5 ; } c5_bmp ;
   bitmap { filename = "images/16b.bmp" ; height = $image_size_5 ;
width = $image_size_5 ; } d5_bmp ;
   bitmap { filename = "images/28b.bmp" ; height = $image_size_5 ;
width = $image_size_5 ; } e5_bmp ;
   bitmap { filename = "images/blankc.bmp" ; height = $image_size_5 ;
width = $image_size_5 ; } blank5_bmp ;
   # objects for the 8-object task
   bitmap { filename = "images/74b.bmp" ; height = $image_size_8 ;
width = $image_size_8 ; } a8_bmp ;
   bitmap { filename = "images/45b.bmp" ; height = $image_size_8 ;
width = $image_size_8 ; } b8_bmp ;
   bitmap { filename = "images/78b.bmp" ; height = $image_size_8 ;
width = $image_size_8 ; } c8_bmp ;
   bitmap { filename = "images/65b.bmp" ; height = $image_size_8 ;
width = $image_size_8 ; } d8_bmp ;
   bitmap { filename = "images/26b.bmp" ; height = $image_size_8 ;
width = $image_size_8 ; } e8_bmp ;
   bitmap { filename = "images/60b.bmp" ; height = $image_size_8 ;
width = $image_size_8 ; } f8_bmp ;
   bitmap { filename = "images/86b.bmp" ; height = $image_size_8 ;
width = $image_size_8 ; } g8_bmp ;
   bitmap { filename = "images/72b.bmp" ; height = $image_size_8 ;
width = $image_size_8 ; } h8_bmp ;
   bitmap { filename = "images/blankc.bmp" ; height = $image_size_8 ;
width = $image_size_8 ; } blank8_bmp ;
   # objects for the 11-object task
   bitmap { filename = "images/zerob.bmp" ; height = $image_size_11 ;
width = $image_size_11 ; }  a11_bmp ;
   bitmap { filename = "images/oneb.bmp" ; height = $image_size_11 ;
width = $image_size_11 ; }   b11_bmp ;
   bitmap { filename = "images/sixb.bmp" ; height = $image_size_11 ;
width = $image_size_11 ; }   c11_bmp ;
   bitmap { filename = "images/twob.bmp" ; height = $image_size_11 ;
width = $image_size_11 ; }   d11_bmp ;
   bitmap { filename = "images/fiveb.bmp" ; height = $image_size_11 ;
width = $image_size_11 ; }  e11_bmp ;
   bitmap { filename = "images/threeb.bmp" ; height = $image_size_11 ;
width = $image_size_11 ; } f11_bmp ;
   bitmap { filename = "images/eightb.bmp" ; height = $image_size_11 ;
width = $image_size_11 ; } g11_bmp ;
   bitmap { filename = "images/tenb.bmp" ; height = $image_size_11 ;
width = $image_size_11 ; }   h11_bmp ;
   bitmap { filename = "images/fourb.bmp" ; height = $image_size_11 ;
width = $image_size_11 ; }  i11_bmp ;
   bitmap { filename = "images/nineb.bmp" ; height = $image_size_11 ;
width = $image_size_11 ; }  j11_bmp ;
   bitmap { filename = "images/sevenb.bmp" ; height = $image_size_11 ;
width = $image_size_11 ; } k11_bmp ;
   bitmap { filename = "images/blankc.bmp" ; height = $image_size_11 ;
width = $image_size_11 ; } blank11_bmp ;
} stims ;

/* array {
```

```
   # objects for the 3-object task
   bitmap { filename = "images/1.bmp" ; height = $image_size_3 ; width
= $image_size_3 ; } a3_bmp ;
   bitmap { filename = "images/2.bmp" ; height = $image_size_3 ; width
= $image_size_3 ; } b3_bmp ;
   bitmap { filename = "images/4.bmp" ; height = $image_size_3 ; width
= $image_size_3 ; } c3_bmp ;
   bitmap { filename = "images/blankc.bmp" ; height = $image_size_3 ;
width = $image_size_3 ; } blank3_bmp ;
   # objects for the 5-object task
   bitmap { filename = "images/6.bmp" ; height = $image_size_5 ; width
= $image_size_5 ; } a5_bmp ;
   bitmap { filename = "images/9.bmp" ; height = $image_size_5 ; width
= $image_size_5 ; } b5_bmp ;
   bitmap { filename = "images/10.bmp" ; height = $image_size_5 ; width
= $image_size_5 ; } c5_bmp ;
   bitmap { filename = "images/14.bmp" ; height = $image_size_5 ; width
= $image_size_5 ; } d5_bmp ;
   bitmap { filename = "images/20.bmp" ; height = $image_size_5 ; width
= $image_size_5 ; } e5_bmp ;
   bitmap { filename = "images/blankc.bmp" ; height = $image_size_5 ;
width = $image_size_5 ; } blank5_bmp ;
   # objects for the 8-object task
   bitmap { filename = "images/24.bmp" ; height = $image_size_8 ; width
= $image_size_8 ; } a8_bmp ;
   bitmap { filename = "images/25.bmp" ; height = $image_size_8 ; width
= $image_size_8 ; } b8_bmp ;
   bitmap { filename = "images/27.bmp" ; height = $image_size_8 ; width
= $image_size_8 ; } c8_bmp ;
   bitmap { filename = "images/30.bmp" ; height = $image_size_8 ; width
= $image_size_8 ; } d8_bmp ;
   bitmap { filename = "images/37.bmp" ; height = $image_size_8 ; width
= $image_size_8 ; } e8_bmp ;
   bitmap { filename = "images/43.bmp" ; height = $image_size_8 ; width
= $image_size_8 ; } f8_bmp ;
   bitmap { filename = "images/44.bmp" ; height = $image_size_8 ; width
= $image_size_8 ; } g8_bmp ;
   bitmap { filename = "images/56.bmp" ; height = $image_size_8 ; width
= $image_size_8 ; } h8_bmp ;
   bitmap { filename = "images/blankc.bmp" ; height = $image_size_8 ;
width = $image_size_8 ; } blank8_bmp ;
   # objects for the 11-object task
   bitmap { filename = "images/70.bmp" ; height = $image_size_11 ;
width = $image_size_11 ; }  a11_bmp ;
   bitmap { filename = "images/79.bmp" ; height = $image_size_11 ;
width = $image_size_11 ; }   b11_bmp ;
   bitmap { filename = "images/87.bmp" ; height = $image_size_11 ;
width = $image_size_11 ; }   c11_bmp ;
   bitmap { filename = "images/95.bmp" ; height = $image_size_11 ;
width = $image_size_11 ; }   d11_bmp ;
   bitmap { filename = "images/108.bmp" ; height = $image_size_11 ;
width = $image_size_11 ; }  e11_bmp ;
   bitmap { filename = "images/111.bmp" ; height = $image_size_11 ;
width = $image_size_11 ; } f11_bmp ;
   bitmap { filename = "images/116.bmp" ; height = $image_size_11 ;
width = $image_size_11 ; } g11_bmp ;
```

```
   bitmap { filename = "images/120.bmp" ; height = $image_size_11 ;
width = $image_size_11 ; }   h11_bmp ;
   bitmap { filename = "images/h1.bmp" ; height = $image_size_11 ;
width = $image_size_11 ; }  i11_bmp ;
   bitmap { filename = "images/rr2.bmp" ; height = $image_size_11 ;
width = $image_size_11 ; }  j11_bmp ;
   bitmap { filename = "images/rr5.bmp" ; height = $image_size_11 ;
width = $image_size_11 ; } k11_bmp ;
   bitmap { filename = "images/blankc.bmp" ; height = $image_size_11 ;
width = $image_size_11 ; } blank11_bmp ;
} stims ; */

# boxes as a border for each image region
$border_color = "175,175,175" ; # border
$border_width = 1 ;
array {
   box { color = $border_color ; height = '$image_size_3 +
$border_width * 2' ;
      width = '$image_size_3 + $border_width * 2' ; } border_3 ;
   box { color = $border_color ; height = '$image_size_5 +
$border_width * 2' ;
      width = '$image_size_5 + $border_width * 2' ; } border_5 ;
   box { color = $border_color ; height = '$image_size_8 +
$border_width * 2' ;
      width = '$image_size_8 + $border_width * 2' ; } border_8 ;
   box { color = $border_color ; height = '$image_size_11 +
$border_width * 2' ;
      width = '$image_size_11 + $border_width * 2' ; } border_11 ;
} borders ;

# boxes for highlighting selections
$box_color = "255,0,255" ; # purple
$box_select_color = "0,0,255" ; # blue
$box_width = 6 ;
# our boxes, based on the images sizes specified above
array {
   box { color = $box_color ; height = '$image_size_3 + $box_width * 2'
;
      width = '$image_size_3 + $box_width * 2' ; } high_box_3 ;
   box { color = $box_color ; height = '$image_size_5 + $box_width * 2'
;
      width = '$image_size_5 + $box_width * 2' ; } high_box_5 ;
   box { color = $box_color ; height = '$image_size_8 + $box_width * 2'
;
      width = '$image_size_8 + $box_width * 2' ; } high_box_8 ;
   box { color = $box_color ; height = '$image_size_11 + $box_width *
2' ;
      width = '$image_size_11 + $box_width * 2' ; } high_box_11 ;
} high_boxes ;

bitmap { filename = "images/asterisk2.bmp" ; transparent_color =
0,255,0 ; } astr ;

# Fixation Pic
picture {
      text { caption = "+" ; font = "Courier" ; font_size = 68 ; } ;
      x = 0 ;
```

```
      y = 0 ;
} fix_pic ;

picture {
   text {
      caption = "Select the object \nwith the \'*\'" ;
      font_size = 68 ;
   } ;
   x = 0 ; y = 0 ;
} cntrl_pic ;

picture {
   text {
      caption = "Select each object \nonly once" ;
      font_size = 68 ;
   } ;
   x = 0 ; y = 0 ;
} task_pic ;

array {
   picture {
      bitmap a3_bmp ;
      x = $3x1 ; y = $3y1 ;
      bitmap b3_bmp ;
      x = $3x2 ; y = $3y1 ;
      bitmap c3_bmp ;
      x = $3x1 ; y = $3y2 ;
      bitmap blank3_bmp ;
      x = $3x2 ; y = $3y2 ;
      box border_3 ;
      x = $3x1 ; y = $3y1 ;
      box border_3 ;
      x = $3x2 ; y = $3y1 ;
      box border_3 ;
      x = $3x1 ; y = $3y2 ;
      box border_3 ;
      x = $3x2 ; y = $3y2 ;
   } obj3_pic ;
   picture {
      bitmap a5_bmp ;
      x = $5x1 ; y = $5y1 ;
      bitmap b5_bmp ;
      x = $5x2 ; y = $5y1 ;
      bitmap c5_bmp ;
      x = $5x3 ; y = $5y1 ;
      bitmap d5_bmp ;
      x = $5x1 ; y = $5y2 ;
      bitmap e5_bmp ;
      x = $5x2 ; y = $5y2 ;
      bitmap blank5_bmp ;
      x = $5x3 ; y = $5y2 ;
      box border_5 ;
      x = $5x1 ; y = $5y1 ;
      box border_5 ;
      x = $5x2 ; y = $5y1 ;
      box border_5 ;
      x = $5x3 ; y = $5y1 ;
```

```
   box border_5 ;
   x = $5x1 ; y = $5y2 ;
   box border_5 ;
   x = $5x2 ; y = $5y2 ;
   box border_5 ;
   x = $5x3 ; y = $5y2 ;
} obj5_pic ;
picture {
   bitmap a8_bmp ;
   x = $8x1 ; y = $8y1 ;
   bitmap b8_bmp ;
   x = $8x2 ; y = $8y1 ;
   bitmap c8_bmp ;
   x = $8x3 ; y = $8y1 ;
   bitmap d8_bmp ;
   x = $8x1 ; y = $8y2 ;
   bitmap e8_bmp ;
   x = $8x2 ; y = $8y2 ;
   bitmap f8_bmp ;
   x = $8x3 ; y = $8y2 ;
   bitmap g8_bmp ;
   x = $8x1 ; y = $8y3 ;
   bitmap h8_bmp ;
   x = $8x2 ; y = $8y3 ;
   bitmap blank8_bmp ;
   x = $8x3 ; y = $8y3 ;
   box border_8 ;
   x = $8x1 ; y = $8y1 ;
   box border_8 ;
   x = $8x2 ; y = $8y1 ;
   box border_8 ;
   x = $8x3 ; y = $8y1 ;
   box border_8 ;
   x = $8x1 ; y = $8y2 ;
   box border_8 ;
   x = $8x2 ; y = $8y2 ;
   box border_8 ;
   x = $8x3 ; y = $8y2 ;
   box border_8 ;
   x = $8x1 ; y = $8y3 ;
   box border_8 ;
   x = $8x2 ; y = $8y3 ;
   box border_8 ;
   x = $8x3 ; y = $8y3 ;
} obj8_pic ;
picture {
   bitmap a11_bmp ;
   x = $11x1 ; y = $11y1 ;
   bitmap b11_bmp ;
   x = $11x2 ; y = $11y1 ;
   bitmap c11_bmp ;
   x = $11x3 ; y = $11y1 ;
   bitmap d11_bmp ;
   x = $11x4 ; y = $11y1 ;
   bitmap e11_bmp ;
   x = $11x1 ; y = $11y2 ;
   bitmap f11_bmp ;
```

```
      x = $11x2 ; y = $11y2 ;
      bitmap g11_bmp ;
      x = $11x3 ; y = $11y2 ;
      bitmap h11_bmp ;
      x = $11x4 ; y = $11y2 ;
      bitmap i11_bmp ;
      x = $11x1 ; y = $11y3 ;
      bitmap j11_bmp ;
      x = $11x2 ; y = $11y3 ;
      bitmap k11_bmp ;
      x = $11x3 ; y = $11y3 ;
      bitmap blank11_bmp ;
      x = $11x4 ; y = $11y3 ;
      box border_11 ;
      x = $11x1 ; y = $11y1 ;
      box border_11 ;
      x = $11x2 ; y = $11y1 ;
      box border_11 ;
      x = $11x3 ; y = $11y1 ;
      box border_11 ;
      x = $11x4 ; y = $11y1 ;
      box border_11 ;
      x = $11x1 ; y = $11y2 ;
      box border_11 ;
      x = $11x2 ; y = $11y2 ;
      box border_11 ;
      x = $11x3 ; y = $11y2 ;
      box border_11 ;
      x = $11x4 ; y = $11y2 ;
      box border_11 ;
      x = $11x1 ; y = $11y3 ;
      box border_11 ;
      x = $11x2 ; y = $11y3 ;
      box border_11 ;
      x = $11x3 ; y = $11y3 ;
      box border_11 ;
      x = $11x4 ; y = $11y3 ;
   } obj11_pic ;
} pics ;

# Simple trials for fixation and instruction screens
trial {
   trial_type = fixed ;
   trial_duration = stimuli_length ;

   picture fix_pic ;
   mri_pulse = 1 ;
   duration = $fix_dur ;
   code = "Fixation" ;
} fixation ;

trial {
   trial_type = fixed;
      trial_duration = stimuli_length;

      picture cntrl_pic ;
      duration = $instr_dur ;
```

```
      code = "Control Instructions" ;
} cntrl_instr ;

trial {
   trial_type = fixed;
      trial_duration = stimuli_length;

      picture task_pic ;
      duration = $instr_dur ;
      code = "Task Instructions" ;
} task_instr ;

##############################################################################
##########
begin_pcl ;

# variables needed for all levels
int pos_x = 0 ;
int pos_y = 0 ;
int selected = 0 ; # array position selected
bool highlighted = false ;
int cell = 0 ;
int try = 1 ;
int astr_part_num = 0 ;
int high_box_part_num = 0 ;
int start_time = 0 ;
int stop_time = 0 ;
int timeout = 600000 ; # bail after 10 minutes
int selected_stim ;   # stimulus selected
int response_count ;
int blank_part = 0 ;
int rndm ;

# level specific variables
#
# I'm doing things a couple different ways here... sometimes I lump
everything in to a big array
# and use level specific indices, other times I'm keeping lots of
things in multidimensional array,
# easy to index since we're going to be in a top level loop, but it
means we have to have a
# couple of place fillers.
array <int> levels[4] = { 4, 6, 9, 12 } ;      # defines number of
stimuli (including blanks) in the tasks
array <int> tries[4] = { 9, 15, 24, 33 } ;    # give up after a while
(3N)
array <int> cntrl_tries[4] = { 3, 5, 8, 11 } ; # should match the
number of stimuli
array <int> dims[4][2] = {    # dimensions of our stimulus arrays.
{rows, columns}
   { 2, 2 },
   { 2, 3 },
   { 3, 3 },
   { 3, 4 }
} ;
```

```
# Since we have all the stimuli specific in a big SDL array, we need to
point to the
# first stimuli for each level task
array <int> stim_ndx[4] = { 1, 5, 11, 20 } ;

array <int> cntrl_task[4][12] = {              # order of which stimuli
get the asterisk in the control task
   { 1, 2, 3, 0, 0, 0, 0, 0, 0, 0, 0, 0 },
   { 1, 2, 3, 4, 5, 0, 0, 0, 0, 0, 0, 0 },
   { 1, 2, 3, 4, 5, 6, 7, 8, 0, 0, 0, 0 },
   { 1, 2, 3, 4, 5, 6, 7, 8, 9, 10, 11, 0 }
} ;

# Here's how we handle moving the blank to the last selected location
# This is certainly not the cleanest way, or most efficient, but this
# is the way I was forced to do it in E-Prime, so I'm just translating
it
# to Presentation until I think of a better way to do this.
#
# We're using stim_ndx to point to placements for the corresponding
levels.
# Have to use some 0 filling.
# We take the last selected position (where the blank needs to go)
# as our index into the array below. Then we'll get a random number
from 1-3
# as our index into the next layer of the array. Finally,
# we're going to go through the non-blank images in order and put them
in
# the locations below.
array <int> placements[31][3][11] = {
   ## 3+1 level
   { # blank in the first (1,1) position
      { 2, 3, 4, 0, 0, 0, 0, 0, 0, 0, 0 },
      { 3, 4, 2, 0, 0, 0, 0, 0, 0, 0, 0 },
      { 4, 2, 3, 0, 0, 0, 0, 0, 0, 0, 0 }
   },
   { # blank in the 2nd (1,2) position
      { 3, 4, 1, 0, 0, 0, 0, 0, 0, 0, 0 },
      { 4, 1, 3, 0, 0, 0, 0, 0, 0, 0, 0 },
      { 1, 4, 3, 0, 0, 0, 0, 0, 0, 0, 0 }
   },
   { # blank in the 3rd (2,1) position
      { 2, 1, 4, 0, 0, 0, 0, 0, 0, 0, 0 },
      { 1, 4, 2, 0, 0, 0, 0, 0, 0, 0, 0 },
      { 4, 1, 2, 0, 0, 0, 0, 0, 0, 0, 0 }
   },
   { # blank in the 4th (2,2) position
      { 1, 3, 2, 0, 0, 0, 0, 0, 0, 0, 0 },
      { 3, 2, 1, 0, 0, 0, 0, 0, 0, 0, 0 },
      { 2, 1, 3, 0, 0, 0, 0, 0, 0, 0, 0 }
   },
   ## 5+1 level
   { # blank 1,1
      { 2, 3, 4, 5, 6, 0, 0, 0, 0, 0, 0 },
      { 4, 2, 6, 3, 5, 0, 0, 0, 0, 0, 0 },
      { 6, 5, 2, 3, 4, 0, 0, 0, 0, 0, 0 }
   },
```

```
{ # blank 1,2
   { 3, 5, 1, 4, 6, 0, 0, 0, 0, 0, 0 },
   { 5, 4, 3, 6, 1, 0, 0, 0, 0, 0, 0 },
   { 1, 6, 4, 3, 5, 0, 0, 0, 0, 0, 0 }
},
{ # blank 1,3
   { 2, 4, 1, 5, 6, 0, 0, 0, 0, 0, 0 },
   { 1, 2, 5, 6, 4, 0, 0, 0, 0, 0, 0 },
   { 4, 6, 2, 1, 5, 0, 0, 0, 0, 0, 0 }
},
{ # blank 2,1
   { 5, 1, 6, 2, 3, 0, 0, 0, 0, 0, 0 },
   { 6, 5, 3, 1, 2, 0, 0, 0, 0, 0, 0 },
   { 3, 2, 1, 5, 6, 0, 0, 0, 0, 0, 0 }
},
{ # blank 2,2
   { 6, 4, 1, 3, 2, 0, 0, 0, 0, 0, 0 },
   { 3, 1, 6, 2, 4, 0, 0, 0, 0, 0, 0 },
   { 6, 2, 4, 1, 3, 0, 0, 0, 0, 0, 0 }
},
{ # blank 2,3
   { 5, 1, 2, 3, 4, 0, 0, 0, 0, 0, 0 },
   { 1, 4, 3, 5, 2, 0, 0, 0, 0, 0, 0 },
   { 4, 5, 1, 3, 2, 0, 0, 0, 0, 0, 0 }
},
## 8+1 level
{ # blank 1,1
   { 2, 3, 4, 5, 6, 7, 8, 9, 0, 0, 0 },
   { 4, 5, 7, 2, 9, 6, 3, 8, 0, 0, 0 },
   { 8, 4, 2, 6, 7, 9, 5, 3, 0, 0, 0 }
},
{ # blank 1,2
   { 5, 1, 6, 4, 3, 9, 7, 8, 0, 0, 0 },
   { 7, 3, 4, 8, 5, 1, 9, 6, 0, 0, 0 },
   { 3, 6, 8, 9, 1, 7, 5, 4, 0, 0, 0 }
},
{ # blank 1,3
   { 4, 7, 5, 6, 1, 8, 2, 9, 0, 0, 0 },
   { 7, 9, 1, 8, 4, 2, 5, 6, 0, 0, 0 },
   { 9, 8, 6, 5, 7, 1, 4, 2, 0, 0, 0 }
},
{ # blank 2,1
   { 6, 5, 1, 2, 9, 7, 3, 8, 0, 0, 0 },
   { 1, 6, 9, 3, 8, 2, 7, 5, 0, 0, 0 },
   { 2, 3, 7, 1, 5, 8, 6, 9, 0, 0, 0 }
},
{ # blank 2,2
   { 7, 1, 9, 3, 4, 8, 2, 6, 0, 0, 0 },
   { 4, 2, 7, 6, 3, 9, 1, 8, 0, 0, 0 },
   { 2, 7, 4, 3, 1, 6, 9, 8, 0, 0, 0 }
},
{ # blank 2,3
   { 5, 4, 7, 1, 2, 9, 8, 3, 0, 0, 0 },
   { 8, 3, 9, 4, 5, 1, 2, 7, 0, 0, 0 },
   { 5, 9, 1, 7, 4, 2, 8, 3, 0, 0, 0 }
},
{ # blank 3,1
```

```
   { 9, 1, 4, 5, 8, 6, 3, 2, 0, 0, 0 },
   { 5, 9, 1, 8, 6, 3, 2, 4, 0, 0, 0 },
   { 3, 5, 8, 4, 9, 2, 1, 6, 0, 0, 0 }
},
{ # blank 3,2
   { 5, 6, 9, 4, 3, 1, 7, 2, 0, 0, 0 },
   { 3, 4, 6, 2, 7, 1, 9, 5, 0, 0, 0 },
   { 4, 2, 7, 3, 1, 5, 6, 9, 0, 0, 0 }
},
{ # blank 3,3
   { 2, 3, 5, 6, 4, 7, 8, 1, 0, 0, 0 },
   { 8, 1, 3, 4, 2, 6, 5, 7, 0, 0, 0 },
   { 6, 7, 8, 3, 5, 4, 2, 1, 0, 0, 0 }
},
## 11+1 level
{ # blank 1,1
   { 2, 3, 4, 5, 6, 7, 8, 9, 10, 11, 12 },
   { 8, 7, 9, 12, 4, 11, 5, 2, 6, 3, 10 },
   { 5, 8, 6, 9, 3, 10, 2, 7, 4, 12, 11 }
},
{ # blank 1,2
   { 12, 4, 3, 5, 7, 6, 1, 11, 10, 9, 8 },
   { 8, 12, 10, 11, 9, 4, 6, 3, 7, 5, 1 },
   { 9, 1, 7, 5, 11, 10, 4, 6, 3, 8, 12 }
},
{ # blank 1,3
   { 4, 7, 5, 2, 8, 11, 9, 12, 6, 10, 1 },
   { 1, 4, 2, 6, 11, 9, 12, 10, 8, 5, 7 },
   { 7, 2, 8, 12, 6, 5, 10, 4, 11, 9, 1 }
},
{ # blank 1,4
   { 5, 6, 11, 10, 3, 2, 7, 9, 8, 12, 1 },
   { 7, 10, 9, 5, 1, 3, 11, 6, 12, 2, 8 },
   { 9, 8, 12, 2, 1, 7, 5, 3, 6, 10, 1 }
},
{ # blank 2,1
   { 7, 11, 6, 12, 4, 10, 3, 9, 2, 8, 1 },
   { 10, 7, 4, 11, 1, 2, 6, 12, 8, 3, 9 },
   { 11, 12, 2, 8, 7, 4, 9, 10, 3, 6, 1 }
},
{ # blank 2,2
   { 2, 4, 3, 10, 5, 8, 11, 7, 1, 9, 12 },
   { 5, 1, 7, 8, 10, 11, 12, 9, 3, 2, 4 },
   { 11, 7, 10, 4, 12, 2, 9, 3, 8, 5, 1 }
},
{ # blank 2,3
   { 10, 4, 8, 12, 9, 5, 3, 2, 11, 1, 6 },
   { 2, 9, 4, 10, 5, 11, 6, 1, 8, 12, 3 },
   { 5, 12, 2, 4, 3, 9, 1, 10, 11, 6, 8 }
},
{ # blank 2,4
   { 9, 10, 5, 12, 6, 1, 2, 4, 7, 3, 11 },
   { 11, 6, 7, 2, 10, 3, 5, 4, 12, 9, 1 },
   { 12, 3, 9, 7, 4, 11, 10, 5, 6, 1, 2 }
},
{ # blank 3,1
   { 7, 1, 6, 4, 2, 8, 5, 12, 3, 11, 10 },
```

```
      { 5, 4, 3, 11, 6, 10, 12, 7, 2, 8, 1 },
      { 3, 8, 11, 6, 1, 12, 10, 2, 5, 4, 7 }
   },
   { # blank 3,2
      { 5, 6, 9, 11, 3, 4, 7, 8, 1, 2, 12 },
      { 8, 4, 12, 9, 7, 2, 3, 1, 5, 6, 11 },
      { 3, 1, 7, 12, 11, 8, 5, 4, 9, 2, 6 }
   },
   { # blank 3,3
      { 7, 12, 5, 8, 9, 3, 2, 6, 4, 1, 10 },
      { 9, 2, 3, 10, 7, 5, 6, 8, 1, 12, 4 },
      { 5, 6, 4, 7, 3, 12, 9, 10, 8, 1, 2 }
   },
   { # blank 3,4
      { 4, 9, 8, 5, 2, 10, 7, 1, 11, 3, 6 },
      { 2, 5, 11, 3, 7, 6, 10, 4, 8, 9, 1 },
      { 5, 3, 9, 1, 10, 2, 6, 11, 4, 7, 8 }
   }
} ;

# We have to keep up with which images have been chosen, so we can
# proceed to next section if all the images have been selected
# before <tries> attempts.
# So here's how I'm doing it... array of int's. The index corresponds
# to whatever image defined above (usually, a3_bmp, b3_, etc...)
# The 2nd value is the current position in the display matrix.
# The second value is 0 for not-selected, or 1 for previously selected
# Again, we're doing one big multidimensional array, so using some
space fillers.
array <int> chosen[4][12][2] = {
   # initial positions have to match the SDL code.
   {
      {1, 0}, {2, 0}, {3, 0}, {4, 0}, {0, 0}, {0, 0},
      {0, 0}, {0, 0}, {0, 0}, {0, 0}, {0, 0}, {0, 0}
   },
   {
      {1, 0}, {2, 0}, {3, 0}, {4, 0}, {5, 0}, {6, 0},
      {0, 0}, {0, 0}, {0, 0}, {0, 0}, {0, 0}, {0, 0}
   },
   {
      {1, 0}, {2, 0}, {3, 0}, {4, 0}, {5, 0}, {6, 0},
      {7, 0}, {8, 0}, {9, 0}, {0, 0}, {0, 0}, {0, 0}
   },
   {
      {1, 0}, {2, 0}, {3, 0}, {4, 0}, {5, 0}, {6, 0},
      {7, 0}, {7, 0}, {8, 0}, {10, 0}, {11, 0}, {12, 0}
   }
} ;

array <int> image_size[4] = { 230, 210, 200, 190 } ; # square
int image_spacing = 20 ; # These values need to match those in SDL

# another multidimensional array for coordinates
# Since I can't see SDL variables, we have to create new ones
array <int> coords[4][12][2] ;
# 2x2, 4 stimuli array
coords[1][1][1] = -(image_size[1] + image_spacing) / 2 ;
```

```
coords[1][3][1] = -(image_size[1] + image_spacing) / 2 ;
coords[1][1][2] = (image_size[1] + image_spacing) / 2 ;
coords[1][2][2] = (image_size[1] + image_spacing) / 2 ;
coords[1][2][1] = (image_size[1] + image_spacing) / 2 ;
coords[1][4][1] = (image_size[1] + image_spacing) / 2 ;
coords[1][3][2] = -(image_size[1] + image_spacing) / 2 ;
coords[1][4][2] = -(image_size[1] + image_spacing) / 2 ;
# 2x3, 6 stimuli array
coords[2][1][1] = -(image_size[2] + image_spacing) ;
coords[2][4][1] = -(image_size[2] + image_spacing) ;
coords[2][1][2] = (image_size[2] + image_spacing) / 2 ;
coords[2][2][2] = (image_size[2] + image_spacing) / 2 ;
coords[2][3][2] = (image_size[2] + image_spacing) / 2 ;
coords[2][2][1] = 0 ;
coords[2][5][1] = 0 ;
coords[2][3][1] = (image_size[2] + image_spacing) ;
coords[2][6][1] = (image_size[2] + image_spacing) ;
coords[2][4][2] = -(image_size[2] + image_spacing) / 2 ;
coords[2][5][2] = -(image_size[2] + image_spacing) / 2 ;
coords[2][6][2] = -(image_size[2] + image_spacing) / 2 ;
# 3x3, 9 stimuli array
coords[3][1][1] = -(image_size[3] + image_spacing) ;
coords[3][4][1] = -(image_size[3] + image_spacing) ;
coords[3][7][1] = -(image_size[3] + image_spacing) ;
coords[3][1][2] = (image_size[3] + image_spacing) ;
coords[3][2][2] = (image_size[3] + image_spacing) ;
coords[3][3][2] = (image_size[3] + image_spacing) ;
coords[3][2][1] = 0 ;
coords[3][5][1] = 0 ;
coords[3][8][1] = 0 ;
coords[3][4][2] = 0 ;
coords[3][5][2] = 0 ;
coords[3][6][2] = 0 ;
coords[3][3][1] = (image_size[3] + image_spacing) ;
coords[3][6][1] = (image_size[3] + image_spacing) ;
coords[3][9][1] = (image_size[3] + image_spacing) ;
coords[3][7][2] = -(image_size[3] + image_spacing) ;
coords[3][8][2] = -(image_size[3] + image_spacing) ;
coords[3][9][2] = -(image_size[3] + image_spacing) ;
# 3x4, 12 stimuli array
coords[4][1][1] = -(image_size[4] + image_spacing) * 3 / 2 ;
coords[4][5][1] = -(image_size[4] + image_spacing) * 3 / 2 ;
coords[4][9][1] = -(image_size[4] + image_spacing) * 3 / 2 ;
coords[4][2][1] = -(image_size[4] + image_spacing) / 2 ;
coords[4][6][1] = -(image_size[4] + image_spacing) / 2 ;
coords[4][10][1] = -(image_size[4] + image_spacing) / 2 ;
coords[4][3][1] = (image_size[4] + image_spacing) / 2 ;
coords[4][7][1] = (image_size[4] + image_spacing) / 2 ;
coords[4][11][1] = (image_size[4] + image_spacing) / 2 ;
coords[4][4][1] = (image_size[4] + image_spacing) * 3 / 2 ;
coords[4][8][1] = (image_size[4] + image_spacing) * 3 / 2 ;
coords[4][12][1] = (image_size[4] + image_spacing) * 3 / 2 ;
coords[4][1][2] = (image_size[4] + image_spacing) ;
coords[4][2][2] = (image_size[4] + image_spacing) ;
coords[4][3][2] = (image_size[4] + image_spacing) ;
coords[4][4][2] = (image_size[4] + image_spacing) ;
coords[4][5][2] = 0 ;
```

```
coords[4][6][2] = 0 ;
coords[4][7][2] = 0 ;
coords[4][8][2] = 0 ;
coords[4][9][2] = -(image_size[4] + image_spacing) ;
coords[4][10][2] = -(image_size[4] + image_spacing) ;
coords[4][11][2] = -(image_size[4] + image_spacing) ;
coords[4][12][2] = -(image_size[4] + image_spacing) ;

# below taken from NBSDemo
sub wait (int wait_time)
begin
      loop int time = clock.time()
      until clock.time() > time + wait_time
      begin
      end;
end;
# end NBSDemo code

# open a file for debugging
output_file dbug = new output_file ;
string dbug_log_file = logfile.subject() ;
dbug_log_file.append( "-so_objects_selection_data.log" ) ;
dbug.open( dbug_log_file, false ) ;

# open a new log file for our performance data
output_file log = new output_file ;
string perf_log_file = logfile.subject() ;
perf_log_file.append( "-so_objects_performance.log" ) ;
log.open( perf_log_file, false ) ;

#=========================================================================
===
# check_timeout()
# subroutine to check if we've gone over the time limit. Bail out with
# a message if so
#=========================================================================
===
sub check_timeout begin
   if ( clock.time() > timeout ) then
      log.print( "\n!!!Timeout!!!\nUnsuccessful in completing within "
) ;
      log.print( timeout ) ;
      log.print( " milliseconds\ntry: " ) ;
      log.print( try ) ;
      exit() ;
   end ;
end ;

#=========================================================================
===
# get_position
# subroutine for determining which cell in the stimuli matrix was
selected
#=========================================================================
===
sub int get_position( int tsk, int x, int y )
begin
```

```
   int rn ;
   int cn ;
   int ro = 0 ;
   int co = 0 ;
   int hw = image_size[tsk]/2 ; # only calculate this once

   # determine what row we're on
   loop int r = 1
   until r > dims[tsk][1]
   begin
      rn = (r-1)*dims[tsk][2]+1 ;
      if ( (y >= (coords[tsk][rn][2]-hw)) && (y <=
(coords[tsk][rn][2]+hw)) )
      then
         ro = r ;
         break ;
      end ;
      r = r + 1 ;
   end ;
   if ( ro == 0 ) then
      return 0 ;
   end ;
   # determine the column
   loop int c = 1
   until c > dims[tsk][2]
   begin
      cn = c ;
      if ( (x >= (coords[tsk][cn][1]-hw)) && (x <=
(coords[tsk][cn][1]+hw)) )
      then
         co = c ;
         break ;
      end ;
      c = c + 1 ;
   end ;
   if ( co == 0 ) then
      return 0 ;
   end ;
   return (ro-1)*dims[tsk][2]+co ;
end ;

#=====================================================================
==========
# Coordinate mapping between the screen and the eye tracker data
#
# Our eye-tracker calibration scenario <eye_calibrate_map.sce> creates
a file
# that looks like 9 lines of...
# screen-x  screen-y eyetracker-x   eyetracker-y
# ...
# ...
#=====================================================================
==========
array <int> screen_coords[9][2] ;
array <double> eye_coords[9][2] ;
input_file mapfile = new input_file ;
mapfile.open( logfile_directory + "\coordinate_map", true ) ;
```

```
loop int i = 1
until ( i > 9 )
begin
   screen_coords[i][1] = mapfile.get_int() ;
   screen_coords[i][2] = mapfile.get_int() ;
   eye_coords[i][1] = mapfile.get_double() ;
   eye_coords[i][2] = mapfile.get_double() ;
   if( !mapfile.last_succeeded() ) then
      exit( "Unable to read coordinates from coordinate_map" ) ;
   end ;
   i = i + 1 ;
end ;
mapfile.close() ;
# solve for some values... this should change to something more
appropriate
# find our offset and scaling factor
# these values should be screen resolution/2
double mx = 0.0 ;
double dx = -512.0 ;
mx = (double(screen_coords[5][1]) - dx) / eye_coords[5][1] ;
double my = 0.0 ;
double dy = 384.0 ;
my = (double(screen_coords[5][2]) - dy) / eye_coords[5][2] ;

# eye tracker set up
eye_tracker tracker = new eye_tracker( "ASLEyeTracker" ) ;
tracker.send_string( "port=1" ) ;
tracker.start_tracking() ;
tracker.start_data( dt_position, false ) ;
int position_count = 0 ;

# spit out some basic info
log.print( "Self-ordered Objects Working Memory Task\n" ) ;
log.print( "-----------------------------------------------------\n" )
;
log.print( "Subject: " ) ;
log.print( logfile.subject() ) ;
log.print( "\n" ) ;
log.print( date() ) ;
log.print( "\n\n" ) ;

# Throw up a fixation screen for the MRI and patient to stabilize
fixation.present() ;

#-------------------------------------------------------------
# our Main() :)
#
# The tasks and the order in which they are presented are set by
# this array...
array <int> tasks[3] = { 2, 3, 4 } ; # just doing the 6-, 9-, and 12-
stimuli tasks for now, and only once
# this number should match the # of tasks...
int ntasks = 3 ;
int task ;

loop int t = 1
until t > ntasks
```

```
begin
   task = tasks[t] ;

   #=============================================================
   # Control Task
   #=============================================================
   cntrl_instr.present() ;

   # make sure images are on top of the background border
   loop int i = 1
   until i > levels[task]
   begin
      pics[task].set_part_on_top( i, true ) ;
      i = i + 1 ;
   end ;

   cntrl_task[task].shuffle( 1, levels[task]-1) ; # randomize the order
of asterisk placement

   # add the asterisk to the picture
   pics[task].add_part( astr, coords[task][cntrl_task[task][1]][1],
coords[task][cntrl_task[task][1]][2] ) ;
   astr_part_num = pics[task].part_count() ;
   pics[task].set_part_on_top( astr_part_num, true ) ;

   # log some task/time information
   log.print( levels[task] ) ;
   log.print( "-word level control task:\n" ) ;
   dbug.print( levels[task] ) ;
   dbug.print( "-word level control task:\n" ) ;
   log.print( "Begin time: " ) ;
   log.print( date_time( "tt" ) ) ;
   log.print( "\n" ) ;

   # display the pic
   pics[task].present() ;

   # set variables
   start_time = clock.time() ;
   try = 1 ;
   blank_part = levels[task] ; # set to the last position (including
border boxes)
   selected = levels[task] ; # set selected to the blank space

   response_count = response_manager.total_response_count() ;
   loop until false
   begin
      if ( response_manager.total_response_count() > response_count )
      then
         response_count = response_manager.total_response_count() ;
         if ( highlighted == false ) then
            continue ;
         end ;
         dbug.print( "selected position " ) ;
         dbug.print( selected ) ;
         dbug.print( "\n" ) ;
         if ( selected == (blank_part) ) then
```

```
          continue ;
        end ;
        # change the highlight color of the selected box
        high_boxes[task].set_color( 0, 0, 255 ) ;
        pics[task].present() ;
        wait( 1500 ) ;
        # reset the highlight box
        pics[task].remove_part( high_box_part_num ) ;
        high_boxes[task].set_color( 255, 0, 255 ) ;
        highlighted = false ;
        # check if we've gone through all the stimuli
        if ( try > (cntrl_tries[task]-1) ) then
           stop_time = clock.time() ;
           log.print( "   control task complete\n" ) ;
           log.print( "   time: " ) ;
           log.print( ( stop_time - start_time ) ) ;
           log.print( "\n" ) ;
           break ;
        end ;
        try = try + 1 ;
        # Set our blank image to the last selected space
        pics[task].set_part( selected,
stims[stim_ndx[task]+levels[task]-1] ) ;
        blank_part = selected ;
        rndm = random( 1, 3 ) ;
        loop int i = 1
        until i >= levels[task]
        begin
           pics[task].set_part( placements[stim_ndx[task]-
1+selected][rndm][i], stims[stim_ndx[task]+i-1] ) ;
           int ndx = placements[stim_ndx[task]-
1+selected][rndm][cntrl_task[task][try]] ;
           pics[task].set_part_x( astr_part_num, coords[task][ndx][1]
) ;
           pics[task].set_part_y( astr_part_num, coords[task][ndx][2]
) ;
           i = i + 1 ;
        end ;
        pics[task].present() ;
     end ;
     if (tracker.event_count( dt_position ) > position_count) then
        position_count = tracker.event_count( dt_position );
        eye_position_data edata = tracker.last_position_data();
        # we have to convert the eye_tracker coordinates to
        # our Presentation screen coordinates
        pos_x = int( edata.x() * mx + dx ) ;
        pos_y = int( edata.y() * my + dy ) ;
     else
        continue ;
     end ;
     cell = get_position( task, pos_x, pos_y ) ;
     if ( cell != 0 ) then
        if ( highlighted == false ) then
           pics[task].add_part( high_boxes[task],
coords[task][cell][1], coords[task][cell][2] ) ;
           high_box_part_num = pics[task].part_count() ;
           highlighted = true ;
```

```
         else
            pics[task].set_part_x( high_box_part_num,
coords[task][cell][1] ) ;
            pics[task].set_part_y( high_box_part_num,
coords[task][cell][2] ) ;
         end ;
         pics[task].present() ;
         selected = cell ;
         continue ;
      end ;
      # I used to un-select/un-highlight cells when the subject was not
looking at any specific cell
      # but found that noise in the system lead to a lot of flicker and
not registering selected cells
      # at a button press. So I now once a cell is
selected/highlighted, it stays selected/highlighted
      # until the subject selects a new cell and won't un-select/un-
highlight if the subject looks in the
      # spaces in between or outside of the stimuli matrix.
      #if ( highlighted == true )
      #then
      #   pics[task].remove_part( high_box_part_num ) ;
      #   pics[task].present() ;
      #   highlighted = false ;
      #end ;
      check_timeout() ;
   end ;
   pics[task].remove_part( astr_part_num ) ;

   #fixation.present() ;

   #=============================================================
   # Working Memory Task
   #=============================================================
   task_instr.present() ;

   # reset the images to their original positions
   loop int i = 1
   until i > levels[task]
   begin
      # reset the stimuli.
      pics[task].set_part( i, stims[stim_ndx[task]+(i-1)] ) ;
      # reset to starting positions
      chosen[task][i][1] = i ;
      i = i + 1 ;
   end ;

   # log some information
   dbug.print( levels[task] ) ;
   dbug.print( "-word level task:\n" ) ;
   log.print( levels[task] ) ;
   log.print( "-word level task:\n" ) ;
   log.print( "Begin time: " ) ;
   log.print( date_time( "tt" ) ) ;
   log.print( "\n" ) ;
   pics[task].present() ;
   start_time = clock.time() ;
```

```
   # reset variables
   try = 1 ;
   selected = levels[task] ;
   blank_part = levels[task] ;
   highlighted = false ;

   response_count = response_manager.total_response_count() ;
   loop until false
   begin
      if ( response_manager.total_response_count() > response_count )
      then
         response_count = response_manager.total_response_count() ;
         if ( highlighted == false ) then
            continue ;
         end ;
         dbug.print( "selected position " ) ;
         dbug.print( selected ) ;
         dbug.print( "\n" ) ;
         if ( selected == (blank_part) ) then
           continue ;
         end ;
         # change the highlight color of the selected box
         high_boxes[task].set_color( 0, 0, 255 ) ;
         pics[task].present() ;
         wait( 1500 ) ;
         # reset the highlight box
         pics[task].remove_part( high_box_part_num ) ;
         high_boxes[task].set_color( 255, 0, 255 ) ;
         highlighted = false ;
         # determine which image was selected, record it, and bail if
all
         # images have been selected
         loop int i = 1
         until i >= levels[task]
         begin
            if ( chosen[task][i][1] == selected ) then
               chosen[task][i][2] = 1 ;
               dbug.print( "word " ) ;
               dbug.print( i ) ;
               dbug.print( " selected at position " ) ;
               dbug.print( chosen[task][i][1] ) ;
               dbug.print( ". selected= " ) ;
               dbug.print( selected ) ;
               dbug.print( "\n" ) ;
            end ;
            i = i + 1 ;
         end ;
         bool all_chosen = true ;
         loop int i = 1
         until i >= levels[task]
         begin
            if ( chosen[task][i][2] == 0 ) then
               all_chosen = false ;
            end ;
            i = i + 1 ;
         end ;
```

```
         stop_time = clock.time() ;
         if ( all_chosen == true ) then
            dbug.print( "all items chosen in " ) ;
            dbug.print( try ) ;
            dbug.print( " attempts.\n\n" ) ;
            log.print( "   SUCCESSFUL\n" ) ;
            log.print( "   tries: " ) ;
            log.print( try ) ;
            log.print( "\n   time: " ) ;
            log.print( ( stop_time - start_time ) ) ;
            log.print( " ms\n" ) ;
            break ;
         end ;
         if ( try > (tries[task]-1) ) then
            log.print( "   UNSUCCESSFUL\n" ) ;
            log.print( "   max attempts: " ) ;
            log.print( try ) ;
            log.print( "\n   time: " ) ;
            log.print( ( stop_time - start_time ) ) ;
            log.print( "\n" ) ;
            break ;
         end ;
         try = try + 1 ;
         # Set our blank image to the last selected space
         pics[task].set_part( selected,
stims[stim_ndx[task]+levels[task]-1] ) ;
         blank_part = selected ;
         rndm = random( 1, 3 ) ;
         loop int i = 1
         until i >= levels[task]
         begin
            int ndx = stim_ndx[task]-1+selected ;
            pics[task].set_part( placements[ndx][rndm][i],
stims[stim_ndx[task]+i-1] ) ;
            chosen[task][i][1] = placements[ndx][rndm][i] ;
            i = i + 1 ;
         end ;
         pics[task].present() ;
      end ;
      if (tracker.event_count( dt_position ) > position_count) then
         position_count = tracker.event_count( dt_position );
         eye_position_data edata = tracker.last_position_data();
         # we have to convert the eye_tracker coordinates to
         # our Presentation screen coordinates
         pos_x = int( edata.x() * mx + dx ) ;
         pos_y = int( edata.y() * my + dy ) ;
      else
         continue ;
      end ;
      cell = get_position( task, pos_x, pos_y ) ;
      if ( cell != 0 )  then
         if ( highlighted == false ) then
            pics[task].add_part( high_boxes[task],
coords[task][cell][1], coords[task][cell][2] ) ;
            high_box_part_num = pics[task].part_count() ;
            highlighted = true ;
         else
```

```
            pics[task].set_part_x( high_box_part_num,
coords[task][cell][1] ) ;
            pics[task].set_part_y( high_box_part_num,
coords[task][cell][2] ) ;
         end ;
         pics[task].present() ;
         selected = cell ;
         continue ;
      end ;
      # Same as above, don't unselect
      #if ( highlighted == true )
      #then
      #   pics[task].remove_part( high_box_part_num ) ;
      #   pics[task].present() ;
      #   highlighted = false ;
      #end ;
      check_timeout() ;
   end ;
   t = t + 1 ;
end ;

tracker.stop_data( dt_position ) ;
tracker.stop_tracking() ;

# close our debug log file
dbug.close() ;
log.close() ;
```

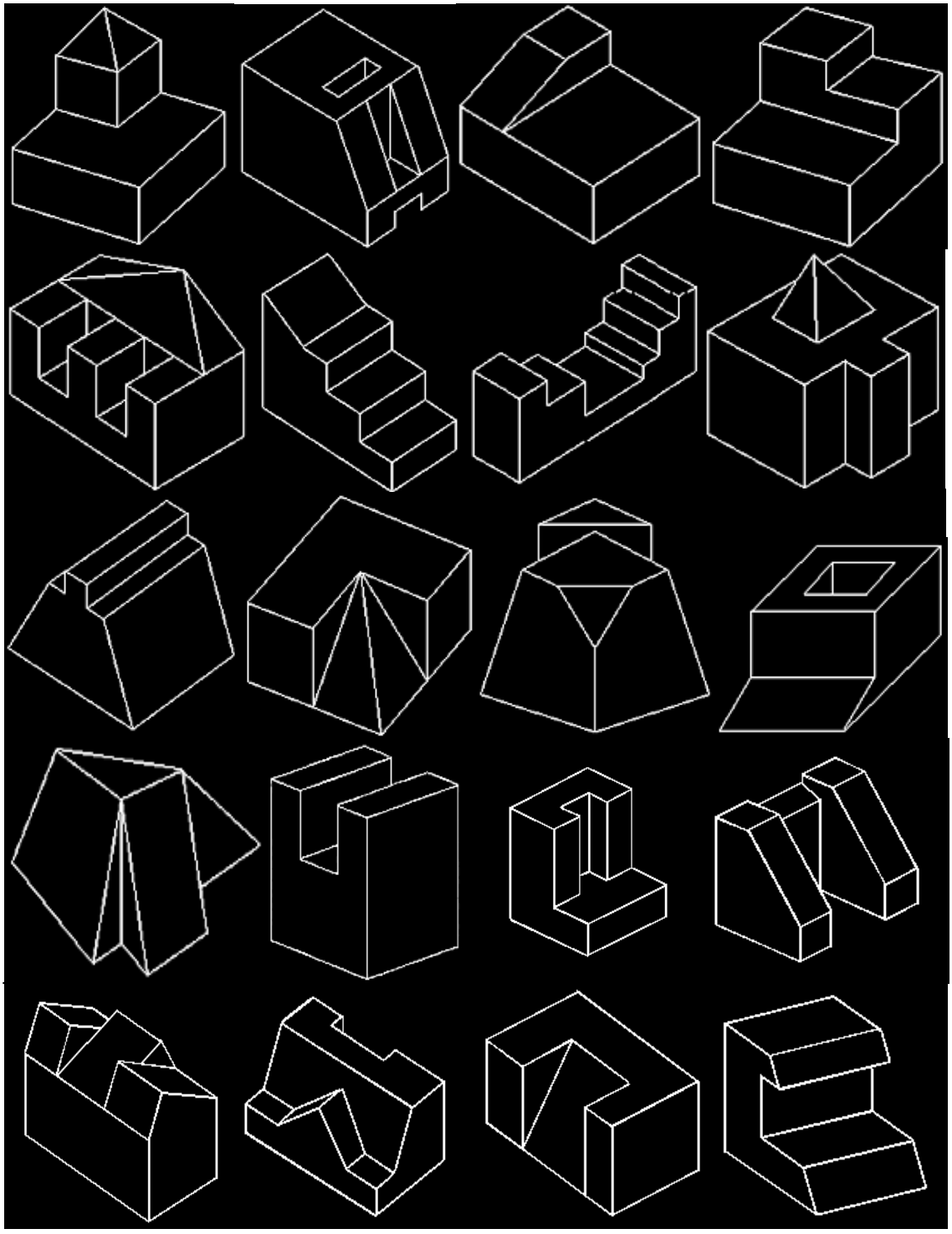

Figure B-1. Objects used in the SOS task.

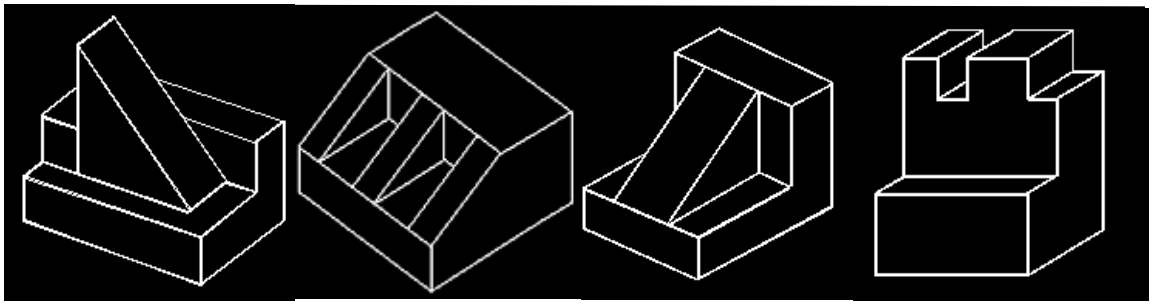

Figure B-1 (continued). Objects used in the SOS task.

Appendix C: N-back Object Scenario

This appendix contains the source code for the N-back object task. Additional scenario files (verbal versions, mouse version, etc…) are available by emailing the author at matthew.scoggins@stjude.org or Dr. Robert Ogg at Robert.Ogg@stjude.org.

N-back Object

The following is the Presentation scenario file for the N-back object task. The objects used in this task are found in Figure 4-4.

```
# n_back_obj.sce
#
# Matt Scoggins
# Radiological Sciences
# St. Jude Childrens Research Hospital
# University of Memphis
#
# The setting of targets and shuffle algorithm for randomization in
this
# task is based on the n-back subroutine in the NBS Demo.
#

# SDL setup stuff
scenario = "n_back_obj" ;

scenario_type = fMRI ;
#scenario_type = fMRI_emulation ;
#scan_period = 2000 ; # for emulation pulse only

no_logfile = false ;

active_buttons = 1 ; #
button_codes = 31 ;

pulses_per_scan = 1 ; #mri send 1 pulse per scan volum (TR)
pulse_code = 100 ;

default_background_color = 32,32,32 ;
default_text_color = 125,125,125 ;
default_font = "arial" ;
default_font_size = 64 ;

begin ;

$n = "2" ;

$xpos = 0 ;
$ypos = 0 ;
```

```
# Timing variables
$instr_len = 2000 ;     # length of instruction screen (ms)
$off_len = 10000 ;      # length of initial rest (ms)
$fix_len = 5000 ; # length of fixation time after instructions
$s_length = 500 ;       # stimulus length (ms)
$isi = 1500 ;           # inter-stimulus-interval (ms)

array {
   bitmap { filename = "images/nb_obj1c.bmp" ; } stim1 ;
   bitmap { filename = "images/nb_obj2.bmp" ; } ;
   bitmap { filename = "images/nb_obj3.bmp" ; } ;
   bitmap { filename = "images/nb_obj4.bmp" ; } ;
   bitmap { filename = "images/nb_obj5.bmp" ; } ;
} stimuli ;

# Fixation Pic
picture {
      text { caption = "+" ; font_size = 30 ;  font = "Courier" ; } ;
      x = $xpos ;
      y = $ypos ;
} default ; # setting this as the default prevents flicker

# Instruction Pic
picture {
      text { caption = "Press the button\nwhen you see" ; } ;
      x = $xpos ;
      y = 150 ;
      bitmap stim1 ;
      x = $xpos ;
      y = -120 ;
} picInstr0 ;

picture {
      text { caption = "Repeating Object?" ; } ;
      x = $xpos ;
      y = $ypos ;
} picInstr1 ;

picture {
      text { caption = "Every other one?" ; } ;
      x = $xpos ;
      y = $ypos ;
} picInstr2 ;


picture {
   bitmap stim1 ;
   x = $xpos ;
   y = $ypos ;
} picStim ;

trial {
   trial_type = fixed;
      trial_duration = stimuli_length;

      picture picInstr0 ;
      duration = $instr_len ;
```

```
      code = "Instr 0-back" ;

      picture default ;
      deltat = $instr_len ;
      duration = $fix_len ;
} trialInstr0 ;

trial {
   trial_type = fixed;
      trial_duration = stimuli_length;

      picture picInstr1 ;
      duration = $instr_len ;
      code = "Instr 1-back" ;

      picture default ;
      deltat = $instr_len ;
      duration = $fix_len ;
} trialInstr1 ;

trial {
   trial_type = fixed;
      trial_duration = stimuli_length;

      picture picInstr2 ;
      duration = $instr_len ;
      code = "Instr 2-back" ;

      picture default ;
      deltat = $instr_len ;
      duration = $fix_len ;
} trialInstr2 ;

trial {
   trial_type = fixed ;
   trial_duration = stimuli_length ;

   picture default ;
   mri_pulse = 1 ;
   duration = $off_len ;
   code = "fix" ;
} trialFix ;

trial {
   trial_type = fixed ;
   trial_duration = stimuli_length ;

   stimulus_event {
      picture picStim ;
      duration = $s_length ;
      code = "stim" ;       # this will change in PCL
   } eventStim ;

   picture default ;
   deltat = $s_length ;
   duration = $isi ;
} trialStim ;
```

```
#===================================================================
# PCL
begin_pcl ;

# PCL variables
int num_stimuli = 5 ;   # number of stimuli in the SDL array above
int num_blocks = 9 ;    # number of stimuli blocks
int num_events = 16 ;   # number of stimuli events in a block
int nbacks = 4 ;        # number of n-back occurances in a block
int n_max = 2 ;
int part = 1 ;

# test order
# number of entries must equal the variable 'num_blocks'
array <int> n[num_blocks] = { 0, 1, 2, 0, 1, 2, 0, 1, 2 } ;

int ndx ;
string txt ;

# list of stimi
array <int> stims[num_events] ;
array <int> last_stims[n_max+1] ;

trialFix.present() ;
loop
   int block = 1
until
   block > num_blocks
begin
   # select the appropriate instruction
   if ( n[block] == 0 ) then
      trialInstr0.present() ;
   elseif n[block] == 1 then
      trialInstr1.present() ;
   else
      trialInstr2.present() ;
   end ;
   ndx = 0 ;
   # clear out our stimulus array
   loop int i = 1
   until i > num_events
   begin
      stims[i] = 0 ;
      i = i + 1 ;
   end ;
   # clear out last_stims array
   loop int i = 1
   until i > (n_max+1)
   begin
      last_stims[i] = 0 ;
      i = i + 1 ;
   end ;
   # set our nback occurances and randomize their placement
   loop int i = (n[block]+1)
   until i > (nbacks+n[block]) || i > num_events
   begin
```

```
      stims[i] = 1 ;
      i = i + 1 ;
   end ;
   stims.shuffle( (n[block]+1), num_events ) ;
   loop
      int e = 1
   until
      e > num_events
   begin
      if ( stims[e] == 1 ) then
         if ( n[block] == 0 ) then
            ndx = 1 ;
         else
            ndx = last_stims[n[block]] ;
         end ;
         txt = " NBACK!"
      else
         if ( n[block] == 0 ) then
            ndx = random( 2, num_stimuli ) ;
         else
            ndx = random( 1, num_stimuli ) ;
            loop
            until ndx != last_stims[n[block]]
            begin
               ndx = random( 1, num_stimuli ) ;
            end ;
         end ;
         txt = "" ;
      end ;
      picStim.set_part( 1, stimuli[ndx] ) ;
      eventStim.set_event_code( "stim" + string(ndx) + txt ) ;
      trialStim.present() ;
      # keep track of the last stimuli
      loop
         int i = (n[block]+1) ; int j = (i-1)
      until
         i == 1
      begin
         last_stims[i] = last_stims[j] ;
         i = i - 1 ;
         j = j - 1 ;
      end ;
      last_stims[1] = ndx ;
      e = e + 1 ;
   end ;
   block = block + 1 ;
end ;
```

Appendix D: Extraction of SOS Timing

The following is the code developed to extract our timing information from the SOS logfiles generated by Presentation. The code consists of a combination of matlab functions and UNIX/LINUX scripting tools BASH, SED, and AWK. Our matlab function *wm_prep2.m* was inserted into the SPM5 batch processing code. This Matlab file makes a *system()* call to our unix shell script *wm_prep2.sh*. The shell script parses the log files and writes the necessary timing information into a new file called *wm_vars.m*, which the original Matlab functions loads into memory.

wm_prep.m

```
function sos = wm_prep2()
% wm_prep.m
%
% Matt Scoggins
% St. Jude Children's Research Hospital
%
% Batching up the spm processing for the working memory task set:
% self-order-search (verbal and objects)
%
% Here we're just loading some variables and calling a little
% shell script to extract some timing and response information from
% the SOS and nback log files. It was just easier to do somethings
% in a shell script rather than use system() commands in here.
% The shell script creates a matlab file that we'll just run from here
% to load those variables.

% building an sos structure with the following fields:
% inst_dur (instruction duration)
% v_resp (verbal responses)
% v_inst_times (times for instruction screens, verbal task)
% v_cntl_1_onset
% v_cntl_2_onset
% v_cntl_3_onset
% v_cntl_1_dur
% v_cntl_2_dur
% v_cntl_3_dur
% o_resp (object responses)
% o_inst_times (times for instruction screens, object task)
% o_cntl_1_onset
% o_cntl_2_onset
% o_cntl_3_onset
% o_cntl_1_dur
% o_cntl_2_dur
% o_cntl_3_dur
```

```
% TR
% Might end up pulling this out of the dicom files
% TR=2.060 ;

% - SOS timing parameters
% most will have to be extracted from the log file
sos.inst_dur = 2.5 ;

% call our shell script to parse out our values and creat another .m
file
rc = system( '/rjo/EXFXN2/SPM5_batch/wm_prep2.sh' ) ;
if ( rc )
   error( 'wm_prep2.sh returned unsuccessful' ) ;
end

wm_vars

if ( sosv_exists )
   % adjust our response times to the start of the scanner sequence
   sos.v_resp = sosv_resp - sosv_start_time ;
   % going for 0.1s resolution
   sos.v_resp = sos.v_resp / 1000 ;
   sos.v_resp = round( sos.v_resp ) ;
   sos.v_resp = sos.v_resp / 10 ;
   % going for 0.1s resolution
   sos.v_inst_times = sosv_inst_times - sosv_start_time ;
   sos.v_inst_times = sos.v_inst_times / 1000 ;
   sos.v_inst_times = round( sos.v_inst_times ) ;
   sos.v_inst_times = sos.v_inst_times / 10 ;
   % find our control and task onsets and durations
   sos.v_cntl_1_onset = sos.v_inst_times(1) + sos.inst_dur ;
   sos.v_cntl_1_dur = sos.v_inst_times(2) - sos.v_cntl_1_onset ;
   sos.v_task_1_onset = sos.v_inst_times(2) + sos.inst_dur ;
   sos.v_task_1_dur = sos.v_inst_times(3) - sos.v_task_1_onset ;
   sos.v_cntl_2_onset = sos.v_inst_times(3) + sos.inst_dur ;
   sos.v_cntl_2_dur = sos.v_inst_times(4) - sos.v_cntl_2_onset ;
   sos.v_task_2_onset = sos.v_inst_times(4) + sos.inst_dur ;
   sos.v_task_2_dur = sos.v_inst_times(5) - sos.v_task_2_onset ;
   sos.v_cntl_3_onset = sos.v_inst_times(5) + sos.inst_dur ;
   sos.v_cntl_3_dur = sos.v_inst_times(6) - sos.v_cntl_3_onset ;
   sos.v_task_3_onset = sos.v_inst_times(6) + sos.inst_dur ;
   % to get the length of the last task we use the last response
   sos.v_task_3_dur = sos.v_resp(length(sos.v_resp)) -
sos.v_task_3_onset ;
end

if ( soso_exists )
   % adjust our response times to the start of the scanner sequence
   sos.o_resp = soso_resp - soso_start_time ;
   % going for 0.1s resolution
   sos.o_resp = sos.o_resp / 1000 ;
   sos.o_resp = round( sos.o_resp ) ;
   sos.o_resp = sos.o_resp / 10 ;
   % going for 0.1s resolution
   sos.o_inst_times = soso_inst_times - soso_start_time ;
   sos.o_inst_times = sos.o_inst_times / 1000 ;
```

```
   sos.o_inst_times = round( sos.o_inst_times ) ;
   sos.o_inst_times = sos.o_inst_times / 10 ;
   % find our control and task onsets and durations
   sos.o_cntl_1_onset = sos.o_inst_times(1) + sos.inst_dur ;
   sos.o_cntl_1_dur = sos.o_inst_times(2) - sos.o_cntl_1_onset ;
   sos.o_task_1_onset = sos.o_inst_times(2) + sos.inst_dur ;
   sos.o_task_1_dur = sos.o_inst_times(3) - sos.o_task_1_onset ;
   sos.o_cntl_2_onset = sos.o_inst_times(3) + sos.inst_dur ;
   sos.o_cntl_2_dur = sos.o_inst_times(4) - sos.o_cntl_2_onset ;
   sos.o_task_2_onset = sos.o_inst_times(4) + sos.inst_dur ;
   sos.o_task_2_dur = sos.o_inst_times(5) - sos.o_task_2_onset ;
   sos.o_cntl_3_onset = sos.o_inst_times(5) + sos.inst_dur ;
   sos.o_cntl_3_dur = sos.o_inst_times(6) - sos.o_cntl_3_onset ;
   sos.o_task_3_onset = sos.o_inst_times(6) + sos.inst_dur ;
   % to get the length of the last task we use the last response
   sos.o_task_3_dur = sos.o_resp(length(sos.o_resp)) -
sos.o_task_3_onset ;
end

clear sosv_exists soso_exists sosv_start_time sosv_resp ...
sosv_instr_times soso_exits soso_start_time soso_resp soso_inst_times
```

wm_prep2.sh

```
#!/bin/bash
#
# wm_prep.sh
#
# Matt Scoggins
# St. Jude Children's Research Hospital
#
# Pull out all timing information from the working memory
# experiment logfiles. We should see 4 files, but might only
# see the nback log files if the Self-ordered search didn't work.
#
# We'll dump all the data into a matlab formatted (*.m) file, so
# we can just run that from the matlab batch file.

mfile=wm_vars.m

echo "% ${mfile} a file to load some timing parameters into our" >
$mfile
echo "% batch script for processing the working memory task set." >>
$mfile
echo "% This file is generated by wm_prep.sh" >> $mfile

#================================================
# Self-ordered Search Verbal Stuff
#================================================
echo -e "\n% SOS verbal stuff..." >> $mfile
# our base log file will either be of the form <patid>-so_verbal.log
# or <patid>-so_verbal2.log going to use brace expansion to take of
that
# bash requires at least one comma, otherwise expansion isn't forced
```

```
if [ -f *so_verbal.log ] || [ -f *so_verbal2.log ] ; then
   echo "sosv_exists = 1 ;" >> $mfile

   # Find which field in the log files contains our time data
   tc=`grep -s "Time" *so_verbal{2,}.log | awk 'BEGIN {FS="\t"} {
      i = 1
      while ( i <= NF ) {
         if ( $i == "Time" ) {
            print i
            break
         }
         ++i
      }
   }'`
   # Echo the field number containing the time to the .m file for
   # debugging purposes
   echo -e "\n% Time values found in field number $tc of the log file"
>> $mfile
   echo -n "sosv_start_time = " >> $mfile

   # parse out start time of the sequence
   grep -s "Fixation" *so_verbal{2,}.log | awk -v TC=${tc} '{print $TC,
" ;" }' >> $mfile

   # parse out all response times
   echo -n "sosv_resp = [ " >> $mfile
   grep -s "Response" *so_verbal{2,}.log | awk -v TC=${tc} 'BEGIN
{ORS=" "} { print $TC }' >> $mfile
   echo "] ;" >> $mfile

   # parse out instruction onset times
   echo -n "sosv_inst_times = [ " >> $mfile
   grep -s "Instructions" *so_verbal{2,}.log | awk -v TC=${tc} 'BEGIN
{FS="\t"} {ORS=" "} {print $TC}' >> $mfile
   echo "] ;" >> $mfile
else
   echo "sosv_exists = 0 ;" >> $mfile
fi

#================================================
# Self-ordered Search Object Stuff
#================================================
echo -e "\n% SOS object stuff..." >> $mfile
# our base log file will either be of the form <patid>-so_object.log
# or <patid>-so_object2.log going to use brace expansion to take of
that
# bash requires at least one comma, otherwise expansion isn't forced
if [ -f *so_objects.log ] || [ -f *so_objects2.log ] ; then
   echo "soso_exists = 1 ;" >> $mfile

   # Find which field in the log files contains our time data
   tc=`grep -s "Time" *so_objects{2,}.log | awk 'BEGIN {FS="\t"} {
      i = 1
      while ( i <= NF ) {
         if ( $i == "Time" ) {
            print i
            break
```

```
         }
         ++i
      }
   }'`
   # Echo the field number containing the time to the .m file for
   # debugging purposes
   echo -e "\n% Time values found in field number $tc of the log file"
>> $mfile
   echo -n "soso_start_time = " >> $mfile

   # parse out start time of the sequence
   grep -s "Fixation" *so_objects{2,}.log | awk -v TC=${tc} '{print
$TC, " ;" }' >> $mfile

   # parse out all response times
   echo -n "soso_resp = [ " >> $mfile
   grep -s "Response" *so_objects{2,}.log | awk -v TC=${tc} 'BEGIN
{ORS=" "} { print $TC }' >> $mfile
   echo "] ;" >> $mfile

   # parse out instruction onset times
   echo -n "soso_inst_times = [ " >> $mfile
   grep -s "Instructions" *so_objects{2,}.log | awk -v TC=${tc} 'BEGIN
{FS="\t"} {ORS=" "} {print $TC}' >> $mfile
   echo "] ;" >> $mfile
else
   echo "soso_exists = 0 ;" >> $mfile
fi

                                exit 0
```

Appendix E: Interface Box

An electronic interface box was designed and created to handle communications between various components of our functional-MRI equipment setup as described in Chapter 4. This intermediary device was necessary due to multiple components using the parallel port on the PC. The following figures are schematic diagrams of the interface box. Light emitting diodes (LEDs) were used to provide visual feedback and verification that trigger pulses from the MRI control unit and response button were being received and directed to the PC running Presentation software.

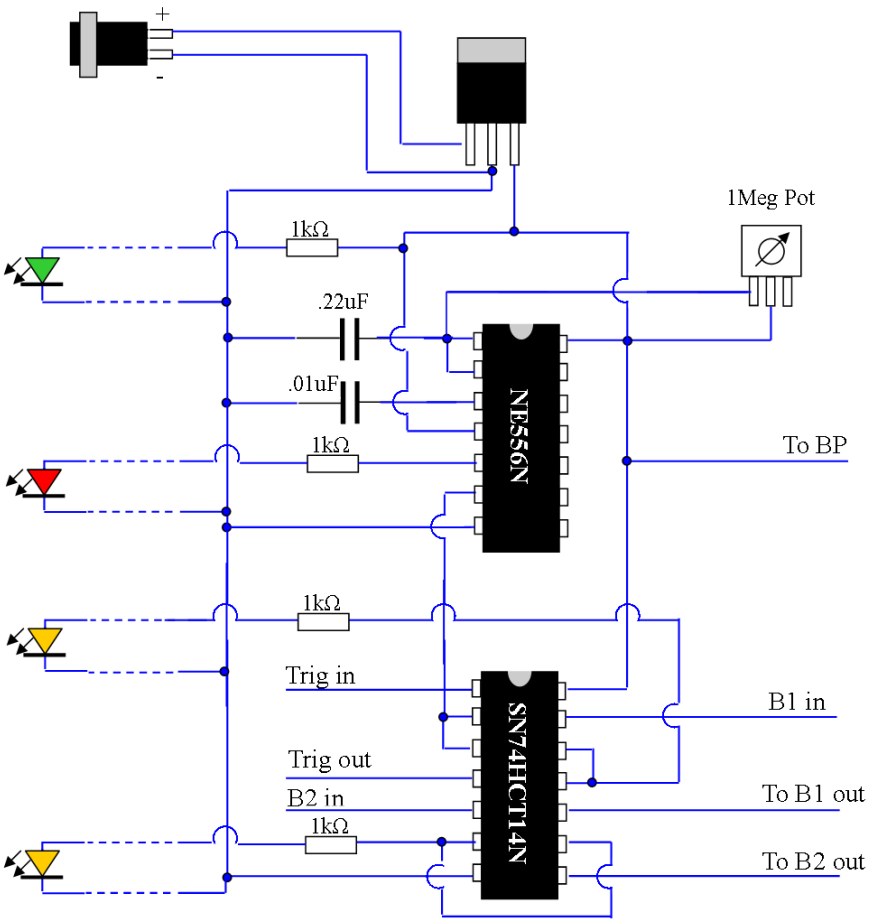

Figure E-1. Electronics layout of the interface box. LEDs provided visual verification that trigger pulses and button responses were being received by the interface box and passed to the PC running Presentation software.

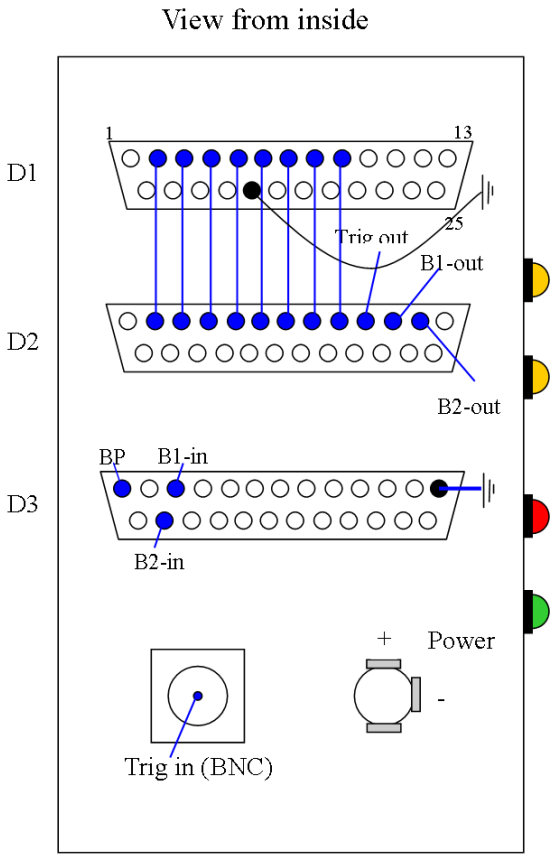

Figure E-2. Pin-diagram of the interface box.

Appendix F: Behavioral Performance

The following tables contain all participant performance data from N-back and SOS tasks. Tables F1-F6 contain inside- and outside-MRI results from the group of healthy young adults in the EXFXN2 protocol. Tables F7 – F9 contain the results from the RT1 patient group.

Table F-1. Outside-MRI N-back (verbal) performance. RT = reaction time. OM = omissions. CO = commissions.

#	0-back RT	0-back OM	0-back CO	1-back RT	1-back OM	1-back CO	2-back RT	2-back OM	2-back CO
1	0.47	1	2	0.58	1	1	0.53	0	0
2	0.41	1	1	0.50	1	0	0.42	2	6
3	0.46	0	0	0.49	0	0	0.55	1	3
4	0.37	0	0	0.33	0	1	0.39	0	1
5	0.45	0	1	0.43	1	3	0.44	4	3
6	0.38	0	0	0.35	0	1	0.39	0	0
7	0.48	0	0	0.55	0	0	0.82	3	1
8	0.36	0	0	0.35	0	0	0.47	0	3
9	0.42	0	0	0.42	0	0	0.56	0	1
10	0.39	0	0	0.35	0	1	0.40	1	2
11	0.42	0	0	0.49	0	0	0.72	1	6
12	0.37	0	1	0.41	0	0	0.68	1	3
13	0.42	0	1	0.40	0	3	0.55	1	3
14	0.50	0	3	0.58	0	0	0.82	0	2
15	0.38	2	1	0.44	0	4	0.42	1	7
16	0.40	0	0	0.41	1	0	0.52	3	4
17	0.52	0	0	0.54	0	0	0.67	4	1
18	0.45	0	0	0.43	0	0	0.61	0	5
19	0.42	0	0	0.43	0	0	0.46	0	1
20	0.59	0	0	0.74	0	0	0.88	0	3
21	0.38	0	1	0.38	0	0	0.56	1	4
22	0.43	0	0	0.43	0	0	0.46	0	0
23	0.40	0	0	0.38	1	0	0.51	0	0
24	0.50	0	0	0.50	0	0	0.52	0	0
25	0.38	0	1	0.39	0	0	0.51	2	1
Mean	0.43			0.45			0.56		
StDev	0.057			0.093			0.140		

Table F-2. Outside-MRI N-back (object) performance. RT = reaction time. OM = omissions. CO = commissions.

#	0-back RT	0-back OM	0-back CO	1-back RT	1-back OM	1-back CO	2-back RT	2-back OM	2-back CO
1	0.43	0	0	0.44	2	1	0.43	0	0
2	0.45	2	2	0.41	4	4	0.39	2	3
3	0.45	0	0	0.47	0	0	0.52	1	1
4	0.39	0	0	0.35	0	0	0.33	1	3
5	0.47	0	0	0.50	0	1	0.42	6	2
6	0.39	0	1	0.34	0	0	0.42	0	1
7	0.41	0	1	0.64	1	2	0.66	3	0
8	0.39	0	1	0.43	0	1	0.43	1	3
9	0.38	0	0	0.37	0	0	0.41	0	0
10	0.42	0	0	0.38	0	1	0.41	0	2
11	0.42	0	0	0.56	0	0	0.63	1	4
12	0.38	0	1	0.55	0	0	0.63	2	0
13	0.46	2	1	0.45	0	0	0.49	1	1
14	0.44	0	2	0.50	0	0	0.97	0	2
15	0.40	0	3	0.38	0	3	0.40	1	11
16	0.39	0	0	0.35	0	0	0.50	6	5
17	0.41	0	0	0.49	1	0	0.73	0	3
18	0.41	0	0	0.39	3	1	0.48	1	3
19	0.50	0	0	0.45	1	0	0.45	0	0
20	0.59	0	0	0.68	2	0	0.70	1	3
21	0.37	1	1	0.36	0	0	0.57	1	5
22	0.45	0	0	0.44	0	0	0.46	0	1
23	0.50	0	0	0.34	0	0	0.50	1	2
24	0.44	0	0	0.45	1	0	0.51	2	1
25	0.39	3	3	0.41	1	0	0.51	1	2
Mean	0.43			0.45			0.52		
StDev	0.050			0.089			0.139		

Table F-3. Inside-MRI N-back (verbal) performance. RT = reaction time. OM = omissions. CO = commissions.

#	0-back RT	0-back OM	0-back CO	1-back RT	1-back OM	1-back CO	2-back RT	2-back OM	2-back CO
1	0.56	0	0	0.54	0	1	0.48	0	1
2	0.54	0	1	0.56	1	0	0.56	0	2
3	0.56	1	0	0.61	0	1	0.74	0	0
4	0.38	0	0	0.39	0	1	0.44	0	2
5	0.47	0	0	0.53	0	0	0.51	1	1
6	0.46	0	0	0.48	0	0	0.55	0	0
7	0.78	0	0	0.95	0	0	1.08	7	2
8	0.44	0	0	0.44	0	0	0.47	0	0
9	0.43	1	0	0.46	0	0	0.63	0	1
10	0.53	0	0	0.40	0	0	0.38	0	0
11	0.53	0	1	0.58	0	0	0.67	0	0
12	0.47	0	0	0.47	0	0	0.82	2	3
13	0.53	0	0	0.46	0	0	0.46	0	1
14	0.66	0	0	0.69	0	0	0.78	0	4
15	0.38	0	2	0.49	0	2	0.56	0	5
16	0.43	0	0	0.44	0	0	0.50	1	2
17	0.56	0	0	0.59	0	0	0.68	2	0
18	0.47	0	0	0.51	0	0	0.61	1	2
19	0.57	0	0	0.48	3	1	0.54	0	1
20	0.67	0	0	0.67	1	0	0.77	1	1
21	0.45	0	0	0.41	0	0	0.67	0	4
22	0.52	0	0	0.60	0	0	0.75	0	4
23	0.53	0	0	0.60	0	0	0.50	0	0
24	0.56	0	0	0.57	0	1	0.62	1	1
25	0.49	4	0	0.49	3	2	0.68	0	5
Mean	0.52			0.54			0.62		
StDev	0.090			0.118			0.153		

Table F-4. Inside-MRI N-back (object) performance. RT = reaction time. OM = omissions. CO = commissions.

#	0-back RT	0-back OM	0-back CO	1-back RT	1-back OM	1-back CO	2-back RT	2-back OM	2-back CO
1	0.55	0	0	0.52	0	0	0.53	2	1
2	0.58	1	0	0.57	3	4	0.57	2	0
3	0.61	0	0	0.61	0	1	0.71	0	1
4	0.41	0	0	0.39	0	0	0.46	1	2
5	0.53	0	0	0.51	0	0	0.58	1	1
6	0.46	0	0	0.46	0	0	0.52	1	1
7	0.89	0	0	0.84	2	0	0.91	6	1
8	0.47	0	0	0.50	0	0	0.60	1	4
9	0.53	0	0	0.48	0	0	0.63	0	0
10	0.47	0	0	0.37	1	2	0.34	0	2
11	0.55	0	0	0.58	0	0	0.84	0	3
12	0.49	0	0	0.45	0	0	0.52	1	3
13	0.58	0	0	0.53	0	0	0.56	1	2
14	0.68	0	0	0.67	0	0	0.87	0	3
15	0.53	0	0	0.41	0	1	0.48	2	5
16	0.43	0	0	0.44	0	1	0.62	0	2
17	0.53	0	0	0.54	0	0	0.96	1	2
18	0.47	0	0	0.46	0	1	0.51	0	2
19	0.52	0	0	0.62	0	0	0.56	2	2
20	0.61	0	0	0.59	0	0	0.66	2	2
21	0.50	0	0	0.46	0	0	0.60	1	4
22	0.54	0	0	0.55	0	0	0.51	4	1
23	0.60	0	0	0.66	1	0	0.64	1	0
24	0.49	0	0	0.53	0	0	0.71	1	0
25	0.51	0	0	0.64	1	2	0.80	1	2
Mean	0.54			0.54			0.63		
StDev	0.096			0.104			0.151		

Table F-5. Outside-MRI SOS performance results for EXFXN2 healthy participants. Times are in seconds.

#	6 word trials	6 word time	9 word trials	9 word time	12 word trials	12 word time	5 obj trials	5 obj time	8 obj trials	8 obj time	11 obj trials	11 obj time
1	6	30.5	9	54.9	22	146.3	5	21.5	12	87.2	11	80.6
2	6	37.0	10	38.7	15	64.8	5	20.1	9	31.9	11	58.8
3	6	17.3	9	35.8	13	66.0	8	32.7	9	42.2	21	110.8
4	6	15.6	9	22.6	14	57.8	9	47.9	8	25.8	23	143.3
5	6	31.5	9	46.1	14	109.0	5	21.1	8	48.9	11	76.3
6	6	28.9	9	33.6	16	157.8	5	17.1	8	30.9	15	173.5
7	6	25.3	16	96.0	19	176.1	5	25.5	8	35.5	11	48.0
8	6	17.9	9	37.9	14	61.1	5	17.1	9	42.0	16	71.9
9	6	17.5	9	39.0	15	71.7	6	23.4	8	38.2	23	157.6
10	6	20.1	9	35.3	35	255.0	5	22.6	16	113.7	12	103.1
11	6	37.4	9	44.9	13	71.9	5	19.4	23	151.2	21	202.4
12	6	27.1	9	35.4	12	56.2	5	15.0	8	31.1	13	112.9
13	6	16.0	9	28.6	26	112.1	5	18.2	8	34.4	11	50.7
14	6	18.3	10	36.4	12	40.4	6	30.6	8	31.0	27	175.7
15	6	17.3	20	114.5	17	71.4	12	52.5	8	34.8	19	82.0
16	6	34.5	9	48.8	12	59.5	5	25.9	8	47.7	13	70.9
17	6	19.7	9	33.3	18	78.6	5	18.1	8	29.7	14	103.4
18	6	37.6	10	54.1	28	198.3	5	16.3	8	41.8	15	103.7
19	6	61.1	9	60.7	12	95.7	5	23.0	9	62.7	13	121.3
20	6	17.5	9	25.5	22	106.1	5	15.7	10	34.9	15	83.8
21	6	29.3	9	37.2	12	47.3	5	17.4	8	30.1	11	49.7
22	6	31.9	10	44.5	20	117.0	5	18.4	9	54.0	21	153.0
23	6	18.1	9	36.9	21	135.8	5	19.7	10	56.6	15	85.5
24	11	49.7	9	40.5	12	75.1	7	28.6	24	104.4	15	95.7
25	6	19.7	9	36.5	14	78.7	5	19.5	11	60.3	11	74.6

Table F-6. Inside-MRI SOS performance results for EXFXN2 healthy participants. Times are in seconds.

#	6 word trials	6 word time	9 word trials	9 word time	12 word trials	12 word time	5 obj trials	5 obj time	8 obj trials	8 obj time	11 obj trials	11 obj time
1	7	34.1	14	111.9	29	243.2	5	19.0	12	72.2	13	84.6
2	7	56.7	9	42.1	12	47.7	5	21.2	8	35.3	13	69.6
3	6	17.8	13	48.3	17	73.6	6	26.8	14	67.0	15	78.9
4	10	38.2	14	59.1	13	42.2	7	25.4	9	28.8	23	158.3
5	7	48.0	17	238.3	12	158.5	6	45.7	8	61.2	11	140.8
6	6	19.6	9	49.9	12	67.8	6	30.6	8	43.5	14	77.8
7	6	29.5	9	37.7	12	55.7	6	38.9	10	57.1	12	70.1
8	6	16.9	12	45.1	17	75.4	6	23.2	10	39.3	11	47.0
9	10	59.0	10	63.8	16	85.5	5	22.6	10	58.8	14	89.6
10	6	21.3	11	42.4	14	77.1	5	20.4	8	33.4	21	163.6
11	6	25.2	11	74.4	14	73.8	6	24.7	10	60.4	13	79.4
12	6	45.1	9	47.8	19	174.1	6	25.3	8	43.5	20	185.1
13	9	35.9	11	51.0	25	104.9	5	24.3	11	57.8	18	104.8
14	7	31.6	9	40.0	20	136.3	7	37.5	11	50.3	14	73.9
15	10	32.2	11	51.2	14	63.5	10	45.3	9	39.1	15	74.1
16	7	41.4	16	84.1	14	86.4	5	24.2	12	98.8	17	145.6
17	7	24.8	10	41.8	28	174.6	5	16.5	14	75.2	22	176.0
18	11	66.5	16	96.1	23	121.6	6	22.3	8	35.7	16	125.3
19	6	17.3	11	47.1	13	55.4	5	19.2	8	38.9	11	81.0
20	6	19.0	10	38.3	13	49.3	6	23.8	18	123.2	23	221.3
21	8	30.5	10	35.1	12	42.9	5	22.1	8	28.5	13	50.5
22	6	22.7	9	53.2	18	121.3	6	20.8	8	28.4	21	98.8
23	7	29.5	13	67.0	13	53.6	7	35.0	18	116.3	21	98.9
24	7	37.1	17	94.2	12	76.7	5	25.3	8	46.5	16	111.7
25	6	30.6	17	141.8	20	184.2	8	47.4	9	49.1	12	84.1

Table F-7. N-back (verbal) performance for RT1 patients. RT = reaction time. OM = omissions. CO = commissions.

#	0-back RT	0-back OM	0-back CO	1-back RT	1-back OM	1-back CO	2-back RT	2-back OM	2-back CO
1	0.46	0	0	0.52	0	2	0.65	1	5
2	0.48	0	1	0.63	1	12	0.82	0	16
3	0.47	0	1	0.55	4	6	0.65	1	11
4	0.72	0	0	1.00	0	1	1.14	1	1
5	0.58	0	2	0.63	4	5	0.66	0	1
6	0.46	0	0	0.51	0	3	0.60	3	2
7	0.55	3	5	0.34	7	17	0.33	0	39
8	0.59	0	20	0.75	0	20	1.07	1	25
9	0.49	0	0	0.54	1	1	0.74	2	20
10	0.46	0	0	0.47	0	1	0.53	1	1
11	0.55	0	0	0.61	5	2	1.24	5	3
12	0.65	0	15	0.69	4	15	0.63	3	29
13	0.57	0	0	0.57	0	1	0.70	1	2
14	0.69	1	9	0.89	6	13	0.95	6	11
15	0.46	0	1	0.54	1	0	0.60	5	2
16	0.54	0	1	0.63	1	5	0.75	3	7
17	0.51	0	2	0.84	1	2	0.93	3	1
18	0.47	0	1	0.49	1	1	0.58	0	4
19	0.48	0	0	0.58	0	0	0.56	0	5
20	0.46	0	0	0.50	0	1	0.85	0	3
21	0.49	0	1	0.62	1	1	0.79	1	1
22	0.48	1	0	0.59	2	0	0.52	1	1
23	0.46	0	0	0.57	0	0	0.57	0	2
24	0.72	2	9	0.76	5	11	0.47	8	13
25	0.81	0	0	0.84	0	0	0.90	0	1
26	0.68	1	5	1.09	8	22	0.75	5	33
27	0.45	0	0	0.48	0	1	0.50	0	3
29	0.67	0	2	0.77	0	3	0.67	7	14
30	0.51	0	0	0.59	0	0	0.78	0	3
31	0.59	0	0	0.85	0	0	0.86	2	6
32	0.55	0	9	0.72	1	11	1.16	5	13
33	0.55	0	0	0.68	1	5	0.74	0	6
34	0.49	0	1	0.54	0	2	0.57	5	3
35	0.62	0	0	0.00	12	5	0.60	4	1
36	0.57	0	0	0.64	0	0	0.85	1	2
37	0.59	0	2	0.57	2	3	0.70	4	2
38	0.46	0	0	0.54	4	4	0.45	9	8
39	0.56	2	11	0.52	7	11	0.60	9	8
40	0.53	0	0	0.54	1	1	0.76	1	1
41	0.51	0	2	0.77	3	1	0.84	4	3
42	0.46	0	0	0.43	0	5	0.45	0	10

Table F-7 (continued). N-back (verbal) performance. RT = reaction time. OM = omissions. CO = commissions.

#	0-back RT	0-back OM	0-back CO	1-back RT	1-back OM	1-back CO	2-back RT	2-back OM	2-back CO
43	0.46	0	0	0.52	0	2	0.65	1	5
44	0.43	0	2	0.43	0	0	0.53	1	2
45	0.60	3	1	0.57	1	0	0.94	2	5
Mean	0.55			0.61			0.72		
StDev	0.09			0.18			0.20		

Table F-8. N-back (object) performance for RT1 patients. RT = reaction time. OM = omissions. CO = commissions.

#	0-back RT	0-back OM	0-back CO	1-back RT	1-back OM	1-back CO	2-back RT	2-back OM	2-back CO
1	0.51	0	0	0.57	0	2	0.51	5	1
2	0.44	0	5	0.41	0	3	0.68	3	21
3	0.53	0	2	0.48	1	3	0.64	3	9
4	0.64	0	0	1.03	0	0	1.10	3	0
5	0.55	0	1	0.57	0	0	0.66	3	3
6	0.47	0	2	0.56	0	2	0.65	3	6
7	0.51	4	2	0.00	12	6	0.36	10	8
8	0.78	5	20	0.86	8	22	1.16	8	20
9	0.44	0	1	0.53	1	0	0.42	6	21
10	0.49	0	1	0.54	1	1	0.56	1	0
11	0.66	0	2	1.05	2	1	0.86	4	1
12	0.56	3	56	0.57	5	23	0.43	7	26
13	0.59	0	1	0.66	0	0	0.91	0	5
14	0.73	0	3	0.56	8	9	0.55	11	3
15	0.54	0	0	0.58	4	1	0.82	5	5
16	0.61	1	2	0.60	2	5	0.56	2	2
17	0.67	2	1	0.77	3	4	1.01	4	4
18	0.50	0	0	0.59	0	1	0.60	1	2
19	0.52	0	3	0.59	0	1	0.69	0	6
20	0.49	6	0	0.56	8	0	0.66	9	0
21	0.68	0	1	0.62	0	0	0.83	2	3
22	0.47	0	0	0.48	3	0	0.60	2	1
23	0.58	0	0	0.59	0	0	0.62	0	3
24	0.74	1	2	0.65	1	4	0.64	9	3
25	0.81	0	0	0.90	0	0	0.76	0	0
26	0.81	0	18	0.54	4	25	0.48	0	49
27	0.53	0	0	0.49	0	0	0.52	0	0
29	0.64	1	8	0.83	3	19	0.58	5	16
30	0.68	0	0	0.57	0	0	0.88	1	1
31	0.61	0	0	0.79	0	1	0.87	5	9
32	0.64	0	11	0.75	7	14	0.96	6	12
33	0.57	0	3	0.65	1	10	0.79	1	11
34	0.53	0	0	0.74	3	0	0.81	9	3
35	0.67	0	0	0.70	10	9	0.58	9	3
36	0.55	0	0	0.58	1	0	0.79	1	1
37	0.66	0	0	0.72	2	1	0.72	3	4
38	0.52	0	2	0.49	3	0	0.59	9	4
39	0.00	0	0	0.00	0	0	0.00	0	0
40	0.64	0	0	0.87	4	0	0.58	4	0
41	0.55	0	1	0.84	3	5	0.83	4	4
42	0.51	0	0	0.57	0	2	0.51	5	1

Table F-8 (continued). N-back (object) performance. RT = reaction time. OM = omissions. CO = commissions.

#	0-back RT	0-back OM	0-back CO	1-back RT	1-back OM	1-back CO	2-back RT	2-back OM	2-back CO
43	0.47	0	7	0.40	1	15	0.40	1	29
44	0.48	0	1	0.48	2	0	0.51	2	5
45	0.71	5	4	0.77	3	0	0.95	5	4
Mean	0.58			0.62			0.68		
StDev	0.13			0.20			0.21		

Table F-9. FRMI SOS performance results for RT1 patients. Times are in seconds.

#	6 word trials	6 word time	9 word trials	9 word time	12 word trials	12 word time	5 obj trials	5 obj time	8 obj trials	8 obj time	11 obj trials	11 obj time
5	6	20	10	52.5	27	187	5	23	8	38.5	11	72
9	10	39	14	73	20	86	8	25	10	39	17	59
10	6	18	9	32	14	48	8	28	16	69	25	116
11	11	70	18	121	28	250	6	27	8	48	26	157
13	7	30	9	41	18	106	5	21	10	44	11	52
15	8	30	11	45	15	56	6	17	11	39	22	87
16	11	64	27	114	31	171	9	58	8	26	22	102
17	10	47	14	74	33	162	9	37	8	42	15	84
18	7	29	10	39	21	146	7	23	9	49	25	208
19	6	25	10	56	15	109	7	72	17	97	13	91
20	6	25	19	134	24	207	6	28	12	80	17	126
21	9	35	9	32	17	75	7	28	8	31	16	74
22	8	32	13	58	14	50	5	14	10	33	33	125
23	7	38	9	45	33	150	5	28	8	43	16	93
25	6	24	27	172	24	186	7	25	9	42	27	109
27	6	16	9	30	12	40	9	27	13	49	22	89
28	13	36	20	54	30	84	13	35	24	70	21	73
30	6	20	11	43	22	148	5	16	9	42	13	113
31	10	31	17	47	20	44	7	24	14	46	30	108
34	7	29	11	57	13	53	12	63	15	81	26	173
35	7	19	12	41	19	60	9	26	13	46	33	143
37	9	37	13	66	26	160	5	25	10	55	29	194
38	7	26	16	59	36	196	11	72	12	53	21	88

Table F-9 (continued). FRMI SOS performance results for RT1 participants. Times are in seconds.

#	6 word trials	6 word time	9 word trials	9 word time	12 word trials	12 word time	5 obj trials	5 obj time	8 obj trials	8 obj time	11 obj trials	11 obj time
39	8	27	24	66	25	84	7	25	21	65	33	80
41	8	48	16	95	18	97	13	51	9	48	28	158
42	12	64	10	67	16	128	6	33	10	60	19	91
43	6	24	9	55	33	500	5	20	8	35	11	98
44	11	52	11	46	24	148	9	33	16	68	20	85